Acta Pharmaceutica Sinica B 2026;16(4):1804−1847

Chinese Pharmaceutical Association
Institute of Materia Medica, Chinese Academy of Medical Sciences

Acta Pharmaceutica Sinica B

www.elsevier.com/locate/apsb
www.sciencedirect.com

REVIEW

From conceptual design to translational progress: Emerging advances in intelligent microneedles for biomedical applications

Yue Yin[a,b,c], Qiaoqiao Zhao[a,b,c], Zihan Wang[a,b,c], Zixuan Li[a,b,c], Hening Liu[a,b,c], Fatemeh Eghbalitabar[a,b,c], Jing Shang[b,c,d,*], Lu Tang[e,*], Wei Wang[a,b,c,*]

[a]*State Key Laboratory of Natural Medicines, Department of Pharmaceutics, School of Pharmacy, China Pharmaceutical University, Nanjing 211198, China*
[b]*NMPA Key Laboratory for Research and Evaluation of Cosmetics, China Pharmaceutical University, Nanjing 211198, China*
[c]*Wuxi Research Center for Innovative Medicines and Life Health, Wuxi Innovation Research Institute of China Pharmaceutical University, Wuxi 214112, China*
[d]*School of Traditional Chinese Pharmacy, China Pharmaceutical University, Nanjing 211198, China*
[e]*Institute for Experimental Molecular Imaging, Uniklinik RWTH Aachen and Helmholtz Institute for Biomedical Engineering, RWTH Aachen University, Aachen 52074, Germany*

Received 10 September 2025; received in revised form 17 October 2025; accepted 12 December 2025

KEY WORDS

Microneedle;
Mimicking strategy;
Stimuli-responsive system;
Bioengineering;
Nanobiotechnology;
Artificial intelligence;
Wearable devices;
Close-loop theranostics

Abstract Microneedles (MNs), as innovative biomedical devices, are undergoing a transformation from basic transdermal devices to intelligent and multifunctional systems. The advancement of intelligent MNs enhances tissue penetration and adhesion, triggers timely, on-demand and precise spatiotemporal controlled release, achieves sequential drug delivery and *in situ* monitoring, and enables close-loop theranostics *via* the integration of flexible electronics, wireless communication, and artificial intelligence. This review not only systematically highlights these cutting-edge breakthroughs, focusing on five major innovative advancements of conceptual design, including mimicking strategies, stimuli-responsive systems, innovative structural designs, living payload, and wearable integration, but also delineates the principal obstacles obstructing the advancement of intelligent MNs. We also emphasize that MN technology

This article is part of special issue entitled: Hot Topic Revs in Drug Delivery (II) published in Acta Pharmaceutica Sinica B.
*Corresponding authors.
E-mail addresses: wangcpu209@cpu.edu.cn (Wei Wang), ltang@ukaachen.de (Lu Tang), shangjing21cn@cpu.edu.cn (Jing Shang).
Peer review under the responsibility of Chinese Pharmaceutical Association and Institute of Materia Medica, Chinese Academy of Medical Sciences.

https://doi.org/10.1016/j.apsb.2026.01.021

is fueling the evolution of next-generation medical paradigms based on its personalized, minimally invasive, and intelligent features through interdisciplinary integration, which is crucial for reshaping the future landscape of disease diagnosis and treatment.

1. Introduction

Microneedles (MNs) are needles measuring tens to thousands of micrometers in length that can mechanically disrupt the superficial skin layer (stratum corneum) barrier or the barriers of necrotic tissue or biofilm to enhance medication penetration[1]. Compared to hypodermic needle injections, MNs offer a less intrusive transdermal approach, making them a possible substitute, particularly for the treatment of chronic diseases and special populations[2,3]. MNs provide many options in material selection and structural configurations for production and alteration, facilitating payload species, dose, and spatiotemporal regulation in drug administration[4]. Besides administering conventional pharmaceuticals, MN delivery platforms are employed to transport diverse nanoparticles (NPs), nucleic acids, proteins, cells, organoids, bacteria, chlorella, and vaccines[5-8]. MNs can provide controlled drug release rates, encompassing rapid release for emergency interventions and sustained release for chronic disease management, by utilizing specific materials at the needle tip, drug delivery mechanisms, and structural design. Moreover, they can facilitate localized drug release to enhance biodistribution, mitigate gastrointestinal exposure, and reduce the loss of drug efficacy due to circulation in the bloodstream, denaturation, clearance, and tissue infiltration[1,9]. Currently, MNs are utilized not just for transdermal administration to the skin but also for targeting other tissues and organs, including the eyes, oral cavity, nasal cavity, joint cavity, heart, spinal cord, gastrointestinal system, and brain[10-19]. MNs exhibit significant potential in the treatment of diverse dermatological conditions, including acne, skin aging, atopic dermatitis, psoriasis, bacterial infections, and skin cancers, as well as localized ailments such as myocardial infarction (MI), obesity, periodontitis, and brain tumors[20-24]. Furthermore, MNs demonstrate considerable potential in preventive medicine due to their ability to interact with the numerous resident immune cells present in the skin. MN-mediated vaccinations have superior immunogenicity and dosage-sparing effects compared to intramuscular injections, as clinically demonstrated for the administration of influenza and polio vaccines[25-27].

Additionally, MNs can also be utilized for diagnosis and monitoring purposes. They can analyze and identify health-related analytes from skin capillary blood and interstitial fluid (ISF) through a porous structure, swelling hydrogel, and biomolecules attached to the needle tips[28-31]. Progress in contemporary MNs, microelectronics, and nanomaterials technology has facilitated the manufacturing of novel wearable MNs capable of detecting and monitoring intricate physiological states, including metabolites that may act as potential biomarkers[32,33]. Concurrently, advanced artificial intelligence (AI) techniques are included with MNs to improve their diagnostic efficiency. AI-driven algorithms enhance data gathering, signal processing, and analysis, facilitating more precise and individualized health insights. The amalgamation of wearable technology with MNs enables the successful implementation of closed-loop systems that modify treatment protocols in real-time, thereby achieving personalized medicine[34].

Intelligent MNs comprise a collection of complex and multifunctional MNs engineered for diverse application contexts. The technological excellence of these MNs is attained through creative material selection, structural design, tailored payloads, and the incorporation of AI. Intelligent MNs can be developed using mimicking strategies that replicate the architecture and functions of real creatures, mimic regular biorhythms, and imitate the activity of natural enzymes. These MNs possess augmented piercing and adsorption properties, enhanced drug penetration effects, adjustable temporal and spatial drug distribution, and precise management of cellular metabolism[35,36]. Moreover, intelligent MNs can be developed by incorporating stimuli-responsive NPs or employing stimuli-responsive matrix materials. These MNs can react to external physical stimuli (such as light, electricity, heat, magnetism, etc.) or internal chemical stimuli (such as pH, reactive oxygen species (ROS), enzymes, glucose, etc.) within the skin and deeper organs, accurately modulating the spatial distribution, release rate, and retention duration of drugs[37-39]. Additionally, progress in materials science and engineering production has facilitated the unique structural design of MNs. Intelligent MNs possess multi-layered, core−shell, hollow, and porous architectures. These varied architectures enable the execution of numerous activities, including the controlled release of drugs, facilitating sequential treatment, and improving the detection efficacy of ISF biomarkers. Intelligent MNs provide innovative options for the delivery of living substances. The advent of hydrogels and cryomicroneedles (cryoMNs) signifies a groundbreaking advancement in the administration of biological materials. These MNs can efficiently preserve the viability of cells, organelles, organoids, and microbes, consequently augmenting the efficacy of disease therapy[40,41]. Furthermore, the advancement of wearable technology facilitates the continuous monitoring of biomarkers in intelligent MNs through real-time feedback, demonstrating significant potential in precision, personalization, and patient comfort in therapy[42-44].

This review summarized the innovative advancements of intelligent MNs, emphasizing how the intersection of biomimicry, intelligent material science, and bioelectronic integration is transforming their applications (Fig. 1[1,32]). By clarifying designing principles, mechanistic insights, and translational achievements across many biomedical fields, we highlighted the revolutionary potential of next-generation MNs. In addition, this review involves the challenges and obstacles faced in the clinical transition of intelligent MNs. Meanwhile, the future perspectives of intelligent MNs are also provided.

2. Mimicking strategy-inspired MNs

Nature has developed numerous systems capable of substantially altering their structures and properties to adapt to their

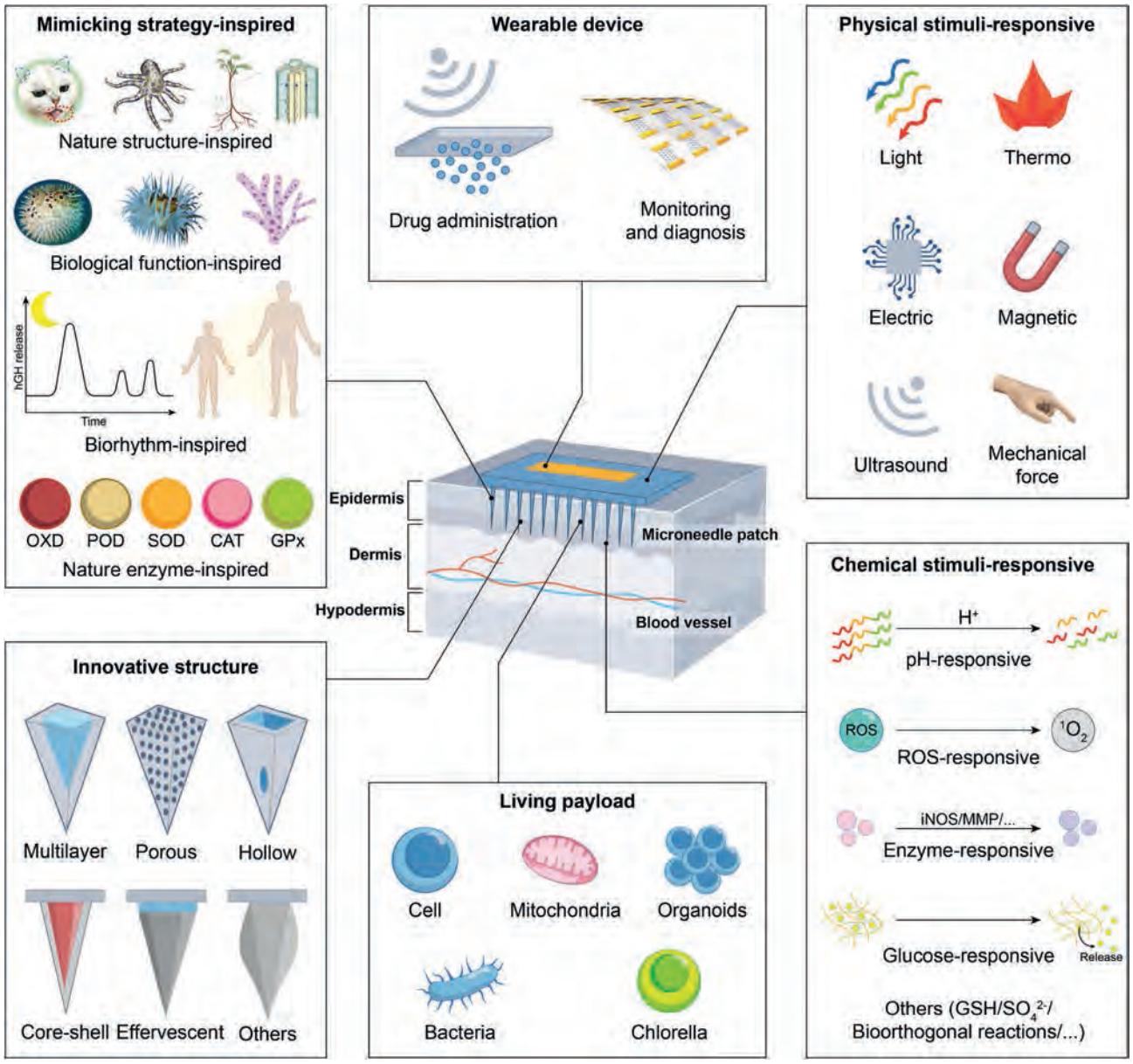

Figure 1 Cutting-edge advancements of intelligent MNs for biomedical applications in mimicking strategies, stimuli-responsive systems, innovative structural designs, living payloads, and wearable integration. Reproduced with permission from Refs. 1 and 32. Copyright © 2023, Springer Nature.

environment. Mimicking the behaviors of animals and the structure of plant organs provides an extraordinary strategy for achieving the needed functionalities[45]. Meanwhile, hierarchical designs and advanced techniques have been developed over the decades to fulfill unique functions[46,47]. Based on these facts, MNs that replicate the structures and biological functions seen in nature have been created. Briefly, these MNs exhibit the following extensive performance: (1) precise spatial localization; (2) enhanced tissue penetration; (3) substantial tissue adherence; (4) effective biomarker absorption. Therefore, nature-inspired MNs encompass a wide range of biomedical applications, including drug administration, tissue regeneration, biodetection, and biosensing[35]. This section comprehensively summarized their diverse biomedical applications. Moreover, the effectiveness of nature-inspired MNs in disease management and diagnostics was clarified. Table 1[16,48-56] and 2[30,57,58] summarized the characteristics and performances of nature-inspired MNs.

Administration time of therapeutics influences therapeutic efficacy and side effects. Adjusting release patterns to align drug concentrations with biological rhythms is essential for maximizing treatment outcoomes[2]. Nonetheless, most of the current delivery systems remain failures in mimicking biological rhythms[59]. Encouragingly, the biorhythm-inspired transdermal MNs with multistage drug release patterns can successfully replicate the normal rhythm of human biological processes. In the second part of this section, a detailed overview of the working principles of biorhythm-inspired MNs for disease treatment was provided. Briefly, these MNs typically consist of materials that encompass both fast-dissolving and slow-dissolving components. The multistage release of drugs loaded in MNs is successfully achieved

Table 1 Summary of nature structure-inspired MNs.

Inspirational source	Working principle	Images of MN	Therapeutic ingredients	Applications	Ref.
The anatomy of a snake's jaw	Once reaching the desired site, the grasper expands to envelop the heart and contracts to position the MNs. Subsequent to the automatic separation of the MNs from the grasper, the device is retracted, resulting in the MNs remaining in the heart.		Exosomes derived from mesenchymal stem cells	Myocardial infarction	16
Tongue prick of cat	Cat tongue prick bionic angle-adjustable MNs are created by angle transform molds to maintain a firm grip on the periwound skin.		Human epidermal growth factor	Wound healing	48
Beetle tentacles	Beetle tentacles structured MNs can realize layered efficacy and improve interaction between MNs and skin tissues.		Metformin	Chronic wound management and therapeutic diagnosis	49
Conical verrucous feet of sea cucumbers	MNs are created by rolling up the MN patch with the needle tips facing outward. This structure can penetrate the muscles and anchor MNs within the muscle.		Zinc oxide NPs	Peripheral nerve injury	50
Suction cup and mouth of blue-ringed octopus	The MNs are composed of cup-shaped suction cups and hydrogel needle tips, which provide wet bonding and puncture the mucus layer or soft barrier on the surface of the tissue, respectively.		Dexamethasone	Oral ulcer and melanoma	51
Xylem vessel structure of wood	MNs have anisotropic pores, possessing superior liquid-absorption capacity.		gamma delta T cells	Xenograft melanoma and pleural mesothelioma	52
The periodic bump structure of the small intestinal villi	The base-layer of MNs exhibits an intestinal villi-like interface, with tips uniformly distributed on it, providing a deep sample collection and promising molecular transfer.	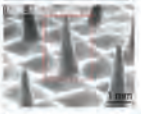	Gentamicin	Mucosal-related diseases	53
The structure of tumbler	MNs possess hollow shell and low center of gravity, and can achieve fast self-oriented when exposure to the mucosa.	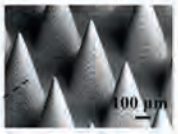	/	Chronic inflammation and cancer of the colon	54
Teeth of shark	MNs are feature of flat and inclined structures, enabling MN patch to penetrate into skin easily and maintain stable adhesion during the long-term recovery process of chronic wounds.		Human epidermal growth factor	Wound healing	55
Feet or stings of ladybugs, gadflies, and wasps	MNs exhibit pagoda-like multilayer structure, which enables strong fix onto diverse tissues *via* physical interlocking and is not affected by large blood loss or other conditions.		Dodecyl-modified chitosan	Hemostasis	56

by adjusting the types and ratios of needle tip materials, thereby simulating biological rhythms. Considering that the majority of hormone medications exhibit rhythm-controlled secretion patterns, these rhythm-inspired MNs provide an effective approach to enhance the advancement of chronopharmacological research.

Enzyme catalysis is a crucial mechanism that supports essential biological processes, such as metabolic regulation, cellular signal transduction, and energy transformation. However, the commercial utilization of enzymes faces technological obstacles, including purification problems, stability drawbacks, high production costs, and restricted modifiability[60]. Surprisingly, Chinese scientists developed a new category of artificial enzymes in 2007, known as nanozymes, which mimic the biological functions of natural enzymes such as peroxidase (POD), oxidase (OXD), and superoxide dismutase (SOD)[61,62]. These nanozymes exhibit biocatalytic properties and can catalyze substrates of natural enzymes *via* specific nanostructures. The desire for nanozymes arises from their unique attributes in comparison to natural enzymes, such as improved catalytic efficiency, increased stability, intrinsic targeting abilities, straightforward modification, and scalable manufacture[63]. Moreover, they can be effectively incorporated with chemotherapy, radiation, phototherapy, and immunotherapy, highlighting the great potential of nanozymes in disease management[64,65]. Over the past decade, applications of nanozymes have encompassed environmental monitoring, industrial catalysis, food safety assessment, biosensing, disease diagnostics and

Table 2 Summary of biological function-inspired MNs.

Inspirational source	Working principle	Images of MN	Therapeutic ingredients	Applications	Ref.
The active predatory behavior of sea anemones through pressure differentials.	MNs have large swelling ratio, showing osmotic pressure characteristic, and can rapidly absorb ISF within 5 min.		/	Ultrarapid sampling and quantum sensing of melanoma-related miRNA	30
Porcupinefish can expand rapidly by imbibing water when threatened.	MNs can rapidly inflate in volume and stick out drug-loaded MNs toward the intestinal wall, leverage the peristaltic force to penetrate the intestine mucus layer and deliver therapeutics.		Insulin	Oral administration	57
Soft coral polyps, which protrude from the openings of coral reefs to feed in the ocean, can shield themselves from the elements by retracting inside the coral reefs.	MNs possess an equally sized porous shell and cavity with functional hydrogel filling in. MN tips absorb exudate to indicate whether anti-infection is needed. Once a positive chronic infection is identified, MNs will activate and release drugs rapidly.	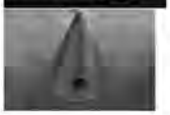	Minocycline hydrochloride	Wound healing	58

therapy, further demonstrating their extensive utility and raising progress in these fields. Generally, nanozymes are modified to facilitate medicinal purposes, including cancer treatment, inflammation management, and wound healing. To optimize the efficacy of nanozymes, a suitable loading platform, which facilitates the stable retention and accurate administration of nanozymes to the damaged tissue, permitting controlled release at designated sites, is essential[66-68]. Encouragingly, MNs can serve as creative vehicles for nanozyme delivery because the combination of nanozymes and MNs establishes a responsive and cascade drug releasing platform that results in a more favorable treatment effect than monotherapy[69]. This section offers a full overview of the applications of nanozymes-integrated MN systems in the treatment of tumors, wound healing, keratitis, periodontitis, endometrial damage, and hair loss. The information has been summarized in Table 3[70-82].

2.1. Nature structure- and biological function-inspired MNs

2.1.1. Nature structure-inspired MNs

MNs inspired by biological structures with superior mechanical qualities are widely employed not only in skin wound healing but also in the treatment of deep organ disorders such as muscle atrophy, nerve regeneration, and MI. For instance, the different phases of wound healing have specific needs, with tension playing a crucial role in enhancing the healing process and minimizing hypertrophic scar development[83]. Motivated by the cat tongue prick, Gan et al.[48] designed tongue prick bionic angel-adjustable

Table 3 Summary of nature enzyme-inspired MNs.

Classification	Matter	Nanozymes in MN	Working principle	Mimicking of nature enzyme activity	Biomedical application	Ref.
Non-noble metal	Fe-based	Fe_3O_4@GO	Induce H_2O_2 to produce highly toxic ·OH	POD	Wound healing	70
		Fe		POD	Keratitis	71
	Cu-based	CuS		OXD	Wound healing	72
				OXD	Periodontitis	73
	Fe/Cu-based	Fe/Cu MOFs		POD	Wound healing	74
	Mn-based	PDA-MnO_2	Scavenge excessive ROS	SOD, CAT	Wound healing	75
		MnOx/GDY		OXD, POD, CAT, SOD	Keratitis	76
	Mo-based	Au@MoS_2	Induce H_2O_2 to produce highly toxic ·OH, deplete the overexpressed GSH	POD, GSHOx	Melanoma	77
Noble metal	Ru-based	PtRu/C_3N_5	Directly convert oxygen molecules around infected sites into ROS.	OXD	Wound healing	78
	Pd-based	CuGQD/PdNPs@PSi	Induce H_2O_2 to produce highly toxic ·OH	POD	Melanoma	79
Rare earth	Ce-based	CeO_2	Scavenge excessive ROS	POD, SOD, CAT	Androgenetic alopecia	80
					Endometrial repair	81
Metal-free	Se-based	Se	Scavenge excessive free radical	POD, SOD	Androgenetic alopecia	82

MNs (TPMNs) for scarless healing (Fig. 2A). Cat tongue pricks possessed a hooked morphology with a U-shaped cavity rather than conventional conical morphologies, providing enhanced gripping and frictional characteristics similar to small tools. Their findings demonstrated that MNs with greater angles displayed enhanced frictional contact performance and increased gripping force, facilitating more secure attachment and extended stable contact in dynamic situations. Moreover, Liu et al.[49] designed a bilayer, tree-shaped, rivet-like hydrogel electroactive MN platform (GP-MN) with an AgNWs-doped gelatin methacryloyl (GelMA) composite hydrogel substrate, adjustable polyvinyl alcohol (PVA) hydrogel tip, and metformin-loaded anti-glycosidic drug (Fig. 2B). GP-MN had a unique double-layer structure that resembled the tentacle structure of elateridae beetles. Meanwhile, the GP-MN had a barb-like microstructure similar to a tree-rivet structure, which allowed mechanically interlock with the skin and firmly cling. Mechanical tests demonstrated that GP-MN had a mechanical strength of 11.0 N, which was much higher than single-layer MN, allowing for deep penetration and smooth subcutaneous drug release. Furthermore, Guo and coworkers[55] discovered that the flat and angled configurations of shark teeth facilitated a firm grip on prey. By replicating these specialized structures, the designed MNs effortlessly infiltrated the skin and sustained solid adherence during the prolonged recovery phase of chronic wounds (Fig. 2C). In addition, inspired by the anatomical structure and physiological properties of sea cucumbers, Fan's group[50] employed micro/nano-manufacturing and three-dimensional (3D) printing technologies to construct MN nerve guidance conduits (MNGCs) (Fig. 2D). The outside layer of MNGCs was mostly made up of a bunch of MN tips, and the inner layer was made up of microchannel guiding structures. This construction allowed exposed needle tips to reach the muscles governed by the nerve defect and deliver electrical stimulation to the muscles, thus attaining the effect of reducing muscular atrophy, and also firmly secured the MNGCs into the muscle, fixing nerve ends and preventing detachment during movement. Moreover, the snake's jaw is distinctively structured with the quadrate bone articulated to the skull instead of being permanently affixed (Fig. 2E(i))[16]. This unique articulation permitted the lower jaws to function independently, granting the snake remarkable flexibility in mouth opening. Inspired by this architecture, researchers created a MN implantation platform that combined MNs with a kidney stone extraction device. The grasper of this device was outfitted with MNs, organized in rows of eight, totaling 24 needles, and infused with medicines (Fig. 2E(ii)). Once reaching designated site, the grasper opened to firmly envelop the heart tissue and subsequently shut to accurately implant the MNs. The mechanical tests of MNs demonstrated that these devices provided adequate mechanical force for myocardial insertion, exceeding 0.2 N/needle. After piercing the tissue, the hyaluronic acid (HA) needle tip was retained within the damaged myocardial tissue, thereby providing a sustained release of therapeutic exosomes (Fig. 2E(iii)). This snakebite-inspired MN device offered a minimally invasive option for internal organ disorders.

For cutaneous, mucosal, or splanchnic disease treatment, ensuring adhesion in physiological fluids is as crucial as overcoming biological barriers. Improving the adherence of drugs reduces drug loss and breaks mucus or exudate barriers obstructing access to the target area. Moreover, improved adhesion facilitates swift initiation and sustained maintenance therapy, which is essential in various contexts, including anti-inflammatory, anti-anginal, and anticancer treatments[84]. Bio-structure inspired MNs offer a solution that demonstrates exceptional capabilities to address clinical requirements for intratissue topical medicine. A wet-bonding MN, silk fibroin-pluronic F127 (Silk-Fp)-poly(*N*-isopropylacrylamide) (PNIPAm)-based, inspired by the predatory behavior of the blue-ringed octopus, was developed by Zhu et al.[51] for tissue surface adherence and efficient topical drug delivery (Fig. 2F). Specifically, Silk-Fp-based hydrogel suction plates, which interior surface was altered with tannic acid, were produced to facilitate a biocompatible chemical adhesion. In addition, the adaptable cup-like structure enabled physical adhesion through the differential air pressure while simultaneously safeguarding the internal chemical bonding contact from the liquid environment. As a result, the Silk-Fp adhered to the wet tissue and maintained stability for several days due to its physical and chemical bonding capabilities. These patches enhanced the healing rate of oral ulcers *via* the release of dexamethasone sodium phosphate and significantly inhibited tumor growth when infused with 5-fluorouracil. Regarding disease treatments, mucosa-interfacing devices derived from bioinspired engineering design have demonstrated significant potential for monitoring infectious mucosal disorders[85]. Conventional swabs utilized for the detection of mucosal diseases (*e.g.*, oral, throat, and nasal swabs) encounter several limitations, including inadequate deep biomarker collection, the potential for false negatives, and unwanted mechanical damage. To address these concerns, a trigonometric function-based periodic pattern was developed and integrated into the base layer of the MNs (IMBEMs) (Fig. 2G(i))[53]. This special shape was inspired by the multilayered villus architecture of the small intestine, which facilitates significant nutritional absorption, potentially due to the multilevel molecular exchange enabled by the periodic protuberances of the intestinal villi. The foundational layer of manufactured MNs displayed an intestinal villi-like interface, which was 20% larger than the flat base, enhancing substance exchange and adherence through increased interfacial regions (Fig. 2G(ii)). Additionally, the sharp MN tip (length/radius = 8:1) significantly enhanced the deep-site biomarker capture on a variety of surfaces. Specifically, the *in vivo* sample collection test included by *Escherichia coli* inoculation on Sprague−Dawley rat skin demonstrated that the colony-forming unit counts of *Escherichia coli* obtained from IMBEMs were much greater than those from other groups, indicating the superior enrichment effectiveness of the IMBEMs. Consequently, induced by the large surface of the base layer and sharp tips of MNs, the IMBEMs concurrently facilitated both biomarker enrichment (from mucosa to device) and medication delivery (from device to mucosa). In addition, drawing inspiration from the hierarchical architecture of insect feet or stings, Zhang et al.[56] developed a dodecyl-modified chitosan-coated, pagoda-like multilayered MN for tissue fixation and expedited hemostasis. The unique multilayer architecture allows the MN to securely adhere to various tissues through physical interlocking, remaining unaffected by significant blood loss or other circumstances. Consequently, acute tissue injuries such as hepatic hemorrhage, splenic hemorrhage, and renal hemorrhage could be promptly addressed with the application of these multilayer MNs.

In addition to animals, plants and inanimate items can also serve as inspiration for the structure and functioning of MNs. For instance, the wood xylem's anisotropic hierarchical porous structures, which have sizes ranging from tens to hundreds of micrometers, offer channels for the quick capillary force transport of water and nutrients. Researchers created an MN with anisotropic pores (APC-MNs) after being inspired by this property

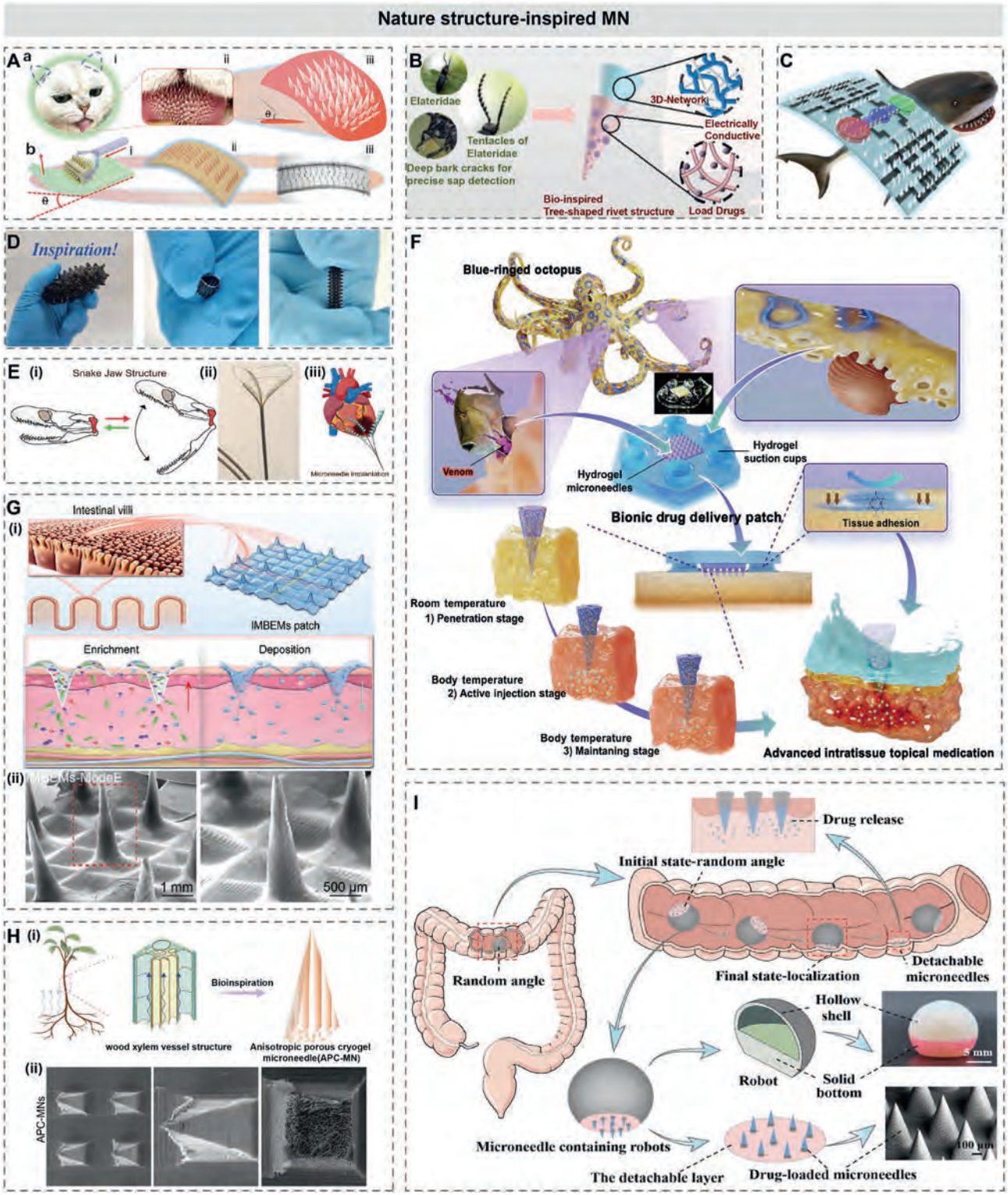

Figure 2 Nature structure-inspired MNs for biomedical applications. (A) Schematic illustration of cat tongue biomimetic inspired MNs. Reproduced with permission from Ref. 48. Copyright © 2025, Wiley. (B) Schematic illustration of insects' special structure-inspired GP-eMN system. Reproduced with permission from Ref. 49. Copyright © 2025, Elsevier. (C) Schematic illustration of shark tooth-inspired MNs. Reproduced with permission from Ref. 55. Copyright © 2021, American Chemical Society. (D) Schematic illustration of sea cucumbers-inspired MNs. Reproduced with permission from Ref. 50. Copyright © 2024, American Chemical Society. (E) Schematic illustration of snakebite inspired MN delivery system for internal organs. Reproduced with permission from Ref. 16. Copyright © 2025, Elsevier. (F) Schematic illustration of blue-ringed octopus-inspired drug delivery MNs. Reproduced with permission from Ref. 51. Copyright © 2023, American Association for the Advancement of Science. (G) Schematic illustration of intestinal villi-inspired mathematically base-layer engineered MNs. Reproduced with

(Fig. 2H)[52]. APC-MNs outperformed isotropic porous MNs in terms of liquid absorption. Thus, these MNs worked well to remove tears from the sensitive area of the eye. Furthermore, this unique shape enabled APC-MNs to load fragile and large-sized pharmaceuticals (*e.g.*, lipid NPs and cells) directly into tips *via* capillary force, without the use of any equipment. Upon treatment with therapeutic gamma delta T cell-loaded APC-MNs, the survival time of melanoma and pleural mesothelioma solid tumor mice was extended for a period of 2 days. In Huang et al.[54] study, in order to achieve precise mucosal drug delivery without the involvement of external fields such as electric and magnetic fields, they developed a millisecond self-oriented MN-containing robot for colonic administration. This robot was inspired by the tumbler that self-rights when shoved over. As illustrated in Fig. 2I, MN-integrated robots were designed with a hollow shell and a low center of gravity. Specifically, the robot's solid bottom bore a large chunk of its weight, causing the center of gravity to shift downward, which increased the robot's stability and made it less susceptible to being pulled down by intestinal peristalsis. Needle tips that were affixed to the robot's solid bottom allowed them to be oriented vertically to the mucosa. The self-orientation capabilities of MN-equipped robots in *ex vivo* swine colon tissue indicated that the self-orientation time of robots on the horizontal mucosa was 1.2 s, while the self-orientation period on a 90° slope was within 0.35 s. Overall, the tumbler structure-inspired MN robots possessed exceptional self-orientation capabilities and potentially resistant to colonic peristalsis, making them a promising candidate for colonic administration systems.

2.1.2. *Biological function-inspired MNs*

The biological processes of animals in nature can drive the design of MNs, endowing them with diverse and distinctive functionalities. For example, porcupinefish swiftly enlarge themselves by absorbing water when they are in danger (Fig. 3A(a, b)). During this process, rigid and tapering spines along the fish's body turn erect, which facilitates the impaling of predators during ingestion. An expandable MN device inspired by porcupinefish, capable of quickly inflating and deploying drug-loaded MNs towards the intestinal wall, could utilize peristaltic force during peristalsis to pierce the intestinal mucus layer and thus administer biologic drugs. Meanwhile, researchers found that specific stinging organisms developed projecting barbs on their spines to improve adherence to tissues post-penetration. This unique structure inspired a barbed MN design that can detach from the MN array and remain in tissues for sustained drug release. Gao et al.[57] developed an MN robot that expanded into a large spiny vesicle in ISFs and injected the MNs into the mucosa during peristaltic contractions for addressing medication absorption challenges and the difficult oral delivery of biologic pharmaceuticals (Fig. 3A(f)). The MNs were equipped with drug-loaded barbs, which could be separated from the microrobotic body and stranded into the mucosa during peristaltic relaxation to facilitate drug release. Specifically, the MN robot was composed of three primary components: (i) drug-loaded barbed needles that were designed to penetrate the mucosa and retain the drug for sustained release (spines, Fig. 3A(c)), (ii) a stretchable basal membrane that was designed to load the MNs and resist continuous peristaltic contraction (skin, Fig. 3A(d)), and (iii) superabsorbent hydrogel particles that provided swelling stress to balance the membrane tension and inflated the device (water in the belly, Fig. 3A(e)). Under dry circumstances, the single MN robot could be encased within a commercial 00# enteric capsule, which preserves its integrity against acidic gastric juices and facilitates its release in the intestine (Fig. 3A(g)). Upon exposure to ISFs, the MN robot rapidly swelled to a predetermined size, while the stretched membrane was tensioned to support the spines broadened towards the luminal wall (Fig. 3A(h)). Relying on the volumetric impact of the microrobots, rhythmic intestinal peristaltic contractions forced the MNs into the mucosa, whereas the relaxation phase detached the barb-equipped, drug-loaded tips from the MN robot, securing the drug-laden barbs within the intestinal wall. The *in vivo* drug delivery evaluations in minipigs confirmed that a rapid hypoglycemic effect was achieved within 60 min, and the oral bioavailability increased to 23.6% during a 4 h observation period, which significantly surpassed the approximately 1% bioavailability noted in existing oral administration of biologic drugs. Unlike the documented spring/balloon-launched or field-controlled actuation mechanisms, the porcupinefish-inspired MN device operated *via* mass transport (absorbing ISFs) and intrinsic intestinal peristalsis, necessitating neither pre-stored energy nor real-time external energy input to administer drugs into the luminal wall. The mimicking strategy of natural organisms' functions significantly influenced the design of this entire system. Similarly, Liu et al.[58] created a biomimetic MN (HepMi-PCL) that emulated the aquatic behavior of coral polyps residing in porous reefs to detect and cure infections in wounds (Fig. 3B). Soft coral polyps, which emerge from coral reef openings to feed in the water, can protect themselves from the environment by withdrawing into the reefs. Inspired by this function, researchers initially reproduced the resilient architecture of coral reefs using polycaprolactone (PCL) MNs to guarantee adequate strength and puncturing ability. Subsequently, they incorporated a heparin composite hydrogel (Hep) inside the PCL MNs to replicate the soft coral polyps found in the reef. Additionally, a pH-induced colorimetric reaction utilizing phenol red was concurrently included into the Hep, endowing the MNs with diagnostic and visualization functions for infections. Moreover, emulating reversible drying−wetting capabilities, hydrochloride encapsulated in Hep was administered into the wound. The bionic MN technology demonstrated a self-regulating medication release behavior for infection treatment, correlating with the swift indication of infection levels *via* the hydrogel's upper surface. This biomimetic MN provided a creative strategy for the diagnosis and treatment of chronically infected wounds. In a separate study, researchers drew inspiration from the active predatory behavior of sea anemones. By immersing PVA/polyvinylpyrrolidone (PVA/PVP)-based MNs in LiCl, which serves as a super-swelling agent for hydrogel due to its hygroscopic characteristics, MNs were equipped with osmotic pressure, facilitating the rapid and efficient absorption of ISF (Fig. 3C)[30]. *Ex vivo* testing indicated that the MNs could readily penetrate the epidermis and stratum corneum, collecting 0.92 ± 0.14 mg of ISF within 5 min, thereby efficiently extracting miRNA. This MN,

permission from Ref. 53. Copyright © 2023, American Chemical Society. (H) Schematic illustration of the wood-xylem-like microstructure-inspired APC-MNs. Reproduced with permission from Ref. 52. Copyright © 2025, Elsevier. (I) Design and mechanism of the tumbler-inspired MN robots for colonic administration. Reproduced with permission from Ref. 54. Copyright © 2023, Wiley.

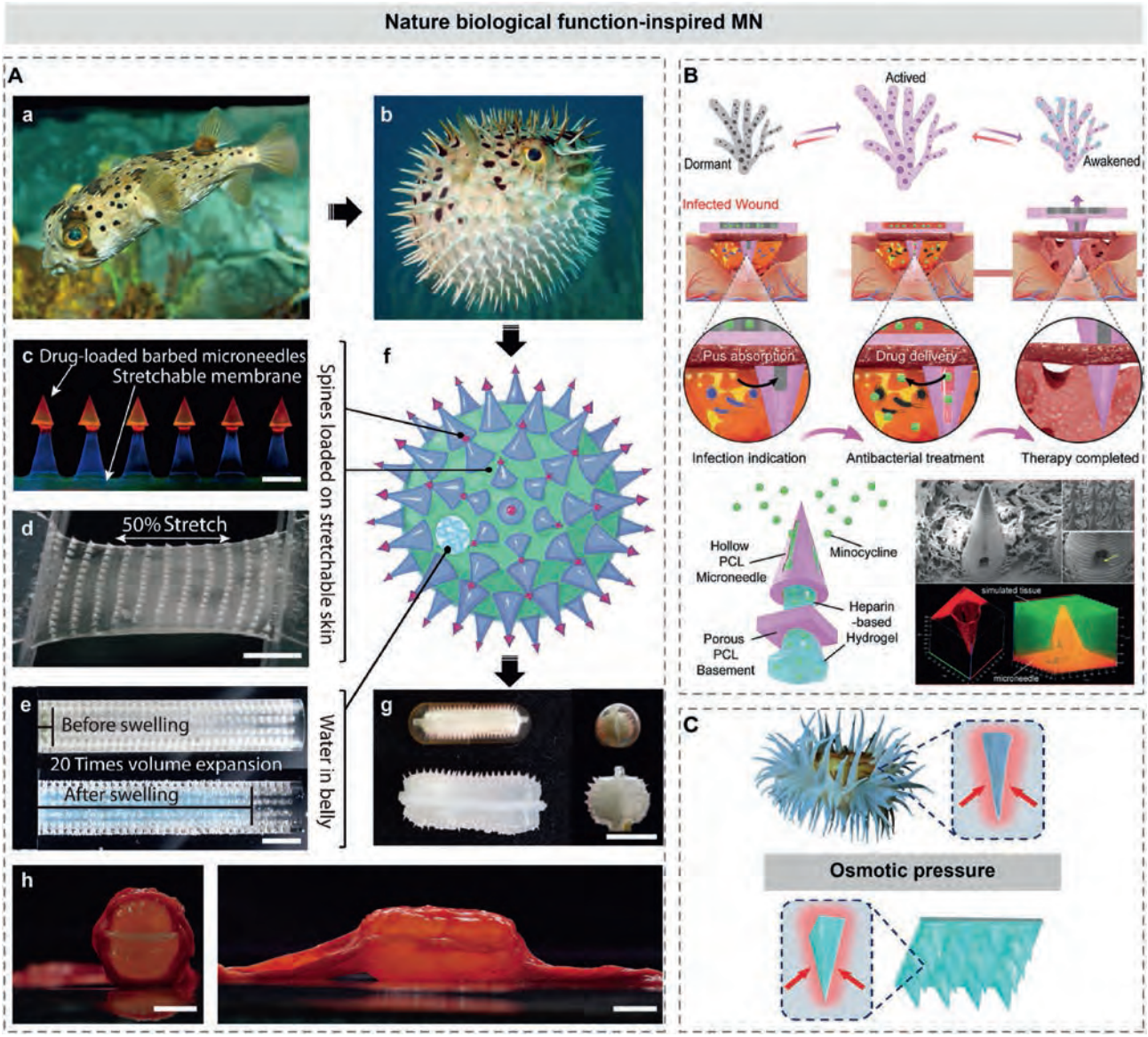

Figure 3 Nature biological function-inspired MNs for biomedical applications. (A) The porcupinefish function-inspired MN for pain-free oral delivery of biologic drugs. Reproduced with permission from Ref. 57. Copyright © 2024, American Association for the Advancement of Science. (B) Schematic illustration of coral-inspired hollow MN for wound infection treatment. Reproduced with permission from Ref. 58. Copyright © 2024, Wiley. (C) Schematic illustration of osmotic pressure-driven MN inspired by sea anemones. Reproduced with permission from Ref. 30. Copyright © 2025, Wiley.

inspired by an osmotic pressure-driven feeding mechanism, showed potential for detecting ISF biomarkers through quick sampling, signal amplification, and machine learning integration.

2.2. *Biorhythm-inspired MNs*

Life on Earth experiences significant environmental variations throughout a typical day, including alterations in light intensity, humidity, and temperature, along with the existence of natural predators and prey[86]. Thus, organisms have developed mechanisms to adapt to and foresee whole-day fluctuations in environmental conditions. In the human body, numerous physiological processes are governed by a 24 h cycle. For instance, remarkable correlations exist between altered circadian rhythms and conditions such as central nervous system illnesses, metabolic disorders, and cardiovascular diseases[87,88]. The drug delivery systems, which are engineered to mimic human circadian rhythms and normal physiological processes, demonstrate significant potential for disease management. For example, human growth hormone (hGH) facilitates longitudinal bone growth and is secreted in accordance with human circadian cycles. The secretion of hGH mainly occurs during the nocturnal hours and manifests in a pulsatile manner, characterized by three distinct pulses throughout the night. Administering GH in pulsed was more effective than continuous administration in accelerating development in mice. Inspired by the overnight pulsatile secretion properties of hGH, Gu's group[2] designed a biorhythm-inspired GH transdermal MN system (BRIGHT) (Fig. 4A(i)). By integrating

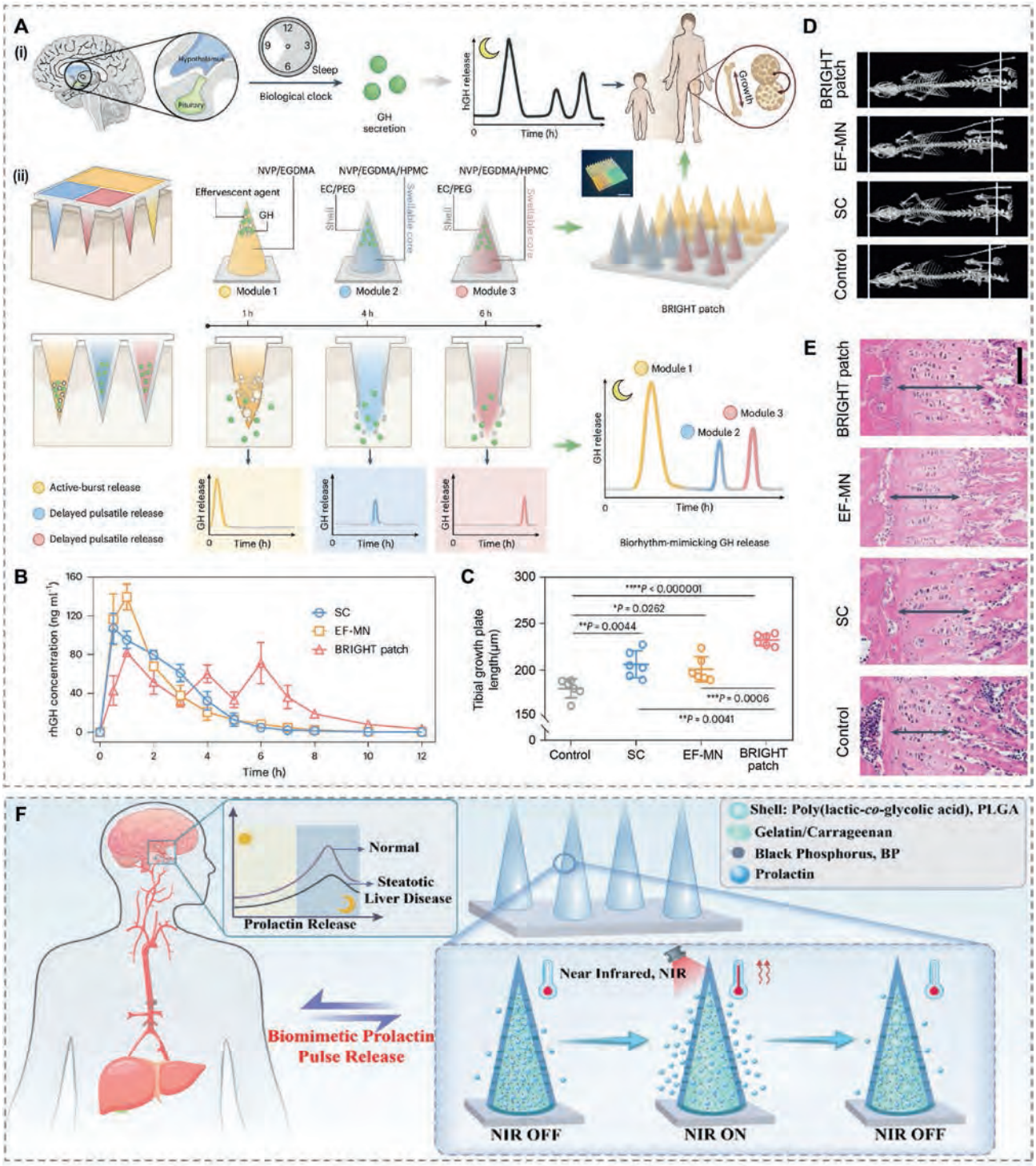

Figure 4 Scheme and therapeutic effects of biorhythm-inspired MNs. (A) Scheme of the BRIGHT. Reproduced with permission from Ref. 2. Copyright © 2025, Springer Nature. (B) Pharmacokinetic profiles of rhGH in rat plasma following several injection routes, including SC, EF-MN, and BRIGHT ($n = 5$). Reproduced with permission from Ref. 2. Copyright © 2025, Springer Nature. (C) Statistical width measurements of the tibial growth plate ($n = 6$). Reproduced with permission from Ref. 2. Copyright © 2025, Springer Nature. (D) Representative X-ray micro-CT images of rats subjected to various administering routes. Reproduced with permission from Ref. 2. Copyright © 2025, Springer Nature. (E) Representative H&E staining slices of the tibial growth plate. Scale bar = 100 μm. Reproduced with permission from Ref. 2. Copyright © 2025, Springer Nature. (F) Designs of the NIR-responsive core−shell MN and its utilization for the treatment of steatotic liver disease. Reproduced with permission from Ref. 90. Copyright © 2025, Wiley.

one "burst-release" module and two "delayed-release" modules, the system could be proposed to autonomously accomplish a time-programmed three-stage drug release, thereby enhancing the growth-promoting effect by mimicking the rhythm of hGH secretion. Specifically, module 1 was prepared from a recombinant human growth hormone (rhGH)-preloaded monomer mixture of *N*-vinylpyrrolidone, ethylene glycol dimethacrylate, and effervescent agent, and subsequently fabricated into UV-crosslinked MNs by *in situ* photopolymerization at 4 °C. Modules 2 and 3 were composed of a core−shell architecture. The MN core comprised a swellable polymeric matrix of hydroxypropyl methyl cellulose, a medical swelling agent, whereas the MN shell was an insoluble structure made of ethylcellulose combined with porogens, specifically polyethylene glycol (PEG). The BRIGHT, with biorhythm-mimicking release behaviors, was manufactured by assembling the three modules into a single patch (Fig. 4A(ii)). Upon immersion of the MNs in phosphate-buffered saline (PBS), a significant quantity of carbon dioxide (CO_2) bubbles from module 1 was rapidly produced, facilitating the release of rhGH due to the rapid disintegration reactions between anhydrous citric acid and sodium bicarbonate. In contrast, modules 2 and 3 comprised MNs featuring a swellable core and a water-insoluble shell, facilitating their optimal delayed-release duration. The pharmacokinetic characteristics of rhGH in rats following subcutaneous injection of rhGH solutions (the SC group), rhGH-loaded effervescent MN (EF-MN), and rhGH-loaded BRIGHT treatments were assessed. Distinctively, in comparison to the SC group and the rhGH-loaded EF-MN group, the rhGH-loaded BRIGHT treatments exhibited a tri-phasic pulsatile release of rhGH, thereby demonstrating their efficacy in replicating a biorhythmic release pattern (Fig. 4B). The biological efficacy in healthy Sprague−Dawley rats showed that the BRIGHT particularly enhanced growth in bone development (Fig. 4C−E). In summary, the BRIGHT facilitated bone formation without disrupting sleep, indicating its potential as a clinically viable technology for achieving circadian-rhythm-mimicking medication release.

Prolactin is recognized for its metabolic protective role in sustaining liver lipid metabolism balance in humans. Similar to the rhGH, prolactin secretion by the pituitary gland follows circadian rhythm[89]. Consequently, motivated by this observation, Yin and colleagues[90] developed a new biomimetic hormone delivery system that incorporated prolactin into intelligent MNs to facilitate fatty liver therapy *via* pulsatile prolactin release. They designed an innovative photothermal-responsive core−shell MN to impede fatty liver development (Fig. 4F). Core−shell structure MNs were manufactured using a repeating mold replication approach, with a shell composed of poly(lactic-*co*-glycolic acid) (PLGA) and a prolactin-loaded core consisting of photothermal agent black phosphorus, phase-change gelatin, and carrageenan. The PLGA shell provided the MNs with sufficient mechanical strength for skin penetration and enabled drug release. By activating the MNs with near-infrared (NIR) light, the black phosphorus in the core absorbed and converted NIR into thermal energy, resulting in a reversible phase transition of gelatin/carrageenan and the release of prolactin[91]. It was established that periodic NIR irradiation induced the cyclic release of prolactin, hence reducing fat buildup in liver cells. The results suggested that photothermal-responsive core−shell MNs with prolactin pulse release could serve as an effective strategy for metabolic dysfunction-associated steatotic liver disease (MASLD) treatment. To date, MN-mediated human circadian rhythms mimicking strategy for disorders regulation has exhibited distinct advantages and considerable developmental potential.

2.3. *Natural enzyme-inspired MNs*

Nanozymes are nanomaterials with enzyme-like characteristics that have been extensively employed in biosensing, bioimaging, antibacterial applications, antioxidation, diseases treatments and environmental protection[92-94]. The nanozymes exhibit catalytic capabilities analogous to POD, catalase (CAT), SOD, glucose oxidase (GOx), and glutathione peroxidase (GPx), as indicated by their enzymatic characteristics[36]. A variety of materials, including metal-based (Ti, V, Cr, Mn, Fe, Co, Ni, Cu, Zn, Zr, Mo, Ru, Rh, Pd, Ag, Cd, Sn, Sb, Ce, Hf, Pt, Au, Bi), metal-free (C, B, Se), as well as their compounds and hybrids, have been utilized to create an array of remarkable nanozymes[95]. They are subsequently encapsulated within MN tips to improve distribution efficiency. To date, the amalgamation of MNs and nanozymes has demonstrated significant therapeutic efficacy in tumor management and bacterial control, tissue regeneration, and inflammatory modulation (Fig. 5).

Melanoma is the predominant malignant skin cancer, distinguished by its complexities, invasiveness, and heterogeneity. Traditional therapy frequently has suboptimal results, presenting considerable clinical difficulties[96,97]. Duan et al.[77] created a MN that combined nanozyme and traditional Chinese medicine for a ferroptosis pathway-dependent therapeutic approach to melanoma. A novel Au@MoS_2 bimetallic plasmonic nanozyme (BPNzyme) was synthesized using a straightforward aqueous method comprising a two-step approach to enhance therapeutic efficacy. This rationally designed BPNzyme, influenced by the synergy of heterostructures, demonstrated an NIR photothermal effect, POD-like activity, and GPx-like properties, which successfully altered the tumor microenvironment (TME) and disrupted redox homeostasis. *In vivo* investigations indicated that the transdermal administration of BPNzyme and TCM β-elemene (β-ELE) *via* a water-soluble HA MN efficiently achieved 99.8% tumor growth inhibition without notable systemic effects. Similarly, in the study by Zhao et al.[79], MN incorporating porous silicon (PSi) infused with dual nanozymes was developed to bidirectionally modulate the TME and precisely administer nanocomplexes to induce ferroptosis for melanoma therapy. The copper-doped graphene quantum dots and palladium NPs co-loaded on PSi (CuGQD/PdNPs@PSi) leveraged the channel confinement effect of PSi, demonstrating a synergistic enhancement in POD and GPx activities, which were approximately 2−3 times higher than those of either monoconfined or nonconfined nanozyme complexes. The incorporation of nanozymes into MNs for delivery achieved a melanoma growth suppression of 98.8% within 14 days. Consequently, MNs encapsulated with CuGQD/PdNPs@PSi offered a promising nanocatalytic approach for triggering ferroptosis in tumor therapy while also addressing the medical requirement of eliminating surface tumors.

Besides the management of malignant melanoma, nanozymes exhibit considerable promise in fighting against bacterial infections. Researchers have reported a diagnostic and therapeutic MN that incorporated the Res@PtZ-Z nanozyme hybrid[98]. Res@PtZ-Z was made up of a zeolitic imidazolate framework (ZIF) shell containing the natural chemical resveratrol (Res) and encapsulating a Pt-doped zinc oxide (ZnO) nanozyme core. The Res component regulated charge distribution on the ZIF shell and

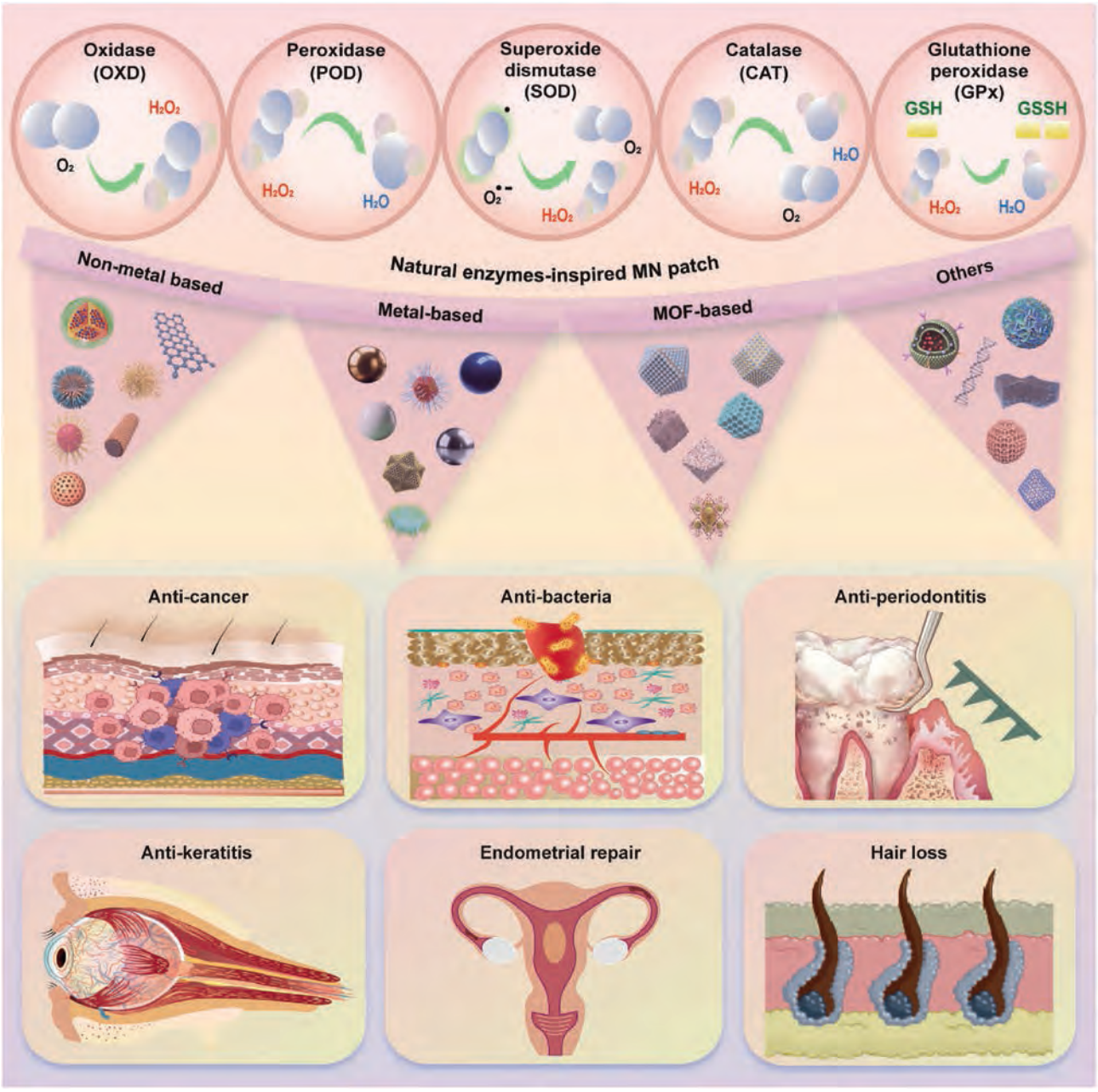

Figure 5 Mechanisms of natural enzyme-inspired MNs and their biomedical applications.

diminished bacterial pathogenicity, hence enhancing the uptake of Res@PtZ-Z by host cells. The PtZ core, infused with Pt^{4+} to create sublattice distortion in ZnO, demonstrated OXD-like, POD-like, and CAT-like activity. Under intracellular hypoxic conditions, the sequence of these enzyme-like actions guaranteed a continuous production of ROS, facilitating strong antibacterial effects. The combined strategy of MNs and nanozymes effectively targeted both the invasion and intracellular persistence of methicillin-resistant *Staphylococcus aureus* (MRSA), enhancing infection management and facilitating wound healing. Besides, a micro-sized ferroferric oxide (Fe_3O_4)/MXene (FM) heterojunction was employed to enhance the healing of diabetic wounds by scavenging extracellular ROS through the CAT-like and SOD-like nanozyme activities[99]. These Fe_3O_4 NP-based pH-sensitive nanozymes could eliminate excessive ROS through CAT-like and SOD-like activities in neutral and mildly alkaline environments. In addition to metal-based nanozymes, Sun et al.[74] proposed an iron-copper bimetallic metal−organic framework (MOF) with POD-like enzymatic activity. They illustrated that Fe and Cu played essential roles in simulating various natural enzymes, displaying higher K_M and analogous V_{max} in comparison to the kinetic parameters of the other POD-like nanozymes. Consequently, Fe−Cu bimetallic metal and MOFs were integrated into hyaluronic acid methacrylic acid (HAMA) MNs to produce MOF-based MN (MOF-MN). When applied to *Staphylococcus aureus* (*S. aureus*)-infected wounds, MOF-MN successfully penetrated the protective biofilm layer and wound exudates, delivering MOFs directly to the infected wound tissues, indicating improved antibacterial

effectiveness. In conclusion, this research emphasized the strengthened antibacterial efficacy and wound-healing capabilities of MOF-MN. Furthermore, ceria nanozymes (CeO_2), copper sulfide nanoenzyme (CuS NE), nanoscale MnO_2, ultrasmall platinum−ruthenium nanoalloys-integrated porous graphitic carbon nitride C_3N_5 nanosheets ($PtRu/C_3N_5$), and manganese oxide nanocluster-decorated graphdiyne nanosheets (MnO_x/GDY) have demonstrated exceptional enzyme-mimicking activity when integrated into MNs, thereby exhibiting remarkable efficacy against refractory bacterial biofilm infections[70,72,73,78,100]. For example, MnO_x/GDY were engineered as multienzyme-like nanozymes and incorporated into HA and polymethyl methacrylate-based ocular MN (MGMN) for the treatment of infectious keratitis[73]. Chen et al.[76] presented a novel therapy strategy for periodontitis utilizing a synergistic CuS nanozyme-catalyzed phototherapeutic and chemodynamic sterilizing approach, along with an *in situ* delivery platform employing MNs.

MNs can directly administer substances through safe channels into the epidermal and dermal layers, where the majority of hair follicles (HFs) are located[101]. Moreover, it has been documented that mechanical stimulation can activate HF cycles, and the mechanical stimulation resulting from the application of MNs in the skin can cause neovascularization, enhance the expression of genes associated with hair development, and stimulate HF stem cells[102]. Androgenetic alopecia (AGA) is characterized by being chronic and progressive and is the most prevalent type of hair loss. Inadequate circulation and/or oxidative stress of the HF niche is the primary cause of AGA. The overproduced ROS induces the premature senescence of dermal papilla cells, hence inhibiting the transition from the telogen to anagen phase of HFs *via* androgen signaling and activation pathways[103]. The synergetic effect of nanozyme and MNs can mitigate HFs oxidative stress and enhance vascularization, hence improving the efficacy of AGA treatment. Gao's group[80] revealed that ceria nanozymes (CeNZs), exhibiting CAT and SOD mimic capabilities, could mitigate oxidative stress in AGA by scavenging excessive ROS. After combining with MNs (Ce-MNs), it not only addressed the low transdermal penetration efficiency of CeNZs but also improved patient compliance. This strategy facilitated a more rapid initiation of the telogen-to-anagen transition in HFs in comparison to minoxidil. Furthermore, contributing to potent antioxidant properties, Selenium (Se) nanozymes have attracted significant interest in hair regeneration. Specifically, ultra-small Se NPs were manufactured and incorporated into hypoxic extracellular vehicles (EVs) to form a Se−HEVs complex, which was then encapsulated within the astragalus polysaccharide MN (AMN)[82]. These MNs penetrated the epidermal barrier and transmitted Se−HEVs to the dermis, indicating antioxidative, pro-angiogenic, anti-inflammatory, and pro-hair growth properties.

3. Stimuli-responsive MNs

The progress of stimuli-responsive materials has resulted in a generation of stimuli-responsive drug delivery systems capable of responding to physical or chemical stimuli for on-demand drug release[104]. The incorporation of stimuli-responsive materials into MNs, along with their flexible structural design and localized drug delivery methods, enables a MN-based stimuli-responsive delivery system to demonstrate superior spatial, temporal, and dosage control attributes. This facilitates tailored, on-demand drug delivery systems (often referred to as "on/off")[105]. Physical stimuli encompass light, electricity, heat, magnetism, and mechanical forces, whilst chemical stimuli comprise pH, ROS, glucose, enzymes, and so on. Physical stimulus-responsive MNs provide remote-controlled drug delivery, enhancing therapeutic efficacy and reducing bodily toxicity. Chemical stimulus-responsive MNs provide independent regulation of medication release in reaction to fluctuating biochemical signals, facilitating a personalized treatment approach that is both efficient and tailored to specific requirements. Furthermore, the multilayered architecture of the skin at the MN application site enables intelligent MNs to leverage the needle tip design for precise cellular targeting across many skin layers, demonstrating spatiotemporal response properties[106]. This section specifically discusses the materials and response mechanisms of responsive MNs, as well as their latest advancements in disease treatment, diagnosis, and monitoring (Fig. 6).

3.1. *Physical stimuli-responsive MNs*

3.1.1. *Light-responsive MNs*

Light possesses advantageous characteristics, including non-invasiveness, high spatial resolution, and temporal control, making light-responsive MNs an appealing mechanism for developing on-demand drug delivery systems. Light-responsive MNs are fabricated through the incorporation of diverse photosensitive materials that react to certain wavelengths of light (*e.g.*, UV light, visible light, NIR light, etc.)[107]. They are mostly utilized for photothermal therapies (PTT) and photodynamic therapies (PDT)[108]. These systems are created by incorporating photosensitive metal or metal oxide NPs or photochromic agents into the MNs. Moreover, MNs infused with light-responsive materials can document information *via* distinct patterns created by the needle tips and the unique fluorescence released by fluorescent dyes. Han et al.[109] encapsulated a quantum dot (QD)-based NIR fluorescent dye within polymethyl methacrylate microparticles and subsequently integrated them into a PVA/PVP dissolvable MN (Fig. 7A). Upon insertion into the skin, this dye was deposited in the dermis and generated distinct NIR signals that correspond to a predetermined pattern associated with a specific set of information in response to the NIR imaging equipment. They developed a comprehensive on-patient medical record-keeping (OPMR) technology utilizing a fluorescent dye-integrated dissolvable MN (MNP) that administered encapsulated information into the skin to encode medical data. Moreover, Yin et al.[110] incorporated inorganic photosensitizer (PS) black phosphorus quantum dots (BPQDs) within a PVP-based dissolvable MN for the pre- and post-operative management of cancer through PTT and PDT (Fig. 7B). When subjected to an NIR laser, the released BPQDs transformed light energy into heat energy and increased ROS generation, resulting in significant PTT and PDT effects that induced tumor cell death and necrosis[111-113]. After integration with PVP-based MNs, BPQDs could be released rapidly and locally, thus triggering efficient tumor management. Likewise, Huang's group[114] self-assembled various hydrophobic PSs, including 2-(1-hexyloxyethyl)-2-divinyl-pyropheophorbide-a, chlorin e6, and zinc (II)-phthalocyanine, with CAT to construct homogenous and stable PS@CAT NPs. These nanostructures were incorporated into MNs, enabling minimally invasive, spatially tailored transdermal delivery. Lai et al.[115] devised a MN theranostic platform (Mn:C/G@MN) to eliminate stubborn bacterial biofilm infections by integrating a novel biophotonic probe

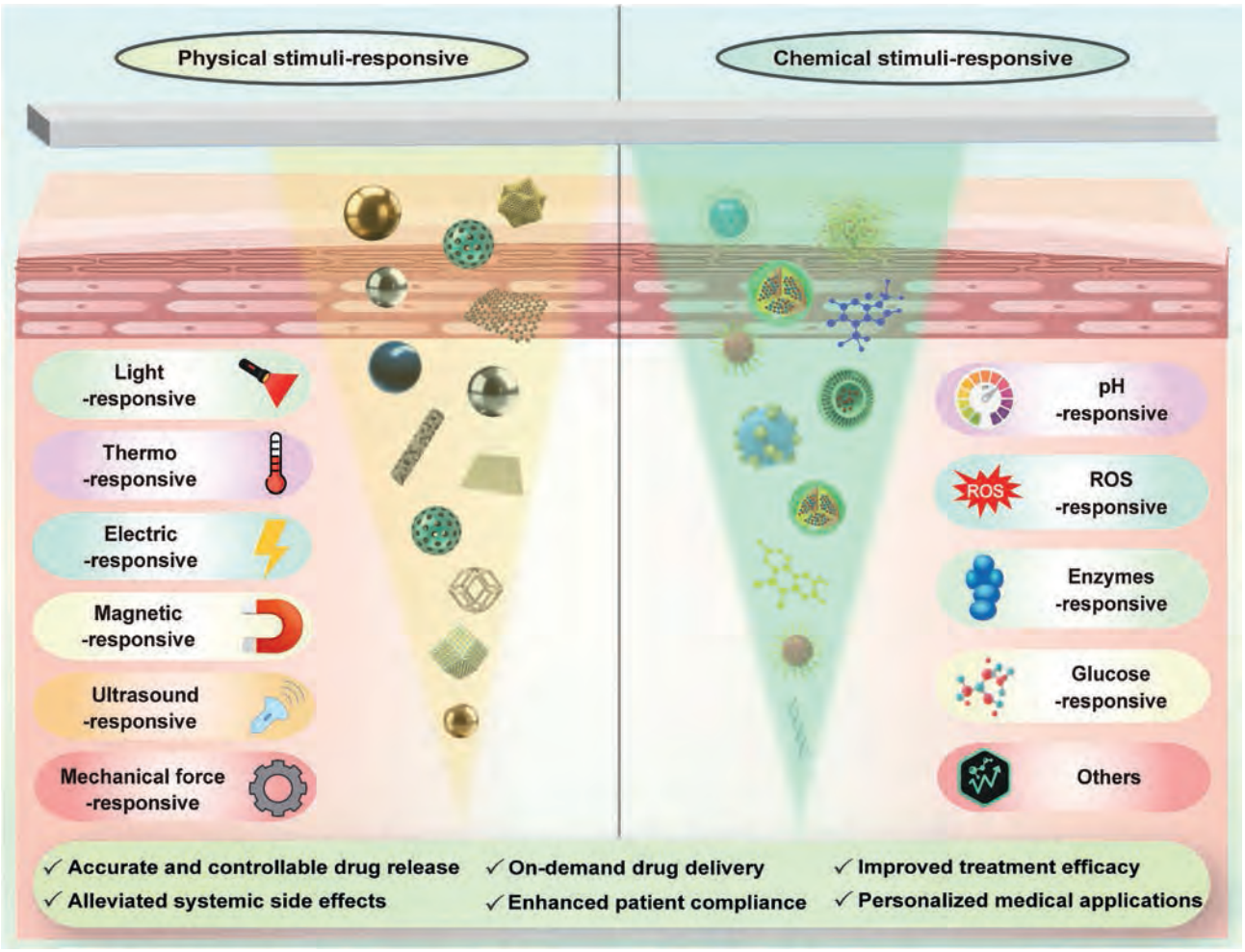

Figure 6 Scheme illustration of stimuli-responsive MNs and their biomedical benefits.

(manganese-doped carbon dots, Mn:CDs) within GelMA for the visual surveillance of biofilm infections and targeted phototherapy (Fig. 7C). The Mn:C/G@MN significantly eliminated biofilm on demand by harnessing the combined effects of localized hyperthermia and a hydroxyl radical (·OH) surge under 808 nm NIR exposure, facilitating the disruption of the extracellular polymeric substances matrix to disperse biofilms and subsequently eradicate detached bacteria. Both *in vitro* and *in vivo* evidence confirmed that the monitoring and treatment of biofilm infections was feasible. This study emphasized the efficacy of the synergy of MNs and phototherapy.

3.1.2. *Thermo-responsive MNs*

Heat has been extensively utilized in domains such as clinical oncology and drug delivery[122]. Simultaneously, the application of heat represents a highly promising technique for improving drug delivery penetration[123,124]. Thermo-responsive MNs are fabricated from materials having a low melting point (<55 °C), allowing them to shift from solid to liquid upon exposure to a heat source[38]. These MNs can absorb heat from a heat source to undergo a phase shift. Both thermal heaters and photothermal agents can be considered as heat sources. Shao et al.[116] engineered a multistage MN featuring multilayer architectures, comprising a degradable needle tip for prolonged drug release, a dissolvable base for accelerated drug release, and a functional substrate with a reservoir (Fig. 7D). The backing layer of the MN consisted of HA, serving as a reservoir for storing Fe micrometer powder-based self-heating materials. The elevated room temperature, increased humidity, and air exposure facilitated the exothermic chemical reaction of the Fe powder-based mixture, demonstrating enhanced self-heating efficacy. This self-heating MN exhibited superior thermally enhanced drug release efficacy compared to traditional MNs. Consequently, self-heating multistage MNs exhibited enhanced therapeutic effects on tumors compared to traditional designs. Similarly, in Cheng et al.'s research[125], a thermo-responsive recombinant adeno-associated virus (rAAVs)-loaded MN (AMNP) was developed to facilitate perivascular gene delivery for the treatment of intimal hyperplasia. AMNP was constructed with gelatin, which possesses a low melting point. This composite material could dissolve at body temperature, facilitating thermally responsive drug release.

3.1.3. *Electric-responsive MNs*

MN, as a novel electroporation device, can effectively traverse the epidermal barrier and penetrate the resistant stratum corneum to deliver targeted electroporation with little invasiveness[126]. Electric-responsive MNs are synthesized through the integration of naturally conductive polymers, including polyaniline,

polyethylene dioxythiophene, and polypyrrole, or conductive nano-architectures comprising metal NPs and carbon-based nanomaterials. Inherently conducting polymers utilize electricity as an external trigger to release their contents, facilitating spatiotemporal control of medication secretion[127]. Hou et al.[128] presented a hydrogel MN predominantly consisting of GelMA, polydopamine (PDA)-modified poly(3,4-ethylenedioxythiophene) NPs (PPEDOT), dopamine (DA), and Lycium barbarum polysaccharide (LBP). PPEDOT not only imparted conductivity to the MNs but also synergized with electroacupuncture to regulate the wound microenvironment. This synergistic action promoted the regrowth of injured tissues and peripheral nerves. In addition to external electric stimuli, the bioelectricity produced by chemical galvanic cells is of great interest to researchers. Lin et al.[117] brilliantly combined galvanic cells and MNs into bipolar MNs (GCMNs). These MNs could minimally and painlessly break the stratum corneum, enabling the *in situ* continuous generation of hydrogen and bioelectricity *via* the reaction between magnesium and water (Fig. 7E). The synergistic properties of hydrogen and bioelectricity facilitated efficient elimination of ROS, thereby promoting cell migration, accelerating collagen synthesis, and establishing an ideal microenvironment for the restoration of UV-damaged regions. Finally, the GCMNs exhibited significant photoaging wrinkle eradication efficiency. Moreover, the cost-effectiveness, superior biocompatibility, and ease of use of this technology addressed the shortcomings of conventional techniques and facilitated extensive application in the treatment of photoaging skin damage.

3.1.4. Magnetic-responsive MNs

Magnetic-responsive MNs are constructed by integrating nanostructures possessing magnetic properties into certain polymer matrices. Magnetic induction technology exhibits characteristics such as long-range guidance, robustness in intricate environments, and adaptability[129]. Upon injection into the tissues, they can be influenced by an external magnetic field gradient, enabling the directed movement of nanoparticles towards target areas[130]. It possesses considerable potential in surgical guidance, drug administration, and medical diagnosis[131]. Fig. 7F illustrates a magneto-responsive MN robot comprising a magnetic substrate, a separable connection, and tips[118]. Upon oral administration, they oriented toward the small intestine wall, traversed the barriers, penetrated the tissue, and released encapsulated active compounds under designated magnetic fields. Overall, the magnetic-responsive MN systems enable accurate and controllable drug delivery.

3.1.5. Ultrasound-responsive MNs

Ultrasound (US) is a biocompatible mechanical wave that has demonstrated practical relevance in biological applications[132]. A broad spectrum of sensitive US materials has been clarified as being influenced by US stimuli through cavitation effects, sonoluminescence, sonoporation, pyrolysis, and many biophysical and chemical phenomena. The US is distinguished by real-time imaging, high permeability, site-specific characteristics, and the absence of radiation. Moreover, the cavitation and heat effects of US can facilitate spatiotemporally focused drug release. A minor fraction of the ultrasonic energy is absorbed by human tissues, resulting in localized heating that facilitates medication release. Research indicated that the extracorporeal US-responsive MN has markedly enhanced the efficacy of transdermal drug delivery[133]. Li et al.[119] described an intelligent spatiotemporally programmable US weight-loss MN that facilitated sono-gene treatment for obesity by upregulating the gene responsible for weight loss and eliminating surplus white adipocytes. Fig. 7G demonstrates that the zinc tetraphenyl (4-carboxyphenyl) porphyrin (Zn-TCPP) MOF, modified with methoxy polyethylene glycol-polyethyleneimine (mPEG-PEI), served as a carrier for the delivery of the CRISPRa-UCP1 plasmid (aUCP1). The loaded system was encased within a HA MN to form a US-controlled weight loss platform (MN-MP/aUCP1). The transdermal characteristics of the MN facilitated the delivery of MP/aUCP1 to the subcutaneous adipose tissue, penetrating the adipocytes, while US irradiation enhanced intracellular plasmid transfection and gene overexpression. This study introduced a standard-of-care framework to address obesity with a spatiotemporally controlled sono-gene therapy approach. Moreover, Xiang et al.'s research[134] presented a HA MN that facilitated the transdermal distribution of US-responsive NPs for the efficacious treatment of acne. The comprised NPs were synthesized from a zinc porphyrin-based MOF and zinc oxide (ZnTCPP@ZnO). They exhibited activated O_2-mediated eradication of *Propionibacterium acnes* with an antibacterial efficacy of 99.73% within 15 min of US irradiation, leading to a reduction in acne-related variables, including tumor necrosis factor α, interleukins, and matrix metalloproteinases (MMPs). This study resulted in a highly efficient approach for acne treatment *via* the engineering of US response interfaces. Moreover, focused ultrasound is a non-invasive technique that can direct sonic waves into a millimetric volume within tissues. At the point of beam convergence, thermal energy can be transferred to the target tissue (*e.g.*, tumor), raising its temperature to 50−60 °C within seconds, hence facilitating immediate and subsequent cancer immunogenic cell death and coagulative necrosis. A study developed an innovative focused ultrasound-thermal monitoring technique utilizing MNs and single molecule arrays to identify alterations in protein expression at the femtomolar level. This study revealed that US-responsive MNs exhibit enhanced tissue penetration, increased permeability, and precise drug delivery, indicating significant promise for advancement in the treatment and detection of obesity and tumors.

3.1.6. Mechanical force-responsive MNs

Mechanical forces can be categorized into three types: compressive, tensile, and shear forces. Such forces naturally exist within the human body and are associated with the onset and progression of different diseases, including musculoskeletal disorders. Mechanical force-responsive delivery devices offer an effective approach for controlled drug release and have garnered increasing interest of scientists. These systems comprise mechano-responsive biomaterials capable of transducing external signals, such as compressive stresses, electrical stimuli, and magnetic stimuli, into mechanical cellular signals[135]. This signal transmission initiates the rapid release of medications while simultaneously providing patients with a self-administered method. Mechanical force-responsive MNs are often constructed by combining triboelectric nanogenerators (TENGs) and piezoelectric nanogenerators (PENGs). TENGs are a cutting-edge technology for transforming ambient mechanical energy into triboelectric energy through the integration of triboelectrification and electrostatic induction. Through intermittent relational contact and separation of disparate frictional materials with varying electron affinities, TENGs

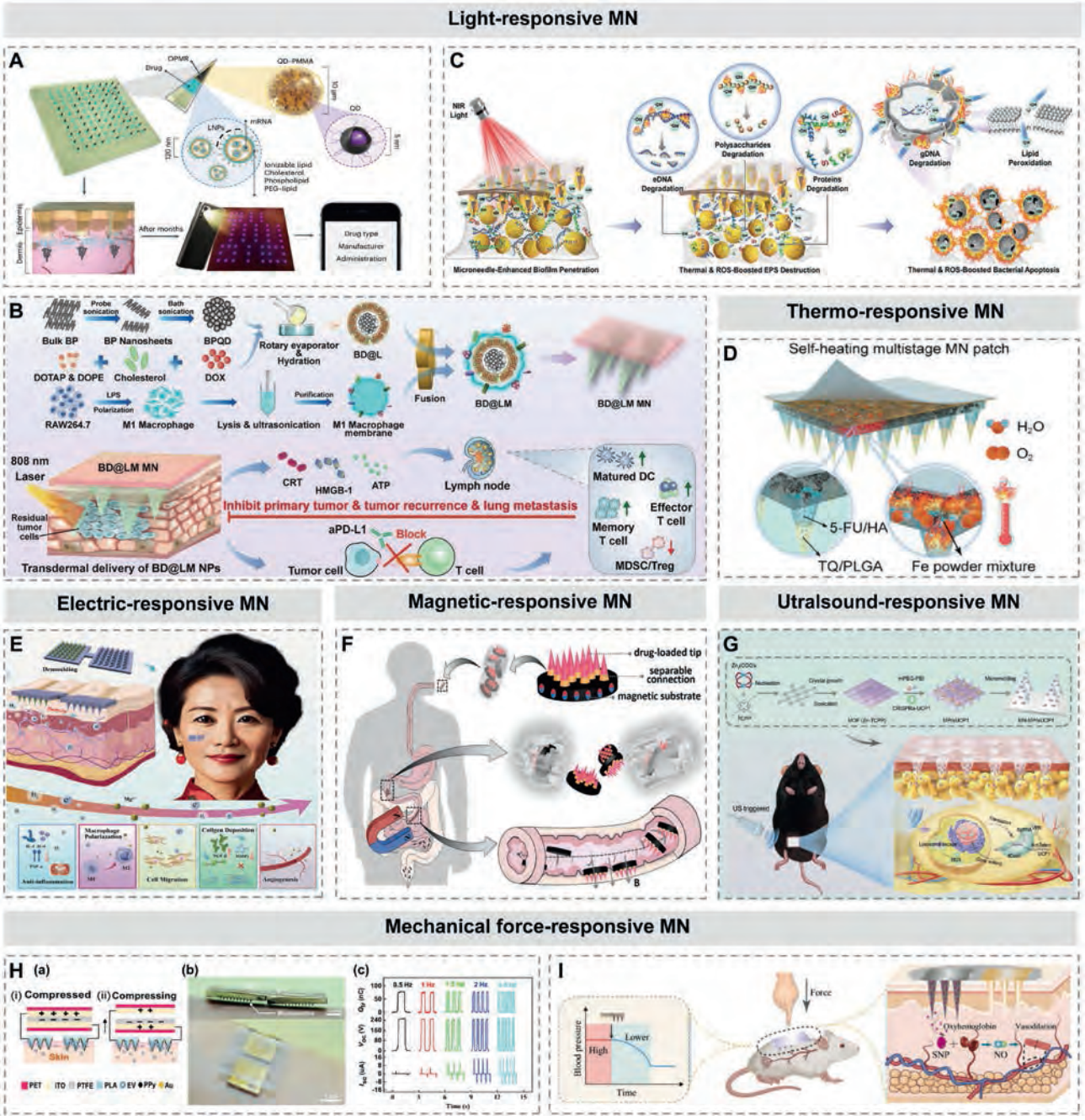

Figure 7 Physical stimuli-responsive MNs for biomedical applications. (A) Diagram of the OPMR technology employed for the maintenance of medical records. Reproduced with permission from Ref. 109. Copyright © 2025, Springer Nature. (B) Diagram illustrating the integration of BPQDs with MNs for cancer management. Reproduced with permission from Ref. 110. Copyright © 2025, Elsevier. (C) Schematic representations of the potential process for biofilm elimination by Mn:C/G@MN under 808 nm NIR irradiation. Reproduced with permission from Ref. 115. Copyright © 2024, Wiley. (D) Schematic representations of the self-heating MN. Reproduced with permission from Ref. 116. Copyright © 2024, Wiley. (E) Schematic representations of the operational principle of the GCMNs. Reproduced with permission from Ref. 117. Copyright © 2025, Wiley. (F) Schematic representations of the drug delivery systems. Reproduced with permission from Ref. 118. Copyright © 2021, Wiley. (G) Preparation technique of MN-MP/aUCP1 and its application in anti-obesity therapy utilizing a spatiotemporally controllable sono-gene therapy platform. Reproduced with permission from Ref. 119. Copyright © 2025, Springer Nature. (H) Self-powered triboelectric-responsive MNs with regulated release of EXPLOR designed EVs. Reproduced with permission from Ref. 120. Copyright © 2024, Springer Nature. (I) Self-powered and controlled MN drug delivery device for expedited blood pressure decrease and its underlying process. Reproduced with permission from Ref. 121. Copyright © 2024, Elsevier.

effectively convert irregular and low-frequency human biomechanical energy from body movements, respiration, cardiac activity, and pressure differentials into electrical energy[136]. TENGs are extensively utilized for health monitoring, minimally invasive diagnosis, and personalized disease therapies due to their low cost, lightweight, structural flexibility, and efficient energy conversion, which also demonstrate remarkable bioelectric properties that influence cellular processes related to functional control and destiny determination[137]. Classical PENGs consist mostly of two electrodes and a single encapsulated piezoelectric layer, exhibiting a comparatively uncomplicated structure in relation to TENGs. The essential element of PENGs is the piezoelectric layer, composed of piezoelectric materials, such as piezoelectric ceramics ($BaTiO_3$, ZnO, GaN, etc.) and/or piezoelectric polymers (polyvinylidene fluoride (PVDF) and its copolymer variants, etc.)[138]. PENGs may transform applied pressure into electrical signals (voltage and current), functioning as both high-performance pressure sensors and energy harvesting devices concurrently[139]. MNs combined with TENGs and PENGs offer a potential approach for various diseases.

Zhang et al.[120] developed a self-powered triboelectric-responsive MN array for the regulated release of optogenetically engineered (EXPLOR) EVs, aiming at repairing intervertebral disc degeneration (IVDD) through an inflammatory regulation technique (Fig. 7H). Self-sustaining triboelectric-responsive MNs, utilizing the triboelectric effect from the relative motion of disparate frictional layers (ITO and PTFE) and the variable electrostatic adsorption properties of polypyrrole (PPy) under triboelectric stimulation, could capture mechanical energy to activate crucial nuclease (TRAM1)-engineered EV release, inhibit TREX1 nuclear localization, and tether TREX1 to the endoplasmic reticulum, thereby enhancing immune surveillance for the removal of damaged DNA, thus significantly mitigating the degeneration of IVDD. Wang et al.[140] similarly created structural color triboelectric MNs with the requisite characteristics using a straightforward mold replication technique. The MNs consisted of a PAM-PEGDA-LiCl ionic hydrogel featuring an inverse opal scaffold structure. The ionic hydrogel, endowed with charge production capability through frictional contact with skin, facilitated efficient and regulated drug release *via* electrostatic repulsion. Simultaneously, the mechanical properties of friction and contact facilitated angiogenesis, which could positively influence on psoriasis treatment.

Chen et al.[121] created MNs integrating with a self-powered module to establish a self-powered and controllable MN drug delivery system (SCMNS) (Fig. 7I). Polylactic acid-gold MNs (PLA-Au MNs) served as electrodes, while PLA-Au-PPy MNs functioned as drug-loading and drug-releasing modules. PENGs consisted of electrospun PVDF and carbon nanotube sheets, functioning as self-sustaining elements. Their findings demonstrated that substantial drug release was achieved under piezoelectric stimulation, showing a voltage-dependent fluctuation drug release model. The PENG transformed mechanical energy from pressure into electrical energy, which was conveyed through copper foil to the MN drug release module. The transdermally released SNP widens blood arteries by generating nitric oxide (NO), hence reducing blood pressure. In comparison to conventional intravenous administration, the device could lower blood pressure gradually, which enhanced patient acceptability. Overall, mechanical force-responsive MNs possess significant clinical application potential.

3.2. Chemical stimuli-responsive MNs

3.2.1. pH-responsive MNs

Under normal physiological settings, the pH of tissues and organs is regulated within a certain range. Nonetheless, the occurrence of a series of diseases such as tumors, inflammation, infections, hypoxia, and ischemia results in substantial alterations in the pH of tissues and organs[141-145]. Leveraging this property, pH-responsive drug delivery systems have been developed to facilitate targeted drug release at designated locations[146,147]. pH-responsive MN delivery systems are constructed utilizing pH-responsive polymers as the needle tip material or by including responsive nanoparticles. They integrated the benefits of pH-responsive delivery systems with MN delivery systems, showcasing significant advantages in conditions affecting the skin and internal organs. Following a MI, a rise of CO_2 content locally, along with the buildup of hydrogen ions and lactate ions within cells, results in a reduction of intracellular pH. Motivated by this feature, Wang et al.[148] developed self-propelled asymmetric microparticles derived from egg-shell membrane for MI treatment (Fig. 8A). Specifically, calcium carbonate ($CaCO_3$), the main component of the eggshell, could react to the localized acidity at the MI site, producing CO_2 that subsequently drove the micro-robots to the remote infarction site. The protein membrane of the eggshell microparticles (ESMPs) associated with the azide monosaccharide Ac4GlcNAz (Glc)-labeled exosome (Exo) through bioorthogonal chemistry. Concurrently, dual complementary liposome NPs (DLC-VEGF) were administered at the needle tips to promote early vascular network reconstruction. The combination of needle penetration and powered particles facilitated the long-distance transport of Exos through micro-robots to remote MI sites, while ESMPs and Exos modulate cardiomyocyte metabolism in hypoxic conditions by enhancing local pH. Furthermore, an unprecedented hierarchical DNA nanocomposite, known as cobalt pyrophosphate/DNA (Co_2PPi/DNA) nanoflower (NF), was composed of an 81-mer GCGR aptamer and a Co_2PPi nanosheet assembled using a coordination-driven self-assembly approach (Fig. 8B)[149]. NFs were included into a soluble HAMA MN. Upon application to the diabetic wound, NFs dissociated to enable the prolonged release of Co^{2+} ions and GCGR aptamer in reaction to the slightly acidic microenvironment of the wound. This study illustrated multifunctional nanocomposites reacted to the mildly acidic conditions of wounds, facilitating diabetic wound healing. Moreover, ZIF-8, a notable subclass of MOFs formed through the self-assembly of zinc ions (Zn^{2+}) and 2-methylimidazole, was selected as a drug delivery carrier owing to its intelligent pH-responsiveness and superior biocompatibility. The pH-responsiveness of ZIF-8 arises from the fact that the acidic environment promotes its breakdown by inducing protonation of organic ligands. A pH-responsive self-assembly nanoplatform was developed in a study by encapsulating silver nanoclusters (AgNCs) and the Chinese herbal drug trigonelline within ZIF-8 for synergistic ferroptosis therapy to target hypertrophic scarring[150]. Similarly, Hao et al.[151] developed a device that integrated mitochondria-targeted doxorubicin-triphenylphosphonium (TPP) into ZIF-67 structures, which were included into rapidly dissolving MNs for localized, organelle-specific drug delivery. The catalytic breakdown of ZIF-67 in acidic, H_2O_2-rich conditions facilitated the targeted buildup of doxorubicin-TPP in mitochondria, leading to mitochondrial malfunction, increased

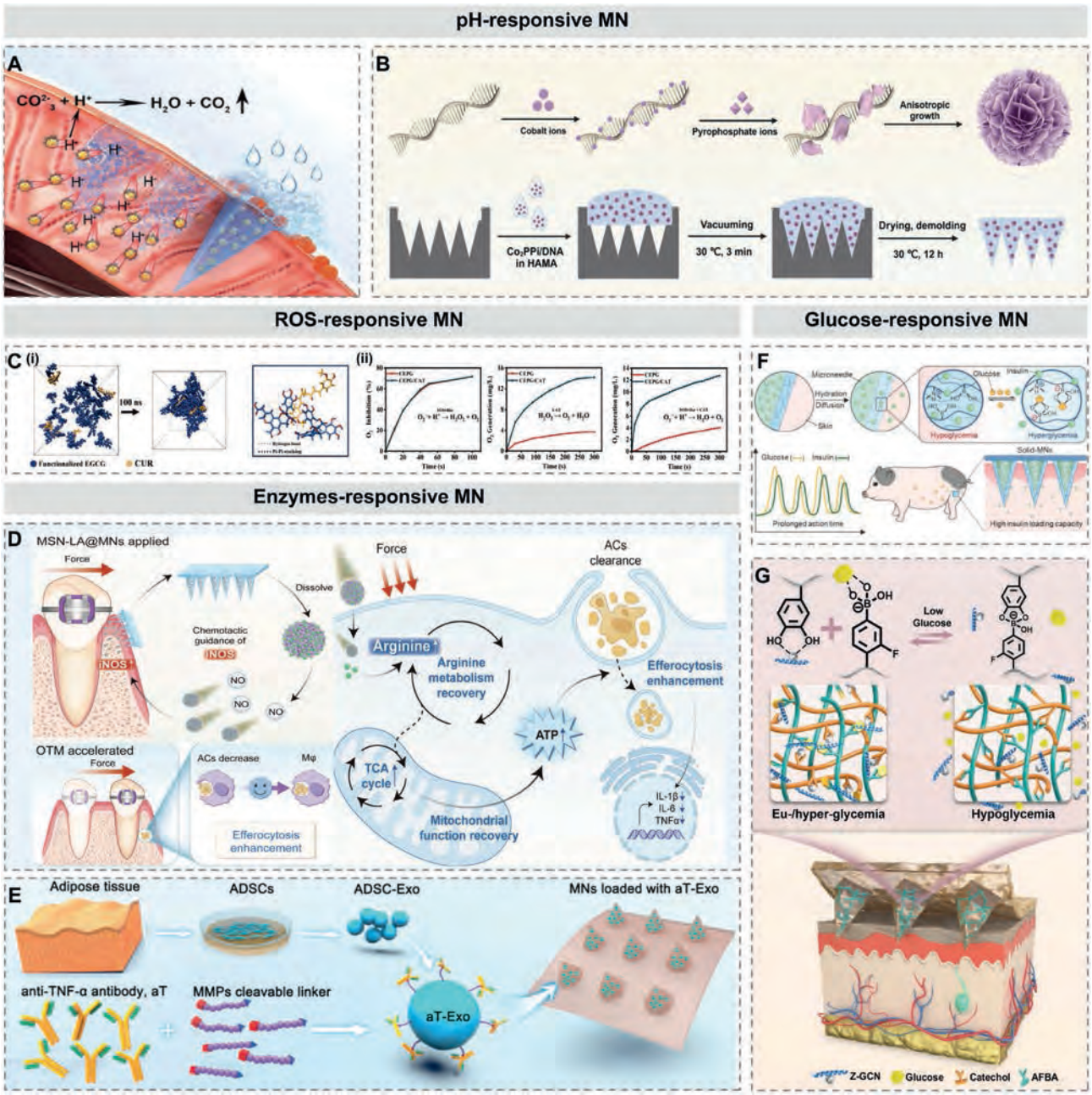

Figure 8 Chemical stimuli-responsive MNs for biomedical applications. (A) Schematic illustration of the exosome and egg-shell-membrane integrated MNs. Reproduced with permission from Ref. 148. Copyright © 2025, Wiley. (B) Schematic showing the preparation of Co_2PPi/DNA@MN. Reproduced with permission from Ref. 149. Copyright © 2025, Wiley. (C) (i) Structural changes of initial CEPG system during ROS simulation. (ii) ROS-integrated cascade catalysis and scavenging abilities. Reproduced with permission from Ref. 154. Copyright © 2024, American Chemical Society. (D) Schematic representation of the fundamental design of MN incorporating NO-driven nanomotors. Reproduced with permission from Ref. 155. Copyright © 2025, American Chemical Society. (E) Schematic illustration of aT-Exo-encapsulated MN for address alkali-burned corneas. Reproduced with permission from Ref. 156. Copyright © 2024, American Chemical Society. (F) Schematic illustration of the glucose responsive Solid-MN. Reproduced with permission from Ref. 157. Copyright © 2024, American Chemical Society. (G) Schematic showing of glucose-responsive glucagon delivery mechanism of Z-GCN loaded MN. Reproduced with permission from Ref. 158. Copyright © 2025, Springer Nature.

ROS generation, and the activation of apoptosis and ferroptosis pathways.

Beyond NP-mediated pH responsiveness, pH-responsive MNs can also be fabricated utilizing pH-responsive tip matrix materials. A study by Sun et al.[152] developed a core−shell pH-responsive MN for orthodontic applications. The MN shell consisted of PLGA supplemented with sodium bicarbonate ($NaHCO_3$). The incorporation of $NaHCO_3$ conferred pH-

responsive releasing characteristics to the MNs. The core of MN consisted of 10% GelMA supplemented with pro-inflammatory macrophage-derived microparticles CQ@PMMPs. The local low pH, generated by force-related aseptic inflammation, initiated the destruction of the MNs and facilitated the gradual release of CQ@PMMPs. Likewise, the $NaHCO_3$-based core−shell MN, incorporating ropivacaine microcrystals, was designed to respond to the acidic milieu at the surgical site for prolonged incisional analgesia[153].

3.2.2. *ROS-responsive MNs*

ROS encompass highly reactive ions and free radicals, such as superoxide (O^{2-}), ·OH, hypochlorite ion (OCl^-), H_2O_2, and singlet oxygen ($_1O^2$). An insufficiency or surplus of ROS can precipitate several diseases, including autoimmune disorders, cardiovascular ailments, and neurodegenerative conditions[159]. These atypical metabolic changes at disease sites have motivated researchers to utilize unregulated ROS levels for the creation of targeted drug delivery devices. ROS-responsive MNs attain their functionality by employing ROS-sensitive materials as the matrix for the tips or by encapsulating ROS-responsive polymeric NPs. ROS-responsive materials typically comprise polymers with chalcogen components, including sulfide, selenide, and telluride[160]. Additional categories of ROS-responsive polymers encompass thioether, diselenide, poly(thioketal), arylboronic acid/ester-containing polymers, aminoacrylate, oligoproline, and peroxalate ester-containing polymers. The drug release mechanisms of these polymers rely on the transformation of polymer solubility from hydrophobic to hydrophilic characteristics or the cleavage of chemical bonds induced by ROS[161].

Owing to the overproduction of ROS and ensuing inflammation, ROS-responsive MNs have been utilized for the treatment of radiation-induced skin injury (RISI). For instance, Epigallocatechin gallate (EGCG) and curcumin (CUR) were co-assembled into NPs (CEPG) through intermolecular interactions. These NPs were subsequently integrated with CAT and MNs to establish a cascade system and facilitate penetration of epidermal keratinocytes that hinder the treatment of RISI. Upon insertion into the dermis, CEPG demonstrated the capacity to react to ROS and breakdown into EGCG and CUR (Fig. 8C(i))[154]. Subsequently, EGCG and CAT transformed superoxide anions into water sequentially, thereby mitigating cellular damage induced by free radicals during the initial phases of radiation for preventative purposes (Fig. 8C(ii)). Similarly, Bi et al.[162] developed detachable H_2O_2-responsive gel-based MNs incorporating methotrexate and EGCG, utilizing EGCG as both cross-linkers for needle-composited materials and anti-inflammatory agents. The gel-based MNs exhibited dual-mode drug release kinetics, facilitating rapid diffusional release of methotrexate and sustained, H_2O_2-responsive release of EGCG. These ROS-responsive MNs enhanced treatment results in both psoriasis-like and prophylactic psoriasis-like animal models.

3.2.3. *Enzyme-responsive MNs*

Enzymes perform important roles in biorecognition and catalysis in living organisms. The existence and expression levels of enzymes differ across various tissues and in pathological conditions. Numerous disorders are associated with enzyme dysfunction or variations in enzyme levels. Meanwhile, enzymes exhibit incredible affinity and selectivity for their substrates, facilitating regulated chemical reactions and biological responses[163]. Consequently, they represent crucial targets for therapeutic investigation and intervention. Enzyme-responsive delivery systems, which integrate the benefits of specific enzyme stimuli with the remarkable properties of nanomaterials, present significant opportunities to enhance the on-demand delivery, tumor accumulation, and efficient cellular internalization of imaging contrast substances or medications[164].

Enzymes utilized in enzyme-responsive delivery systems often comprise MMPs, phospholipases, hyaluronidases (HAase), cysteine caspases, nitric oxide synthase (iNOS), cathepsins, and others[165]. A study by Tan et al.[155] developed a MN drug delivery system using NO-driven nanomotors (MSN-LA@MNs) for the targeted administration of L-arginine (Arg) to address mechanical force-induced sterile inflammation (Fig. 8D). Arg encapsulated in MN tips could respond to iNOS, which is strongly expressed in mechanically stressed tissues, hence producing NO to facilitate autonomous propulsion. Additionally, MMP-9 can be upregulated in alkali-injured corneas. Motivated by this, Yu's research[156] attached antitumor necrosis factor α antibodies (aT) to the surface of adipose-derived stem cell exosome (ADSC-Exo) by utilizing MMP-cleavable peptide chains and subsequently incorporated them into a PVA-based soluble MN to develop tailored aT-Exo with synergistic effects (Fig. 8E). Upon exposure to MMP-9, aT could be effectively liberated from aT-Exo. This design concept provided a dual-targeting capability that enhanced corneal repair following chemical injury. Similarly, Zeng et al.[166] introduced an MMP-9-responsive cascade bilayer MN (G/AZ-MN) that designed to enhance diabetic wound healing through localized glucose depletion and prolonged NO release, and provide enduring antibacterial and anti-inflammatory benefits. The MN featured a degradable GelMA tip containing GOx and a dissolvable base layer encapsulating Arg-loaded NPs. After administration on the wound site, MMP-9 was degraded by the GelMA tip, thus leading to the release of GOx. This profile catalyzed the conversion of glucose into gluconic acid and H_2O_2, which not only diminished glucose levels in the diabetic wound but also triggered a cascade reaction between H_2O_2 and the Arg, resulting in the sustained production of NO for seven days. Furthermore, HAase-responsive, thrombin-responsive, and bacterial lipase-responsive MN systems were established for targeted and precise tumor therapy, thrombosis prevention, and combating antibiotic resistance[167,168].

3.2.4. *Glucose-responsive MNs*

For diabetic patients, inadequate regulation of blood glucose levels may result in various risks, including renal failure, visual impairment, hypoglycemia, neurological damage, cognitive decline, and seizures. Therefore, patients must regularly monitor their blood glucose levels to administer appropriate treatment interventions promptly. The dynamical regulation of the secretion of insulin and glucagon based on the body's glucose levels is of important place[169]. Glucose-responsive MNs offer an efficient and painless strategy for insulin or glucagon delivery. More importantly, they can adeptly regulate the dynamics of medication release in response to variations in blood glucose levels. The majority of chemically driven glucose-responsive drug delivery systems utilize concanavalin A, GO_X, or phenylboronic acid as glucose detecting elements[170,171]. For instance, Gu's team[172] delineated a transdermal polymeric MN for glucose-responsive closed-loop delivery of insulin and glucagon to attain glycemic management while minimizing the danger of hypoglycemia. The glucose-responsive phenylboronic acid units could bind to glucose, resulting in a reversible alteration of the net charge of the entire polymeric matrix within MNs, shifting from positive to

negative. Consequently, the release ratio of negatively charged insulin and positively charged glucagon analogs from the MN could be dynamically adjusted in response to fluctuations in blood glucose levels to achieve glycemic homeostasis. Additionally, to attain a substantial loading capacity of insulin, they enclosed solid insulin powder into the core of negatively charged glucose−boronate complexes constructed in MN tips (Fig. 8F)[157]. This glucose-responsive MN has been shown to effectively regulate blood glucose levels for extended periods in both type 1 diabetic mice and minipigs, achieving up to 48 h of control with MNs of 3.5 cm^2 for minipigs weighing over 25 kg.

Nonetheless, several obstacles, including design intricacy, convoluted manufacturing procedures, degradation of the bioactivity of encapsulated drugs, and sluggish reaction kinetics, constrained the implementation of the aforementioned methods. Currently, dynamic metal−ligand complexation has garnered considerable attention in both theoretical and practical material science. The dynamic binding contacts may rapidly disassociate, exchange, and rebuild. Consequently, they can be utilized in the construction of "smart" fabrics including reversible "ON/OFF" bindings[173]. Catechols are recognized for forming reversible complexes with metal ions, metalloproteins, and boron-containing compounds, with the binding affinity contingent upon the characteristics of the molecules involved[174]. Monomers containing boronic acid represent a distinct category of molecules capable of forming complexes with catechol groups. These interactions may be competitively impacted by glucose molecules. At elevated glucose concentrations, boronic acids interact with glucose molecules to form cyclic boronate esters. As the glucose content diminishes, the boronic acid derivatives dissociate and competitively associate with catechol groups. In this case, if the catechol groups are pre-chelated with a metal-containing molecule that possesses a lower binding affinity than boronic acid, the boronic acid will displace the metal-containing compound. Inspired by this property, researchers developed a closed-loop self-crosslinked hydrogel-based MN utilizing DA and 4-amino-3-fluorophenylboronic acid (AFBA)-functionalized HA-derived polymers (Fig. 8G)[158]. This design allowed AFBA functional groups to reversibly interact with glucose at elevated concentrations, forming cyclic boronate esters. During hyperglycemia, boronic acids interacted with glucose to produce cyclic boronate esters. Concurrently, the catechol functional groups of DA interacted with Zinc-Glucagon (Z-GCN) *via* metal−ligand complexation. As glucose concentration diminishes, AFBA will preferentially bind with DA over Z-GCN, owing to its superior binding affinity and free energy value. This innovative design established a revolutionary framework for the regulation of blood glucose levels.

3.2.5. Others

By choosing the matrix material at the MN tips and the type of loaded NPs, the MNs can demonstrate responsiveness to glutathione (GSH), sulfate ions, and physiological fluids. For instance, Luan and coworkers[175] engineered a carrier-free self-assembled CuTG-Cas9@PLL nanohybrid-encapsulated MN for anti-tumor immunotherapy (Fig. 9A). The carrier-free nanohybrids, designated as CuTG, were synthesized using the coordinated self-assembly of the telomere-targeting drug 6-Thio-dG and copper ions (Cu^{2+}). The CRISPR/Cas9 ribonucleoprotein (RNP) complex was captured onto the CuTG surface and subsequently shielded and encapsulated by BSA and poly-L-lysine (PLL). Considering that Cu^{2+} can be reduced to Cu^{+} by GSH, which is subsequently oxidized to GSSG, GSH may facilitate the disassembly of CuTG-Cas9@PLL, resulting in the release of Cu^{2+}, 6-Thio-dG, and CRISPR/Cas9. This method enabled precise and regulated drug release, offering a viable strategy to boost anticancer immunotherapy. A separate study by Wang et al.[176] developed a MN composed of PLGA infused with magnesium hydride (MgH_2) (MN-MgH_2). Upon interaction with bodily fluids, MgH_2 could produce H_2 and Mg^{2+}, thereby diminishing the generation of ROS and altering the pathogenic microenvironment caused by diabetes. Moreover, Zhang et al.'s study[177] revealed that PVA hydrogel needle tips exhibited ionic responsiveness attributable to Hofmeister effects. The hardness of the PVA tips could be enhanced by sulfate ions and decreased by nitrate ions.

The skin, serving as the organ for MN administration, possesses a hierarchical structure and a diverse array of cell types, offering numerous internal indicators for spatiotemporal responses[178]. Intelligent MNs can be designed to respond to specific cell types in the skin by adjusting the type of matrix material of needle tips and the application site. For instance, Gao et al.[179] suggested a spatiotemporal segmentation immunotherapeutic approach capable of differentiating the treatment requirements of various locations within the local niche (Fig. 9B). This study posited that a keratin-based module MN (CLP@K^2MN), which was intended to enhance wound healing and regulate the tumor immune microenvironment in the postoperative context, could decrease tumor recurrence and enhance the survival outcome of mice with partially resected breast cancer. The SRK84-T-based needle root layer, mostly located in the epidermis, augmented the recruitment, antigen absorption, and activation of dendritic cells (DCs) *via* stable hydrogen bonds binding to the DC surface receptor DEC205, hence significantly enhancing the efficacy of antigen presentation. Conversely, the RK81-1Aα-based needle tip layer infiltrated the dermis extensively, markedly expediting wound healing. *In vivo* experiments indicated that, when cancer cell membrane-coated AS01 liposomes (CLPs) were administered into K_TMN and released intradermally, the dispersed CLPs co-localized with an elevated presence of DCs, including Langerhans cells in the epidermis. Consequently, CLP@K^2MN therapy elevated the infiltration of innate immune cell types in tumor-bearing animals, achieving the response to DCs *via* the specific binding between tail domains of SRK84-T proteins and cell receptors.

In addition, intelligent MNs can also be designed to respond to T cells that resident in the epidermis and dermis. Prior research has shown that transdermal delivery techniques based on MNs enhanced the transport of medicinal agents to lymph nodes through lymphatic channels[180,181]. Motivated by this, Li et al.[182] created a spatially distributed MN system (SDMNS) that utilized bioorthogonal processes to activate and direct endogenous T cells to tumors for efficient elimination (Fig. 9C). The SDMNS comprised two MNs of dissolving needles, each containing complementary bioorthogonal groups, administered individually to lymph nodes and tumor locations. An MN containing two dibenzocyclooctyne (DBCO)-modified antibodies stimulated T cells and marked them with bioorthogonal groups in lymph nodes. The alternative MN comprising *N*-azidoacetylmannosamine-tetraacylated (Ac4ManNAz) for glycometabolic marking of cancer cells, together with the T cell chemotactic factor IP10, was administered directly to the tumor location. Bioorthogonal groups, such as azide (N_3) groups, were integrated into cellular glycans and presented on the cell surface by the manufacture of synthetic sugars. These bioorthogonal groups then established persistent and

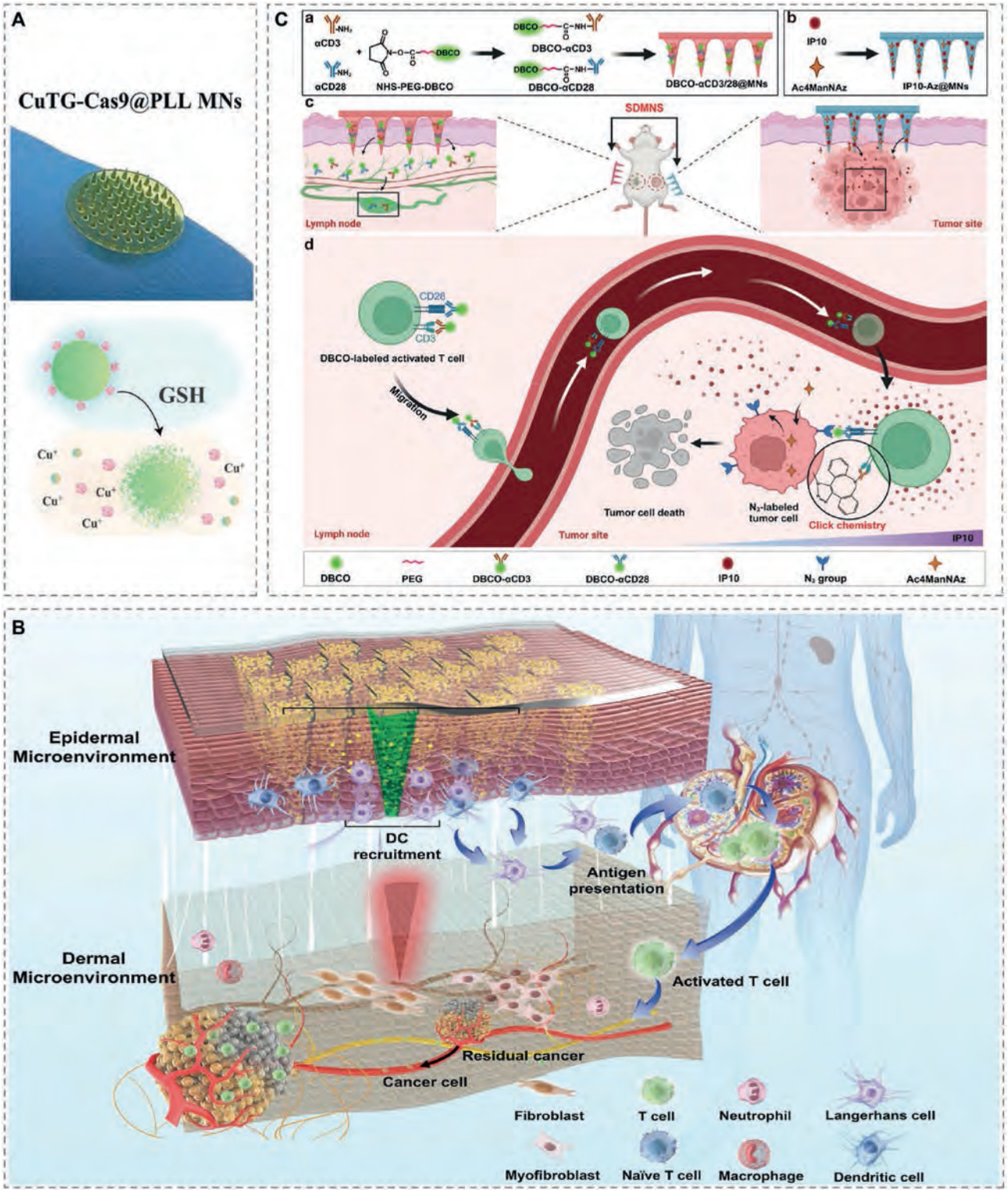

Figure 9 Others stimuli-responsive MNs for biomedical applications. (A) Schematic showing the GSH-responsive capability of CuTG-Cas9@PLL. Reproduced with permission from Ref. 175. Copyright © 2024, Wiley. (B) A spatiotemporal segmentation immunotherapy approach utilizing modular MNs to regulate paradoxical postoperative immunization microenvironments. Reproduced with permission from Ref. 179. Copyright © 2025, Wiley. (C) Schematic representation of the SDMNS and its prospective mechanism of antitumor immune responses. Reproduced with permission from Ref. 182. Copyright © 2025, Wiley.

resilient chemical bonds with the complimentary group (*e.g.*, DBCO) *via* strain-promoted azide-alkyne cycloaddition (SPAAC) reaction[183]. The engineered MN facilitated the effective conjugation of antibodies containing a DBCO group to azide-functionalized cancer cell surfaces, demonstrating improved infiltration, recognition, and selective cytotoxicity towards N_3-labeled cancer cells *via* bioorthogonal chemistry-mediated antibody−cell interactions. Anticancer results based on the 4T1 bilateral tumor-bearing mouse model revealed that the combination of MNs led to elevated infiltration of $CD4^+$ and $CD8^+$ T cells in both primary and distant tumors than the individual applications of DBCO-αCD3/28@MNs or IP10-Az@MNs groups. In summary, the spatially distributed MN improved lymphatic targeting and facilitated localized drug delivery for more powerful therapeutic results.

4. Innovative structural-designed MNs

The biomedical functions of intelligent MNs rely on the properties of the constructing materials and structural designs. Due to the restricted tissue penetration, inadequate cellular absorption, and diminished bioavailability, which hinder the effectiveness of drug delivery systems, more complete, integrated, multi-layered, and specifically constructed MNs have been developed to accommodate diverse complex disease states and fulfill a broader spectrum of biomedical applications. To date, there are multilayer, core−shell, porous, hollow, effervescent, nested, grooved, and thread-structured MNs. The innovative structural design can assist the intelligent MNs to realize multiple functions: (1) delivering or absorbing different types of cargoes; (2) regulating the release pattern, release speed, and release depth of the drug in the tip of the needle; and (3) adjustable mechanical strength. It is critical to understand the capability and features of this parameter to improve the functions of MNs when developing intelligent MNs platforms.

4.1. Multilayer MNs

The tips and bases of multilayer MNs consist of different substrate materials. Controlling the types of materials and the degree of cross-linking allows for exact control over drug release rate, penetration depth, and mechanical strength of the tips. Additionally, the diverse spatial structure design of multilayer MN allows for spatiotemporal regulation of disease treatment and promotes multimodal combination therapy. Furthermore, the incorporation of multilayer MN with sensors establishes a novel paradigm for real-time monitoring and on-demand therapy.

Jiang and colleagues[10] developed a double-layered MN system (SOP MN), wherein the outer layer consisted of non-photo-crosslinked single-layered HA, while the inner layer was composed of photo-crosslinked HAMA (Fig. 10A). Upon penetrating tumor tissue, the outer layer immediately dissolves, liberating the NIR laser-sensitive PROTAC prodrug for acidic activation within tumor cells, while the inner layer progressively degrades, facilitating a sustained release of bovine serum albumin-coated manganese oxide (BM NPs) serving as an "oxygen supply station". This pioneering MN-based technology effectively accomplished spatiotemporally restricted protein degradation and combinatorial therapy for glioblastoma. In Qu's research[184], a dual-layer MN (d-MN) was developed to concurrently regenerate both soft and hard periodontal tissues (Fig. 10B). The d-MNs base layer consisted of gelatin GelMA infused with nano-HA (nHA), which enhanced the differentiation of osteogenic cells into osteoblasts, therefore facilitating alveolar bone regeneration. The tips of the d-MNs consisted predominantly of HA integrated with an Mg-based MOF (Mg-MOF) infused with GO_X. When applied at periodontitis lesion, the synergistic interaction between the d-MNs base layer and tips efficiently enhanced the regeneration of both soft and hard tissues. In the same vein, Zhang et al.[185] constructed a double-layer nucleoside-MN. The MN tips consisted of a guanosine-quadruplex hydrogel formed by the interlacing of guanosine-quadruplex nanowires. The backing layer consisted of a swiftly dissolving PVA substrate to ensure prompt mucosal adherence and to reduce disruption of normal mouth function. This multiscale engineering methodology tackled significant obstacles in oral medication retention and pseudomembrane infiltration.

Interestingly, Song and collaborators[186] established a triphasic MN to improve tendon-to-bone repair (Fig. 10C). The tips of the MN were engineered to infiltrate the tendon-to-bone interface, the stem was intended to gradually release small EVs (sEVs), and the base was utilized for incorporating and distributing tendon-derived decellularized extracellular matrix (ECM) (T-dECM). Moreover, Xu's team[187] manufactured a dual-layered "microneedle rocket" (Fig. 10D). Specifically, the upper layer of the MN consisted of photodynamically active mesoporous silica NPs covalently bonded to PSs. The bottom layer consisted of an enzyme-mediated HA-tyramine hydrogel with collagenase, functioning as rocket thrusters for the remodeling of the ECM within the TME[188]. A multifunctional bilayer MN was created as a theranostic platform for effective wound care by Wang and colleagues (Fig. 10E)[189]. The bilayer MN consisted of a soluble PVP MN (pMN) mounted on a conductive stainless-steel MN (sMN). The tough sMN penetrated the necessary skin depth, while the pMN, loaded with antibiotics, guaranteed continuous drug release upon disintegration in the ISF. Additionally, the silver and carbon nanotube-coated sMN (CNT/Ag/sMN) served as a transdermal electrochemical sensor to evaluate wound conditions by measuring H_2O_2 and uric acid levels. The design enabled the integration of real-time monitoring with on-demand therapy.

4.2. Core−shell MNs

The core−shell MNs design primarily serves to modulate the drug release patterns from the needle tip, providing the MNs with biphasic or multiphasic release profiles that facilitate both rapid and sustained drug release. Additionally, core−shell MNs may establish an *in situ* drug reservoir, significantly prolonging the drug's retention time in the skin. Shan et al.[190] established a dual nanozyme-loaded core−shell MN exhibiting antibacterial and neutrophil extracellular traps (NETs)-degradation dual functionalities for the treatment of periodontitis (Fig. 10F). The outside shell comprised methacrylated hyaluronic acid (MeHA) encapsulating DNase-like dendritic mesoporous silica NPs-cerium nanozyme (DMSN-Ce), whereas the inner core employed HA loaded with Pd nanozymes. The Franz cell apparatus indicated that Pd exhibited a swift release from the rapidly disintegrating HA layer, achieving a total release of $89.50 \pm 2.88\%$ within 5 h. Conversely, Ce included in the MeHA outer layer exhibited an extended-release profile. The biphasic release profile of Pd/Ce MNs promptly elicited an antibacterial response and consistently degraded NETs. Similar to this, Li and colleagues[198] developed a ROS-responsive core−shell MN, whereby the shell comprised a soluble HA containing hypocrellin B-cationic PSs (HB-TTP),

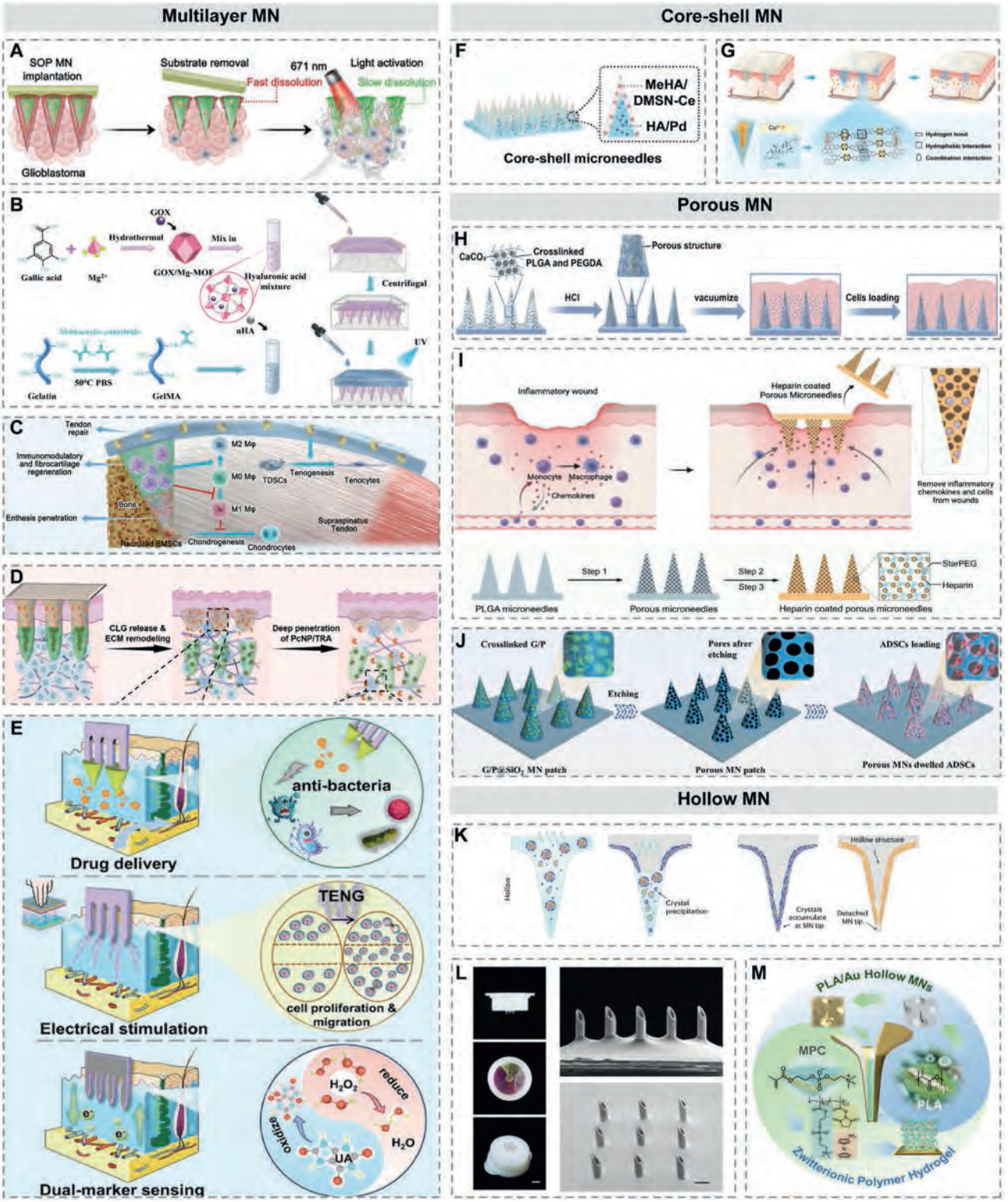

Figure 10 Innovative structure designed MNs for disease treatment and diagnosis. (A) Schematic of the SOP MN. Reproduced with permission from Ref. 10. Copyright © 2025, Wiley. (B) Schematic of the preparation process of d-MNs. Reproduced with permission from Ref. 184. Copyright © 2025, Wiley. (C) Schematic illustration of CR-sEVs/MN for enhancing rotator cuff tendon-to-bone healing. Reproduced with permission from Ref. 186. Copyright © 2024, Wiley. (D) Schematic illustration of multifunctional rocket-like MN for deep drug penetration and combination treatment in melanoma. Reproduced with permission from Ref. 187. Copyright © 2024, Wiley. (E) Schematic image for working principles of MN-TENG-based theranostic platform. Reproduced with permission from Ref. 189. Copyright © 2024, Wiley. (F) The structure of core−shell Pd/Ce MNs. Reproduced with permission from Ref. 190. Copyright © 2025, Elsevier. (G) Schematic illustration of the design of *in situ* supramolecular hydrogel MNs (DexP HMNs). Reproduced with permission from Ref. 191. Copyright © 2025, Elsevier. (H) Schematic

while the core consisted of a ROS-responsive degradable PVA hydrogel infused with recombinant human epidermal growth factor (EGF). Upon the MN's penetration of the biofilm, the MN shell rapidly dissolved and released HB-TTP to kill the bacteria. The MN core was gradually degraded by endogenous ROS in the wound, enabling a prolonged release of EGF. Likewise, Gu's team[199] developed an MN consisting of a ROS-degradable PVA shell and a crosslinked heparin core for immunological regulation. The swift deterioration rate of the shell and the release profile of core-encapsulated medication might be dynamically adjusted in accordance with the inflammatory state of the wounds, thus enhancing individualized treatment in clinical settings. Xu et al.'s study[200] also developed a core−shell MN for the prolonged treatment of osteoporosis. The tip's core−shell architecture comprised a core of alfacalcidol-loaded PLGA microparticles and a shell of ethylcellulose. This structure functioned as a drug reservoir within the epidermis, facilitating the prolonged release of alfacalcidol over a period of 14 days.

More intelligently, the core and shell of the MNs can be considered as an *in situ* chemical reaction chamber. He et al.[191] constructed a core−shell MN (CSMN) capable of *in situ* generation of supramolecular microhydrogels within the dermis (Fig. 10G). The concept was actualized by utilizing the interaction between the medicinal agent dexamethasone sodium phosphate (DexP) and calcium chloride ($CaCl_2$), in conjunction with the differential biphasic release technology (DexP HMNs). Upon application to the skin, the core of the MN swiftly released $CaCl_2$, which diffused to the shell and created a hydrogel containing DexP, establishing reservoirs for a continuous release of DexP. Transdermal permeation assays indicated that DexP HMNs significantly extended the skin storage time of DexP.

4.3. Porous MNs

Porous MNs are commonly used to deliver and capture cells and EVs. This is because MNs have a porous structure, with pore sizes that are suitable for serving as channels for cell infiltration, thereby efficiently loading cells or capturing cells within the skin. Generally speaking, the tips of porous MNs are formed by the polymerization of polymers and $CaCO_3$ particles, and then the tips are etched with hydrochloric acid to form the porous structure. In addition, porous MNs can also be directly constructed into porous structures using chemically crosslinked methacrylic acid. For instance, Liu et al.[192] created a microporous MN incorporating CAR-TREM2-macrophages for scar treatment (Fig. 10H). The MN tips were fabricated using the polymerization of PLGA, poly (ethylene glycol) diacrylate (PEGDA), and $CaCO_3$. The $CaCO_3$ particles were etched in a hydrogen chloride dioxane solution to create a microporous structure on the surface of the tips. This construction demonstrated effective cell loading capacity and markedly preserved the viability of living cells. Likewise, Le et al.[193] constructed a porous MN using the identical methodology, which crosslinked a heparin/4-arm PEG-NH_2 network onto the MN surface post-etching to spatially attract and sequester various inflammatory chemokines (Fig. 10I). These inflammatory chemokines attracted and retained inflammatory monocytes within the porous architecture of the needle tips, effectively mitigating inflammatory skin conditions.

In addition, SiO_2 glass spheres can be utilized to create a porous MN. Fan et al.'s research[194] fabricated porous MNs by utilizing a hybrid of UV-curable GelMA and PEGDA. They applied glass microspheres to occupy negative molds, thereafter subjecting them to overnight etching (Fig. 10J). The stem cells were introduced by perfusing human ADSCs coated in Matrigel into the porous MNs. This biocompatible Matrigel replicated the extracellular matrix, thus simulating the microenvironment of the stem cell niche conducive to the formation of ADSCs. Due to the numerous holes presented on porous MNs, ADSCs had ample opportunity to absorb nutrients, multiply significantly, and effectively release factors. Notably, Fang et al.[201] discovered that GelMA hydrogel alone as needle tips matrix might be formed into porous structures to facilitate the transport of extracellular vesicles.

4.4. Hollow MNs

Hollow MNs comprise hollow needles that facilitate the continuous delivery of the medicine into the skin or the absorption of the drug from the tissue. The operational principle of hollow MNs closely resembles that of hypodermic needles. Over the past decade, hollow MNs have been utilized for insulin delivery. In comparison to solid MNs, hollow MNs can administer insulin more rapidly[202]. Currently, hollow MNs are increasingly utilized in the fields of diagnostics and monitoring. Cao et al.[195] demonstrated the regulation of silk fibroin assembly using inorganic nucleation at the phase front, enabling the nanomanufacture of hollow MNs capable of interfacing with plants (Fig. 10K). Hollow MN facilitated the systemic administration of plant micronutrients to address chlorosis in tomato plants and enhance crop biofortification by transporting human micronutrients injected into the petiole and incorporated into tomato fruits. Hollow MN also facilitated access to plant vasculature for sap extraction, allowing for continuous monitoring and early identification of phytoaccumulation of environmental pollutants like cadmium. Furthermore, Lu et al.[196] designed a hollow MN for *in situ* monitoring of neutrophils (Fig. 10L). This comprised a hollow MN featuring a vacuum chamber for the extraction of ISF. They could swiftly and effortlessly ascertain neutrophil levels without vascular intrusion. A study similarly combined an electrochemical glucose sensor with a hollow MN, constructed from biodegradable PLA and metallized with Au, enabling quick continuous transdermal monitoring (Fig. 10M)[197]. Nonetheless, the intricate fabrication method and elevated costs may impede the advancement of hollow MNs.

4.5. Effervescent MNs

Effervescent MNs are MNs containing effervescent agents at the needle tips or on the substrate. The incorporation of effervescent

diagram of mMNs fabrication and cell loading. Reproduced with permission from Ref. 192. Copyright © 2024, Wiley. (I) Schematic illustration of the mechanisms of HPMN. Reproduced with permission from Ref. 193. Copyright © 2024, Wiley. (J) Schematic diagram of the preparation of porous MNs loaded with ADSCs. Reproduced with permission from Ref. 194. Copyright © 2024, Wiley. (K) Nanofabrication of silk hollow MN for high-throughput micronutrient delivery and continuous sap monitoring in plants. Reproduced with permission from Ref. 195. Copyright © 2025, Springer Nature. (L) Photographs and SEM images of the MN for neutrophil detection. Reproduced with permission from Ref. 196. Copyright © 2025, Wiley. (M) Schematic illustration of the zwitterionic hydrogel-encapsulated PLA/Au hollow MNs. Reproduced with permission from Ref. 197. Copyright © 2024, American Chemical Society.

agents in basement layer of MNs can facilitate rapid separation of the substrate and needle tips while simultaneously improving permeation efficiency. Li et al.[203] developed an effervescent MN patch utilizing PVP-based MN tips and $NaHCO_3^-$ and citric acid (CA)-based effervescent backing for the sustained release of levonorgestrel (Fig. 11A). Upon contacting ISF in the skin, sodium bicarbonate and CA in the MN patch backing reacted to form CO_2 bubbles that weaken MN attachment to the patch and enable separation within 1 min of skin insertion, thereby providing a simple-to-administer approach for improved family planning. Based on this work, Li and colleagues[204] further developed an MN patch that incorporated an effervescent backing (13% PVP containing $NaHCO_3$ and CA) and core−shell tips (levonorgestrel-loaded PLGA core, poly(L-lactide) (PLLA) shell, and a poly(D,L-lactide) (PLA) cap). Similarly, Luo et al.[205] developed an effervescent MN for the simultaneous delivery of chitosan NPs and indocyanine green to address diet-induced obesity (Fig. 11B). The MN consisted of 3 layers: a backing layer comprising 30% PVP, an effervescent layer containing 13% PVP with 5% CA and 4% $NaHCO_3$, and a tip made of HAMA and a photoinitiator. The effervescent MNs required merely 5.1 ± 1.9 s to detach from the effervescent backing. Longitudinal sections of pig skin revealed that effervescent MNs were situated beneath the skin surface at a depth of around 300−600 μm, far deeper than traditional MNs.

Interestingly, incorporating effervescent agents into MN tips can create an ultra-rapid delivery system that facilitates immediate drug release. For instance, You et al.[206] encapsulated biological therapeutic agents such as liraglutide, insulin, and heparin into MN tips that incorporate effervescent agents ($NaHCO_3$ and CA) to establish an ultrarapid-acting MN patch (URA-MN) (Fig. 11C). Upon insertion into the skin, URA-MN generated CO_2 bubbles rapidly, releasing biotherapeutics within 5 min, thereby facilitating immediate transdermal drug delivery. Noteworthily, due to the short application period and little residuals of the MN matrix in the skin, the URA-MN patch demonstrated favorable biocompatibility following six weeks of treatment. Moreover, the CO_2 produced from the hydration of effervescent agents can be repurposed, which can be transformed into carbon monoxide (CO) by photocatalytic technology, consequently exhibiting a deadly impact on tumor cells. Based on this principle, Yu et al.[207] created a detachable photocatalytic MN for the administration of CO to improve chemosensitization (Fig. 11D). The MN utilized a copolymer of hydroxyethyl methacrylate and *N*-vinylpyrrolidone as the hydrogel matrix, incorporating effervescent agents (tartaric acid and $NaHCO_3$), medicinal payloads, and photocatalysts. Upon application, the hydration of the needle body resulted in the release of payloads and the production of CO_2 through the reaction of effervescent agents. They demonstrated that CO may be generated and supplied in a regulated manner *via* photocatalysis initiated by 660 nm light irradiation. These MNs produced an improved anticancer impact in the A375/CDDP melanoma model.

Effervescent MNs not only facilitate transdermal delivery but also penetrate the intestinal barrier for effective oral delivery of macromolecules. Cai et al.'s team[208] manufactured the intended rocket-inspired effervescent motors (RIEMs) *via* a two-step negative replica molding technique. These patches were composed of sharp needle tips for cargo loading and effective penetration and tail wings for fuel (effervescent powders) storage and perforation prevention (Fig. 11E). Attributed to the incorporated effervescent powders, the RIEMs generated substantial CO_2 bubbles upon exposure to water, which propelled the motors to operate at high velocity. This characteristic extremely facilitated the penetration of adjacent mucosa for *in vivo* drug delivery.

4.6. Others

The effectiveness of drug delivery systems, including hydrogels, scaffolds, and ointments, is frequently affected by multiple matters, such as restricted tissue penetration, inadequate cellular absorption, and diminished bioavailability. Consequently, more complete, integrated, multi-layered, and specifically constructed MNs have been developed to accommodate diverse complex disease states and fulfill a broader spectrum of biomedical applications. Xie's team[209] produced an innovative hybrid-nested scaffold (MQW-CMg-MOF) featuring a nested MN at the base and a cryogel layer (CMg-MOF) atop it, aiming at achieving the efficient treatment of diabetic wounds (Fig. 12A). The MQW MN utilized its microtip to facilitate early mechanical rupture and enhanced the diffusion of vancomycin for efficient biofilm eradication, succeeded by the sequential release of tailored antibacterial (W379) and angiogenic (QK) peptides to avert recurrent infections and foster angiogenesis, respectively. The MN eliminated biofilm and sequentially delivered medications customized for the various healing phases of infected diabetic wounds. Zhou's research[210] developed a grooved MN to improve adoptive T cell therapy for solid tumor treatment (Fig. 12B). The grooved design of the MN was optimized for adequate T-cell loading. Additionally, previous research established a self-locking MN for adipocyte-targeted anti-obesity gene therapy (LMN) (Fig. 12C)[211]. The LMN form uniquely extended from a 2 μm tip to a 340 μm mid-body and thereafter narrows to a 250 μm base. This design yielded a remarkably uniform and accurate rate of skin penetration and adherence. Furthermore, this shape facilitated the distribution of encapsulated chemicals mostly towards the tip, hence improving micro-dose delivery precision relative to traditional MNs. Xu et al.[212] invented a smart hydrothermally responsive MN including a grooved shape for localized tumor therapy (Fig. 12D). The grooved shape on each needle would enhance the directional formulation and melt movement towards the deeper tumor locations by capillary action. Interestingly, Hu et al.[213] presented a thread-structured MN for the treatment of IVDD by mending the injured annulus fibrosus (Fig. 12E). The thread structure design successfully emulated the layered annulus fibrosus structure, resulting in enhanced adhesion. In conclusion, the unique structural design of the MNs significantly enhanced their functionality, facilitating more efficient drug distribution and enabling successful, sequential disease therapy.

5. Living MNs

Cell therapy, mitochondrial transplantation, and organoid transplantation have realized considerable benefits in the management of many diseases, providing optimism for certain ailments previously seen as incurable[214]. Nonetheless, other barriers exist in the delivery of cells and organoids, including viability concerns, permeability issues, and patient adherence difficulties. MNs can preserve cell viability and organoid stemness, thereby achieving superior therapeutic outcomes. Furthermore, certain microbes have demonstrated specific roles in disease therapy. Some bacteria can successfully eliminate pathogenic microorganisms, regulate cellular metabolism, and improve drug penetration by generating gas, thereby offering enhanced therapeutic outcomes. Certain

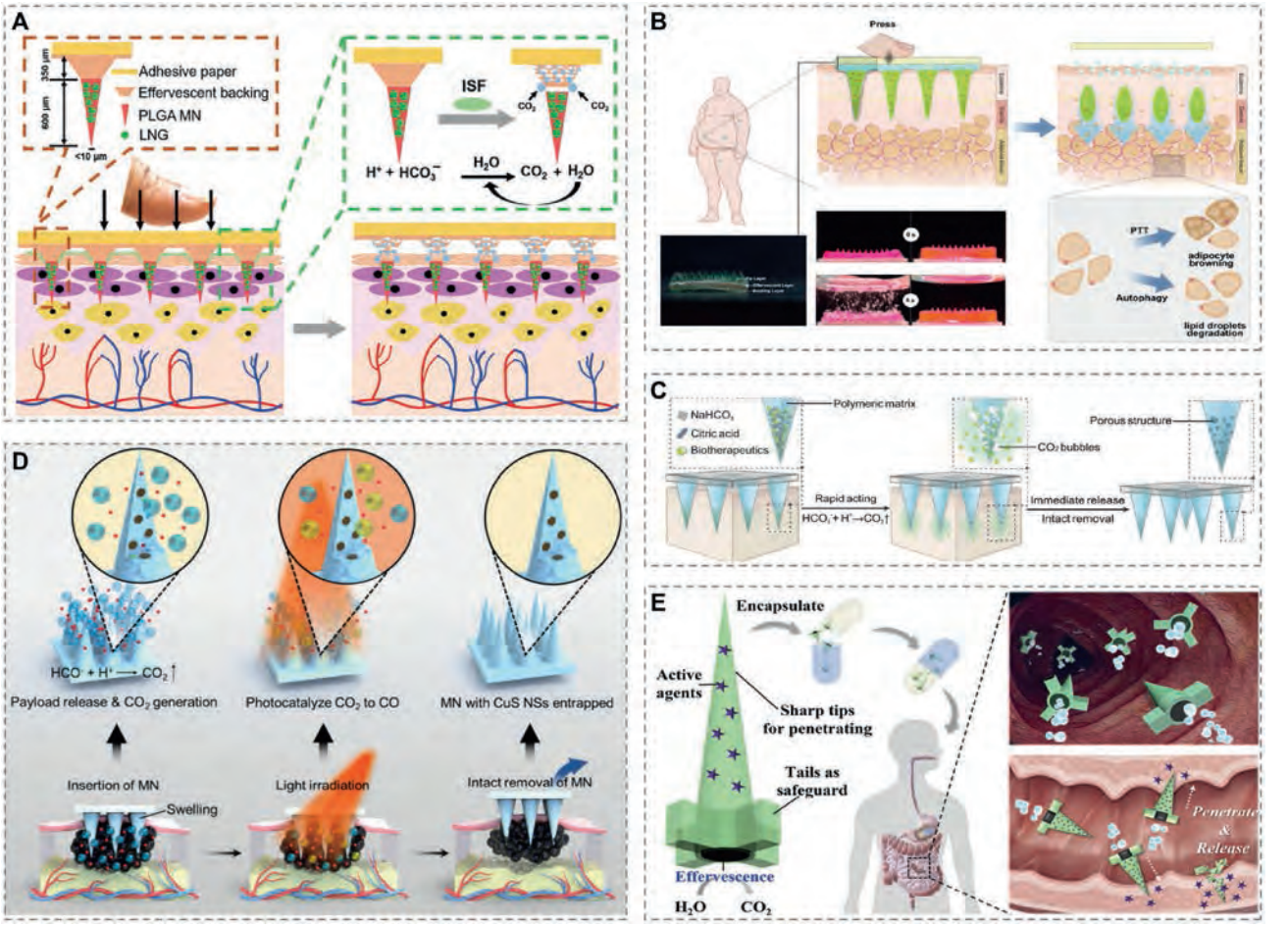

Figure 11 Effervescent MNs for disease treatment. (A) Schematic illustration of effervescent MNs for contraception. Reproduced with permission from Ref. 203. Copyright © 2019, American Association for the Advancement of Science. (B) Schematic representing of the effervescent MN for diet-induced obesity treatment. Reproduced with permission from Ref. 205. Copyright © 2025, American Chemical Society. (C) Schematic illustration of immediate delivery of biotherapeutics *via* the ultrarapid-acting URA-MN patch. Reproduced with permission from Ref. 206. Copyright © 2023, Wiley. (D) Schematic showing of photocatalysis-mediated CO delivery *via* an effervescent MN. Reproduced with permission from Ref. 207. Copyright © 2024, American Chemical Society. (E) Schematic illustration of the rocket-like effervescent micromotors. Reproduced with permission from Ref. 208. Copyright © 2023, Wiley.

algae, including chlorella, possess a significant potential for O_2 generation, rendering them prime candidates for the treatment of diabetic wounds. However, bacteria and chlorella encounter challenges related to inadequate permeability and a propensity to elicit immunological responses. Intelligent living MNs containing bacteria and chlorella can maintain the survival of these microorganisms while integrating them with other therapies to synergistically improve treatment outcomes for diseases. Living MN necessitates specialized matrix materials and fabrication methodologies. Hence, in this section, we summarized the manufacturing progress of living MNs and examined their application and advantages in depth.

5.1. Cell-loaded MNs

Recent advancements in cell therapy offer optimism for diseases that were previously deemed incurable and untreatable[215,216]. For instance, genetically engineered epidermal stem cells can be transplanted to rebuild skin in individuals with epidermolysis bullosa, whereas melanocytes can be transplanted to address vitiligo[217]. DC-based immunotherapy has demonstrated safety as an alternative therapy for melanoma[218]. Chimeric antigen receptor (CAR)-T cells, designed to target specific tumor-associated antigens, have demonstrated significant efficacy in B cell malignancies. At present, these therapeutic cells are administered *via* bolus injection for systemic health conditions (such as cancer) or scaffold transplantation for localized symptoms (such as eczema). However, these approaches struggle to ensure controlled and exact delivery of targeted cells without compromising patient comfort, posing obstacles for their clinical application. Specifically, unlike small molecules and protein therapeutics, the substantial bulk of many medications hinders cellular penetration and diffusion inside specific tissues[219]. MNs for transdermal distribution may address the inherent constraints of cell-based treatments. To transport and administer cells, MNs should preserve the viability of the encapsulated cells and possess sufficient mechanical strength to penetrate the dermis. Consequently, MNs used for living cell delivery require a distinctive design strategy.

Gu's team[219] fabricated a polymeric porous MN (PMN) to retain CAR T cells (Fig. 13A). Biocompatible PLGA was selected

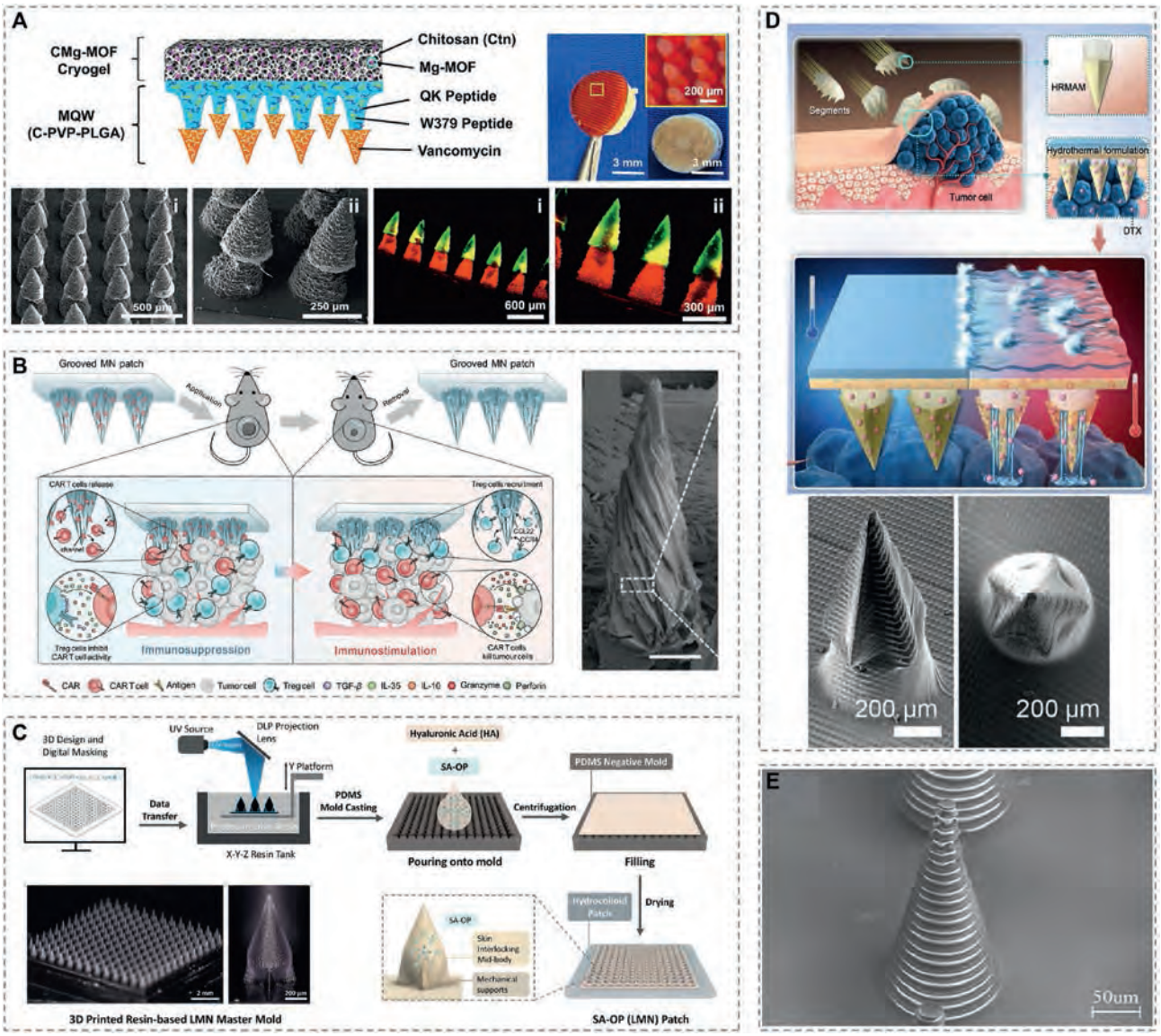

Figure 12 Innovative structure designed MNs for disease treatment and diagnosis. (A) Characterizations of hybrid-nested MN. Reproduced with permission from Ref. 209. Copyright © 2025, Wiley. (B) Schematic illustration of augmented adoptive T cell therapy through a grooved MN. Reproduced with permission from Ref. 210. Copyright © 2024, Wiley. (C) The fabrication method for the self-locking MN. Reproduced with permission from Ref. 211. Copyright © 2024, Wiley. (D) Schematic of the smart hydrothermally responsive MN including a grooved shape for localized tumor therapy. Reproduced with permission from Ref. 212. Copyright © 2023, Elsevier. (E) SEM image of thread-structured MN. Reproduced with permission from Ref. 213. Copyright © 2024, Elsevier.

to prepare porous MNs and load CAR T cells due to the fact that PLGA has adequate mechanical force for implantation into the tumor site. CLSM and 3D reconstruction verified that CAR T cells were located within the internal space of the MN tip. During tumor implantation, the pores of MNs protected CAR T cells from abrasion. Upon insertion, over 50% of the cells were transferred to the tumor within 15 min. More importantly, CAR T cells administered by PMN exhibited more efficient tumor infiltration in comparison to intratumoral injection. Overall, the MN served as a multipoint, dispersed delivery tool for CAR T cell seeding, enhancing T cell infiltration in tumors by mitigating inadequate T cell biodistribution due to physical barriers in solid tumors. This technique can be expanded as a localized therapeutic platform for the delivery of living cells for the treatment of various disorders.

Chang et al.[8] reported the building and proof-of-concept application of cryogenic MNs for the transdermal administration of living cells (Fig. 13B). The MNs were produced using a sequential cryogenic micromoulding process using a cryogenic medium composed of PBS enriched with 2.5% DMSO and 100 mmol/L sucrose, together with pre-suspended cells. This MN could be effortlessly implanted into pig skin and dissolved following the deployment of the cells. In mice, cells administered *via* cryoMNs maintained their viability and proliferative capacity. In murine models with subcutaneous melanoma, the

administration of ovalbumin-pulsed DCs by cryoMNs induced superior antigen-specific immune responses and resulted in reduced tumor growth compared to intravenous and subcutaneous injections of the cells. Therefore, biocompatible cryoMNs may provide minimally invasive cellular administration for various cell-based treatments.

Stem cells have shown efficacy in the treatment of diabetic ulcers (DUs). Xu et al.[40] developed an innovative living MN that encapsulated bioactive platelet-derived growth factor D (PDGF-D) and human ADSCs for DU wound therapy. In contrast to conventional complex stem cell carriers, the MN maintained the survival of encapsulated ADSCs and exhibited sufficient mechanical strength to non-invasively penetrate local skin wounds. This delivery technique demonstrated substantial angiogenesis stimulation and a marked proliferation of ADSCs, indicating its potential utility in DU wound healing and other therapeutic applications in the field of tissue regeneration.

5.2. *Mitochondria-loaded MNs*

Mitochondria are important organelles in eukaryotic cells and play an important role in a variety of metabolic pathways and cellular processes. Mitochondria participate in oxidative phosphorylation, fatty acid oxidation, urea cycle, Krebs cycle, ketone production and gluconeogenesis, and can regulate calcium homeostasis, lipid metabolism, amino acid metabolism, heme biosynthesis and heat production[225]. Therefore, it is very important to preserve mitochondrial homeostasis. Mitochondrial dysfunction can lead to the occurrence of a variety of mitochondrial diseases. Mitochondrial transplantation is an innovative technique to address mitochondrial dysfunction. It restores dysfunctional mitochondria by transplanting normal mitochondria into defective cells. Methods for integrating exogenous mitochondria into recipient cells include direct injection, co-incubation, centrifugation, magnetic mitochondrial transfer, cell-penetrating peptides, biocompatible polymers, photothermal nanoknives, and FluidFM. However, only direct injection is suitable for *in vivo* mitochondrial transplantation among the above methods, and the remaining methods are only suitable for *in vitro* delivery of mitochondria due to technical or immunogenicity and cytotoxicity reasons. Encouragingly, MNs provide a new solution for mitochondrial transplantation. The activity of mitochondria extracted by traditional methods can only be maintained for 1−2 h on ice, while the activity of mitochondria can be extended to seven days after loading mitochondria into dissolvable MNs[226]. Yao and colleagues[220] enclosed stem cell-derived mitochondria-rich EVs in a Decellularized Adipose Matrix (DAM)/HAMA-based MN patch, which efficiently preserved mitochondrial bioactivity, delivered mitochondria to wound tissues, and improved wound healing (Fig. 13C). They validated that intact mitochondria-rich EVs were carried by the lyophilized scaffold material with highly biocompatibility. Meanwhile, gradually degradation property of scaffold material enabled sustainable releasing profile of mitochondria, with approximately 80% of the EVs being released cumulatively in the first 4 days. Additionally, in Dong et al.'s work[227], they encapsulated functional mitochondria into PVA-based MN patch, which not only facilitated the transdermal delivery but also retained the overall structural integrity of mitochondria for at least 3 days at 4 °C and 7 days at −80 °C. In conclusion, MN can be regarded as a versatile delivery vehicle for mitochondria that has shown great promising for treating mitochondrial dysfunction and aging-related conditions.

5.3. *Organoids-loaded MNs*

Decades of research in developmental biology and stem cell biology have boosted the capability to reproduce vital elements of organogenesis *in vitro*. In recent years, significant advancements have been made in harnessing the self-organizing capabilities of pluripotent or adult stem cells to produce organotypic multicellular structures referred to as organoids. Organoids are developing as a potential method for simulating the development, homeostasis, and diseases of numerous human organs due to their capacity to replicate the microarchitecture and functional properties of genuine organs[228]. In this respect, techniques have been established for the *in vitro* creation of organoids that mimic various tissues, such as the intestine, lung, brain, retina, and kidney. These organoids act as robust platforms for mimicking human organ development and chronic diseases. Moreover, organoids may function as tissue sources for personalized regenerative therapies. To date, most existing protocols for organoid generation necessitate the encapsulation of spheroids within biologically derived materials like Matrigel, which are poorly characterized and demonstrate significant lot-to-lot variability, inadequate experimental control, and the inability to separate their biochemical and biophysical properties[229]. Besides, the derivation of Matrigel from neoplastic mouse cells constrains its translational applicability. Significantly, hydrogel-based organogenesis (hydrogel-SC) scaffolds have been created for wound treatment by integrating stem cells with biocompatible materials[230]. Nonetheless, the practical utility of hydrogel−organogenesis complexes has remained limited, including inadequate structural design, hindering precision delivery and substance exchange. Of note, the efficacy of utilizing MNs for the delivery of pharmaceuticals, cell-secreted active substances (such as exosomes and genes), metal ions, gasses, and NPs demonstrate that MNs are regarded as a promising, micrometer-scale, minimally invasive delivery method for organogenesis. MNs can preserve the viability and stemness of organoids while retaining significant mechanical strength[5]. Consequently, MNs encapsulated with organogenesis exhibit significant potential in recent years.

Zheng et al.[5] constructed GelMA-cryoMNs loaded with HF organoids, which effectively facilitated transdermal distribution while preserving the vitality of the embedded organoids. The GelMA-cryoMNs were produced by a sequential cryogenic molding technique based on a balanced proportion of cryopreservation chemicals and GelMA hydrogel (Fig. 13D)[5]. Both *in vitro* and *in vivo*, organoids administered *via* cryoMNs maintain cell survival, self-assembly, and differentiation capabilities. In mice, HF organoid-loaded GelMA cryo-MNs were administered to the superficial dermis, leading to subsequent HF development and the emergence of a series of biomimetic hair tufts that penetrated the skin surface. This work presented a potential technique for biomimetic hair neogeneration characterized by minimal invasiveness, cost-effectiveness, and straightforward production. In addition, Zhao's team[221] utilized microfluidic flow to evenly disperse stem cells spheroids (SPs) into MNs on a specifically engineered microfluidic chip (Fig. 13E). HAMA pregel solutions were injected into the template to encapsulate the SPs and subsequently underwent polymerization through UV light. The SPs in the MN@SPs sustainedly survived and increased the expression of

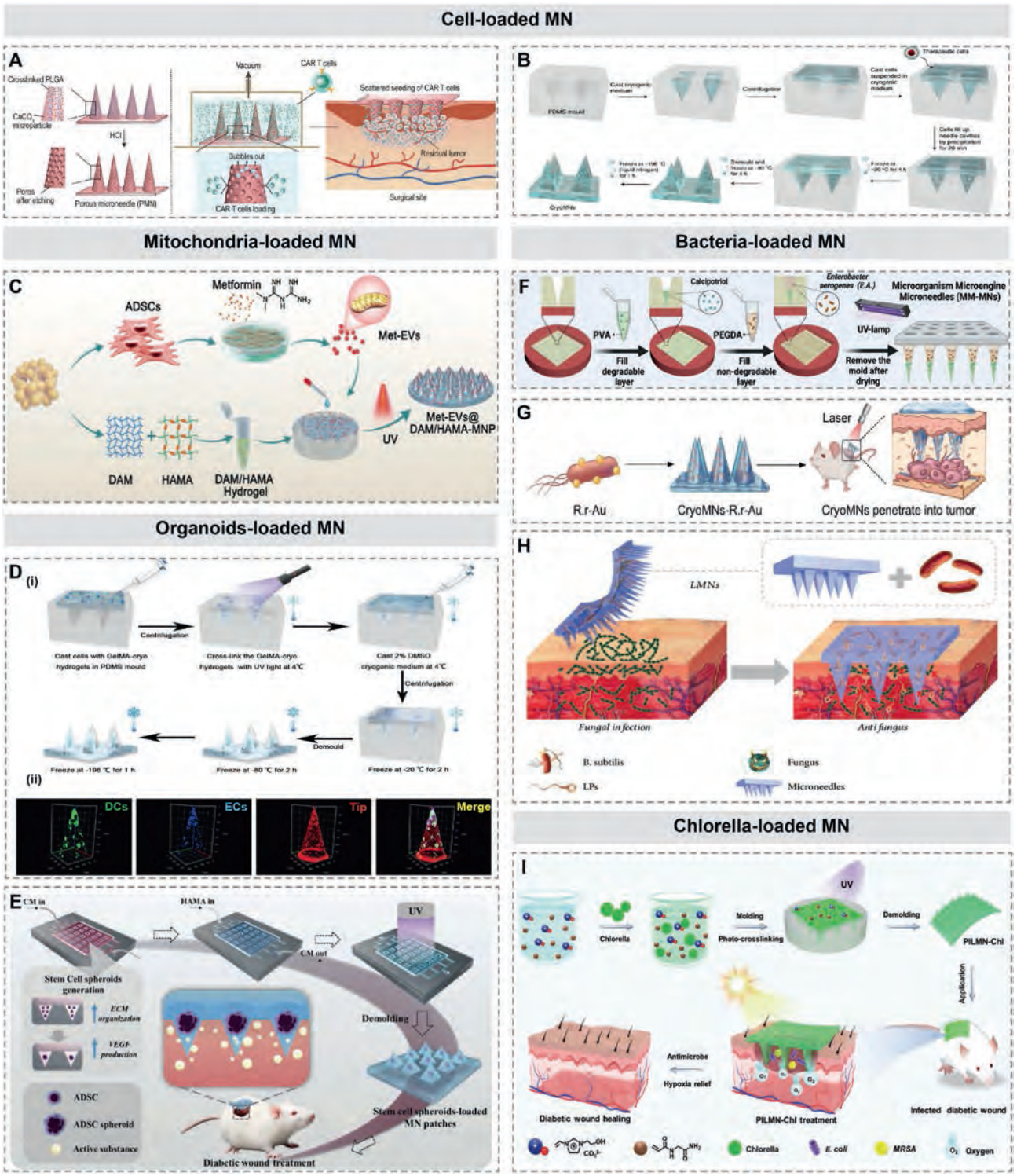

Figure 13 Living MNs for biomedical applications. (A) Schematic representation of PMN manufacture, CAR T cell loading, and the implantation of PMN@CAR T within the tumor bed post-surgery. Reproduced with permission from Ref. 219. Copyright © 2022, Oxford University Press. (B) Schematic of cryoMN fabrication. Reproduced with permission from Ref. 8. Copyright © 2021, Springer Nature. (C) Schematic illustration of the fabrication of mitochondria-loaded MNs. Reproduced with permission from Ref. 220. Copyright © 2024, American Chemical Society. (D) Schematic diagram of hierarchical organoids-loaded cryo-MNs fabrication and programmed freezing process. Reproduced with permission from Ref. 5. Copyright © 2023, Wiley. (E) Schematic representation of the fabrication of microfluidic templated MN@SPs and its operational mechanism for the treatment of diabetic wounds. Reproduced with permission from Ref. 221. Copyright © 2023, Wiley. (F) The preparation procedure of double-layer microbiota-assisted gas dynamic MNs. Reproduced with permission from Ref. 6. Copyright © 2024, Springer Nature. (G) Utilization of CryoMNs-R.r-Au for the transdermal administration of nanogold-engineered *Rhodospirillum rubrum via* optical biotherapy to modify the TME. Reproduced with permission from Ref. 222. Copyright © 2024, Elsevier. (H) Schematic illustration of the

genes that link to ECM organization and pro-angiogenesis. Subsequent animal investigations revealed that the wounds of diabetic mice exhibited enhanced neovascularization, collagen deposition, and tissue regeneration following treatment with MN@SPs.

5.4. Bacteria-loaded MNs

The inherent bioactive behaviors and physiological characteristics of certain living microorganisms present an opportunity for disease treatment. For instance, the inherent competition among beneficial bacteria and other microbes allows dominant bacteria to repel, obstruct, and disrupt the reproduction of other microorganisms while securing living space through rapid, extensive reproduction and colonization, thereby demonstrating a diverse array of bioactivities, including antimicrobial, anticancer, immunosuppressive, and anti-mycoplasma effects[231-233]. Furthermore, several bacteria can modulate the metabolic processes present in the TME, presenting a potential avenue for cancer therapy. Moreover, certain bacteria, like *Enterobacter aerogenes*, can generate gas that may enhance drug penetration into tissues[6]. Nonetheless, living bacterial therapy is frequently suboptimal due to unpredictable bacterial sequelae, inherent bacterial toxicity, restricted medication production, and contraindications with other treatments. Furthermore, colonizing bacteria at the target site and safeguarding them from the immune system poses significant challenges to achieving favorable therapeutic outcomes[234,235]. Consequently, there is a necessity to establish a platform for the efficient administration of alive bacteria for practical therapeutic applications. Numerous investigations have demonstrated that administering living bacteria using MNs can not only preserve their viability but also shield them from the host immune response. Thus, MN-based living bacteria transport presents an innovative framework and solution for on-demand and regulated delivery.

E. aerogenes can produce gas by fermenting many sugars, including glucose, lactose, and sucrose. It mainly resides in the intestines of humans and animals, functioning as a component of the natural flora in the body[236]. Zheng et al.[6] created a living microbacterial MN system featuring an adjustable propelling force that utilized gas-producing microorganisms internally to provide robust gas dynamics (Fig. 13F). These MNs were constructed using *E. aerogenes*-contained PEGDA, demonstrating enhanced properties in sustained gas generation, increased total gas output, and instantaneous release rate relative to metallic substrates. These bacteria sustained remarkable biological activity for several hours post-formation. The sustained gas propulsion force produced by these microbes could exceed 0.04 N, allowing the drug to penetrate the skin into a maximum depth of 1000 μm. In contrast to traditional MNs that depend on passive diffusion for drug administration, the living microbial pneumatic MN microengine system could enhance drug delivery depth by over 200%. In a murine model of psoriasis, substantial amelioration of overall symptoms was noticed following the administration of the medication calcipotriol *via* pneumatic-active MNs.

Rhodospirillum rubrum (*R. rubrum*) is a representative anaerobic photosynthetic bacterium possessing a P870 photosystem that utilizes tiny organic acids as electron donors. Under light irradiation, *R. rubrum* effectively reduces lactate and produces H_2 *via* nitrogenase. H_2 is a therapeutic medical gas, and due to its intrinsic biosafety, it represents a highly promising approach for various ailments[237]. Shi's research[222] employed a sequential cryogenic micromolding technique to fabricate a transdermal therapeutic cryoMN embedded with R.r-Au (CryoMNs-R.r-Au) to enable the safe and efficient *in situ* administration of living bacterial therapeutics (Fig. 13G). Specifically, they suspended bacteria in the optimum cryogenic medium (5% glycerol in PBS) and poured the combination into a negative polydimethylsiloxane mold. Following low-speed centrifugation and freezing, bacteria were introduced into the tip cavities. Long-term storage tests showed that the survivability of R.r-Au in CryoMNs exceeded 90%, therefore substantially enhancing bioavailability. CryoMN demonstrated adequate mechanical strength, achieving 0.2−0.3 N per needle. Following insertion into mouse skin, they immediately disintegrated and effectively delivered the bacterial medicines. The integration of laser biotherapy and CryoMNs had enabled minimally invasive *in situ* administration of alive bacterial therapeutics.

Bacillus subtilis 3610 (*B. subtilis*), a species of gram-positive bacterium, is naturally present on human skin. They demonstrate antifungal efficacy by secreting substantial antimicrobial compounds and show significant potential for the treatment of fungal infections. Wang et al.[223] encased *B. subtilis* within photocured MNs composed of PEGDA and PVA (Fig. 13H). CLSM images revealed that *B. subtilis* maintained vitality during UV irradiation. Furthermore, the integrity of the MNs was well-preserved in PBS (pH 7.4) after Days 1, 3, and 7. These MNs effectively generated and released many potential antifungal agents, including lipopeptides, directly retrieved proteins linked with fungal cell surfaces, compromised cell walls, and eradicated the target fungi. Consequently, LMNs demonstrated exceptional antifungal efficacy. In summary, the combination of living bacteria and MNs demonstrated distinctive efficacy in treating fungal infections.

5.5. Chlorella-loaded MNs

Diabetes can hinder the angiogenic capacity of wound tissue, leading to persistent ischemia and sustaining a hypoxic environment for the wound. The hypoxic condition may significantly impede wound healing by exacerbating tissue necrosis and interrupting critical processes, such as ECM formation and wound re-epithelization[238,239]. Mitigating or eradicating hypoxia can enhance the microenvironment and facilitate wound healing, addressing an urgent therapeutic need in the management of chronic diabetic wounds. *Chlorella* is a type of algae that can generate O_2 *via* photosynthesis, exhibiting a far greater O_2-producing capacity than plant cells. They are extensively utilized in pharmaceutical applications due to their nutritional value, therapeutic potential, nontoxicity, and low immunogenicity[240]. Notably, due to their superior O_2-generation capacity, they show significant potential in the treatment of infected diabetic wounds. Nonetheless, the limited tissue penetrating ability of chlorella impedes the advancement of chlorella-based treatments for infected diabetic wounds (IDWs). The MN, composed of sharp

application of the LMNs for fungal infection treatment. Reproduced with permission from Ref. 223. Copyright © 2020, American Association for the Advancement of Science. (I) Schematic illustration of the synthesis of PILMN-Chl. Reproduced with permission from Ref. 224. Copyright © 2024, Wiley.

needles, efficiently breaks the epidermal barrier to deliver the encapsulated therapeutic agents *in situ*. Consequently, the MN offers a practical approach for chlorella delivery.

In a study of Wang et al.[7], they developed a living micro-ecological MN (LMMP) that could improve IDW sites' O_2 levels and lower inflammation and bacterial infection. A flexible sheet-like hydrogel substrate of these patches was produced by cross-linking oxidized HA and gallic acid-modified carboxymethyl chitosan *via* Schiff base reaction. Subsequently, chlorella-integrated MN were fabricated on hydrogel substrate using the photo-cross-linking of HAMA-*Chlorella* mixtures *via* polymer casting. High-resolution SEM images revealed that chlorella were clearly localized at the tips of MNs. Additionally, *Chlorella* remaining in the needle tips could be released in response to hyperglycemia and increased ROS stress due to the utilizing of gallic acid. Significantly, the chlorella produced substantial O_2, ameliorating the hypoxic condition of the IDWs and subsequently activating the related pathways in fibroblasts and endothelial cells, which facilitated tissue repair and wound vascularization. Gao et al.[224] conducted an MN system (PILMN-Chl) that could *in situ* and long-term generate O_2 *via* photosynthesis (Fig. 13I). The PILMN-Chl was synthesized *via* photo-crosslinking *N*-(2-amino-2-oxoethyl)-2-propenamide and 3-(2-hydroxyethyl)-1-vinylimidazolium bromide with live chlorella, subsequently incorporating CO_3^{2-} through anion exchange to serve as a stable carbon source for chlorella's photosynthesis and ongoing O_2 production. Encouragingly, this system could constantly generate O_2 for up to 30 h. PILMN-Chl showed superior efficacy in enhancing chronic diabetic wound healing.

6. Wearable MNs

The rising demand for healthy lifestyles and well-being has propelled the advancement of wearable biosensor technologies. The comprehensive advancement of wearable devices allows for the continuous and non-invasive monitoring of vital signs, physiological signals, and biomarkers in biological fluids[241]. Furthermore, they provide the identification of metabolic and electrophysiological signals, offering a non-invasive diagnostic alternative that eliminates the necessity for blood draws. The integration of reading systems and smartphone sensors has markedly enhanced the accessibility of wearable biosensors, consequently facilitating individualized medical services[20].

Wearable MNs are devices that integrate wearable biosensors into MNs. They have garnered heightened interest in recent years from both academic and commercial sectors. In contrast to traditional wearable devices that depend on surface contact, which often cause discomfort and are susceptible to detachment or signal disruption, MN-based wearable systems adhere tightly to the skin and penetrate solely the superficial layers. Additionally, wearable MNs offer the advantage of controlled drug release, enabling precise and on-demand dose control[43]. Considering these benefits, MNs provide an optimal option for minimally invasive diagnostics of diverse diseases, such as cancer and autoimmune disorders. In terms of therapeutic drug delivery, wearable MNs offer a sustainable, controllable, non-invasive, and highly compliant closed-loop therapeutic diagnostic strategy.

Furthermore, AI represents a machine's capacity to communicate, think, and function autonomously in both familiar and unfamiliar contexts, similar to human behavior. Nowadays, AI are frequently used interchangeably with "machine learning" or "deep learning", and the latter is regarded as a specific subset of machine learning. Machine learning indicates algorithms and statistical models that derive knowledge from labelled training data, enabling them to identify and deduce patterns[242]. AI technology creates adaptive biosensing systems capable of detecting subtle changes in biomarker levels, predicting disease progression, and providing real-time feedback to users[44]. The combination of AI and wearable MNs indicates a significant advancement in wearable diagnostic devices, enabling the development of more intelligent, responsive, and user-centered health monitoring platforms[243]. AI-equipped wearable biosensors are crucial for enabling users to analyze and derive advantages from complex, multi-faceted data. Specifically, the data collected by wearable MN sensors may be affected by noise, drift, and patient-specific variations, while AI can quickly denoise and calibrate these signals through machine learning and deep learning methods, and transform them into actionable insights, so as to achieve more timely and informed decisions. Moreover, AI-driven models proficiently detect nuanced trends in time-series biosignals, facilitating the modification of personalized treatment regimens in response to continuous physiological alterations. Consequently, AI supports closed-loop MN therapies capable of administering medications in reaction to fluctuations in biosignals[44]. These AI-enhanced MN wearable devices are expected to fully unleash the potential of next-generation biosensing, providing unprecedented opportunities for early disease detection and personalized treatment.

This section presented wearable MNs utilized for drug administration and diagnostic evaluation by thoroughly examining their design tactics, mechanisms of action, and application effects.

6.1. Wearable MNs for drug administration

Wearable MNs have been extensively utilized in the management of pain, cancers, and diabetes due to their ability to be remotely controlled, release drug in a timely and exact manner, and provide long-term consistent drug delivery. Wearable MNs enable precise and on-demand drug delivery by utilizing external stimuli such as light, temperature, magnetism, pH, and electrical current[244]. In the following content, we classify wearable MN devices based on their drug release profiles and systematically introduce their working mechanisms and drug delivery efficacy.

Firstly, the combination of MNs and iontophoresis (ITP) improves transdermal delivery by combining electrical stimulation from ITP with the microchannels generated by MNs to increase drug penetration. ITP uses a low-intensity current (<0.5 mA/cm^2) to deliver charged drug molecules into the skin. Jiang's team[244] demonstrated an integrated ITP-driven fiber-based MN patch (IFMP) controlled by a smartphone for precise, long-lasting lidocaine transdermal delivery (Fig. 14A). The transdermal drug delivery patch was made up of six components: Ag/AgCl electrodes on flexible polyimide, an enclosed shell, cathode gel, drug-loaded conductive gel, MN patch grooves, and fiber-based dissolving MNs. When the patch was placed to the skin, the MNs penetrated the outer layers while the cotton fiber substrate absorbs the medication solution from the hydrogel. When an external power source was connected, current flows from the flexible electrode's anode to the drug-loaded conductive hydrogel, fiber substrate, skin, and cathode gel before exiting the flexible electrode's cathode. This resulted in a completely conductive circuit for iontophoretic drug delivery. Furthermore, this device was

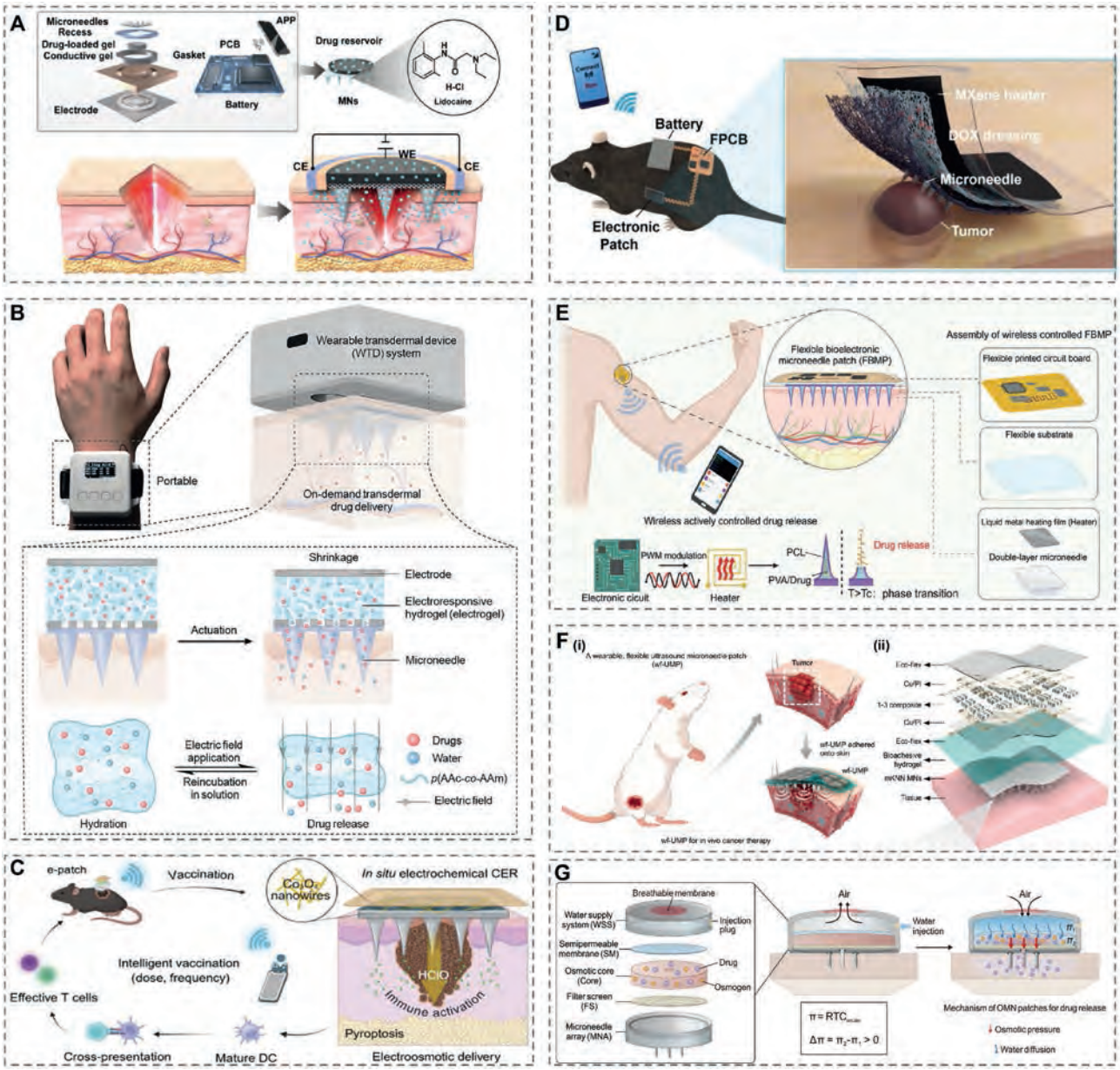

Figure 14 Wearable MNs for drug administration. (A) Schematic of IFMP and its drug delivery mechanism. Reproduced with permission from Ref. 244. Copyright © 2024, Springer Nature. (B) Schematic illustration WTD system incorporated with MNs. Reproduced with permission from Ref. 245. Copyright © 2025, Elsevier. (C) Schematic showing of electrochemical MN-induced HClO-driven immune activation. Reproduced with permission from Ref. 246. Copyright © 2025, American Chemical Society. (D) Schematic representing of a stretchable MN-integrated electronic MN for wearable cancer therapy. Reproduced with permission from Ref. 248. Copyright © 2025, Wiley. (E) Schematic illustration of the designing and operation principles of FBMP. Reproduced with permission from Ref. 249. Copyright © 2025, Wiley. (F) Schematic illustration of wf-UMP application for cancer therapy. Reproduced with permission from Ref. 250. Copyright © 2025, Springer Nature. (G) Schematic of the components of the OMN patch and the mechanism of osmotic pressure-triggered drug release. Reproduced with permission from Ref. 251. Copyright © 2024, American Chemical Society.

Bluetooth-connected to a mobile application, allowing for a real-time visual curve of drug dosage, providing immediate onset and long-term pain relief. Similarly, Gu's team[245] developed a wearable transdermal device (WTD) system for diabetes treatment that allowed for controlled distribution based on blood glucose levels, eliminating the need for numerous injections (Fig. 14B). This system consisted of a portable iontophoresis device integrated with an electroresponsive hydrogel (electrogel) and polymeric MNs. Upon activation by a preset current from the WTD, the macroporous electrogel contracted to regulate the release of the drug solution and facilitated its transport into the skin through microchannels created by MNs, therefore enabling effective, on-demand transdermal drug delivery. This device tackled the restricted drug loading capacity of MN systems, offering a highly efficient, minimally invasive, and on-demand solution for drug delivery. More intelligently, Zou et al.[246] introduced an

electrocatalytic regulatory system for chemical messengers *via* a bioelectronic (e-patch) (Fig. 14C). This e-patch combined electrocatalytic HClO production with electroosmotic flow-enhanced transdermal administration to facilitate *in situ* electrochemical tumor vaccination. The e-patch utilized Co_3O_4 nanowires as electrocatalysts for the chlorine evolution reaction to locally produce HClO. Leveraging the electroosmotic flow mechanism, the electrogenerated HClO was unidirectionally and continuously administered into tumor tissues through porous needle tips, offering a non-invasive and confined alternative to improve the spatial accuracy of electrochemical message delivery. Furthermore, this electro-vaccine was wireless manipulated from a mobile phone, enabling exact control of dosage and frequency, hence improving patient compliance and portability. While MNs and ITP techniques have increased transdermal drug delivery efficiency, obstacles such as skin flexibility, high electrical resistance of the stratum corneum, and the need for an external power supply limit their effectiveness in treating deep-seated diseases. In order to address these limitations, Qian et al.'s study[247] presented a wearable, self-powered, multi-component drug-loaded electronic MN patch (mD-eMN) to accelerate tissue repair of inflammatory skin disorders. Specifically, this system was integrated with remodeled metal MNs loaded with multi-component chemical drugs and flexible TENGs. Owing to the pulsed electrons originating from the TENG, this wearable patch realized an efficient penetration into cell body and specific immunomodulation.

Secondly, an electronically controlled and wearable MN can successfully integrate hyperthermia with regulated drugs delivery. Yang et al.'s work[248] developed a heater integrated wearable MN. Specifically, the MN featured a flexible heater made of 2D MXene with wrinkled microstructures to reduce resistance fluctuations and temperature variations during stretching (Fig. 14D). Additionally, an extra element of microfiber textile dressing was adorned with phase-change microcarriers, facilitating the regulated release of anticancer therapeutics following thermal activation. Furthermore, the patch was linked to a flexible integrated circuit and a lithium-ion battery, forming an untethered electronic system that executed therapeutic commands sent remotely from a smartphone. Therefore, the stretchable MN-integrated electrical patch exhibited considerable effectiveness in suppressing cancer proliferation. Similarly, Jin et al.'s study[249] introduced a flexible bioelectronic MN (FBMP) that integrated a flexible printed circuit board (FPCB), a eutectic gallium-indium (EGaIn) heating film, and dual-layer MNs comprising a PVA core and a PCL shell (Fig. 14E). This design enabled real-time modulation of the heat response rate by smartphone-controlled Bluetooth, facilitating rapidly drug release within 2 min or a continuous release over 10 h. This study presented a versatile, global electronic MN platform with considerable promise to enhance precision and personalized therapy through customizable, dynamically regulated drug delivery.

The wearable MNs can provide consistent and efficient therapy or monitoring over a period without requiring coupling agents or external fixation by integrating lead-free ultrasound transducers and biodegradable MNs. For example, Xue and colleagues[250] manufactured a cohesive wearable flexible ultrasonic MN (wf-UMP) (Fig. 14F). The wf-UMP implemented a comprehensive bioelectronic concept that incorporated a stretchable lead-free US transducer array for acoustic emission, a bioadhesive hydrogel elastomer for strong adhesion and acoustic coupling, and a dissolvable MN infused with biocompatible piezoelectric NPs for painless drug delivery and ROS generation. When coupled with anti-PD1, this device exhibited synergistic therapeutic activity, suppressing distant tumor development and recurrence.

In addition to external stimuli, drug release from wearable MN devices may also be osmotically mediated. Gu's team[251] constructed a wearable osmotic MN (OMN) patch that enables sustained drug administration for a minimum of 24 h without the use of electronic components (Fig. 14G). The OMN patch consisted of multiple unique subcomponents: a water supply system; an osmotically active unit featuring a semipermeable membrane, an osmotic core containing the medication and osmogen, and a filter screen; and a MN array unit. The drug in the osmotic core was dissolved to form a saturated solution, thereby leading to an osmotic pressure difference on both sides of the semipermeable membrane. The osmotic pressure difference formed by this dissolution drives the drug solution to penetrate the skin through the hollow MN array. This approach achieved continuous release of the small-molecule chemotherapeutic drug cytarabine, and offering a novel strategy for reliable high-dose drug delivery with convenience and safety.

In summary, wearable MNs address the challenges of inadequate drug loading capacity, restricted penetration depth, and the intricacies of controlled-release formulations in MNs, providing an innovative option for the accessibility and cost-effectiveness of cancer and diabetes treatment.

6.2. Wearable MNs for diagnosis and monitoring

MN-based electrochemical sensors have been developed to facilitate continuous health monitoring and molecular-level illness diagnosis through the utilization of chemical markers. Minimally invasive sensing devices facilitate the real-time acquisition of critical diagnostic information by persistently accessing the dermal ISF through swellable or porous hydrogel needle tips. Furthermore, the MN, comprising many individually addressable sensing electrodes functionalized with various receptors, may acquire significant dynamic chemical data by simultaneously detecting numerous ISF indicators[252]. In addition, to mitigate the effects of bias, location, and individual variances in the perception of external stimuli and enhance feature recognition rates, wearable MNs for diagnosis and monitoring are also integrated with AI technology. To date, wearable MNs are mostly utilized for the control of diabetes and associated cardiovascular concerns.

Wang's team[253] combined the rich multiplexed chemical sensing capability of MN sensor patches with crucial physical sensors to create a single flexible platform (Fig. 15A). The hybrid monitoring system incorporated a multiplexed MN that concurrently monitors various interstitial fluid chemical markers (glucose, alcohol, and lactate) through specific oxidase-based recognition processes and amperometric signal transduction. Meanwhile, this wristband device utilized a soft ultrasonic sensor array to detect essential physiological data such as blood pressure and heart rate in real-time on a single soft wristband. This multimodal platform offered continuous, complete metabolic and cardiovascular monitoring, significantly enhancing tailored diabetes care, sustaining glycaemic control, and warning to cardiac dangers. Yang's study[254] presented a wearable dual-modal MN that integrated a surface-enhanced Raman scattering (SERS) MN with flexible electronics for the prehospital diagnosis of acute MI (Fig. 15B). The MNs was seamlessly incorporated into a stamp-sized adhesive bandage, supplemented by a smartphone

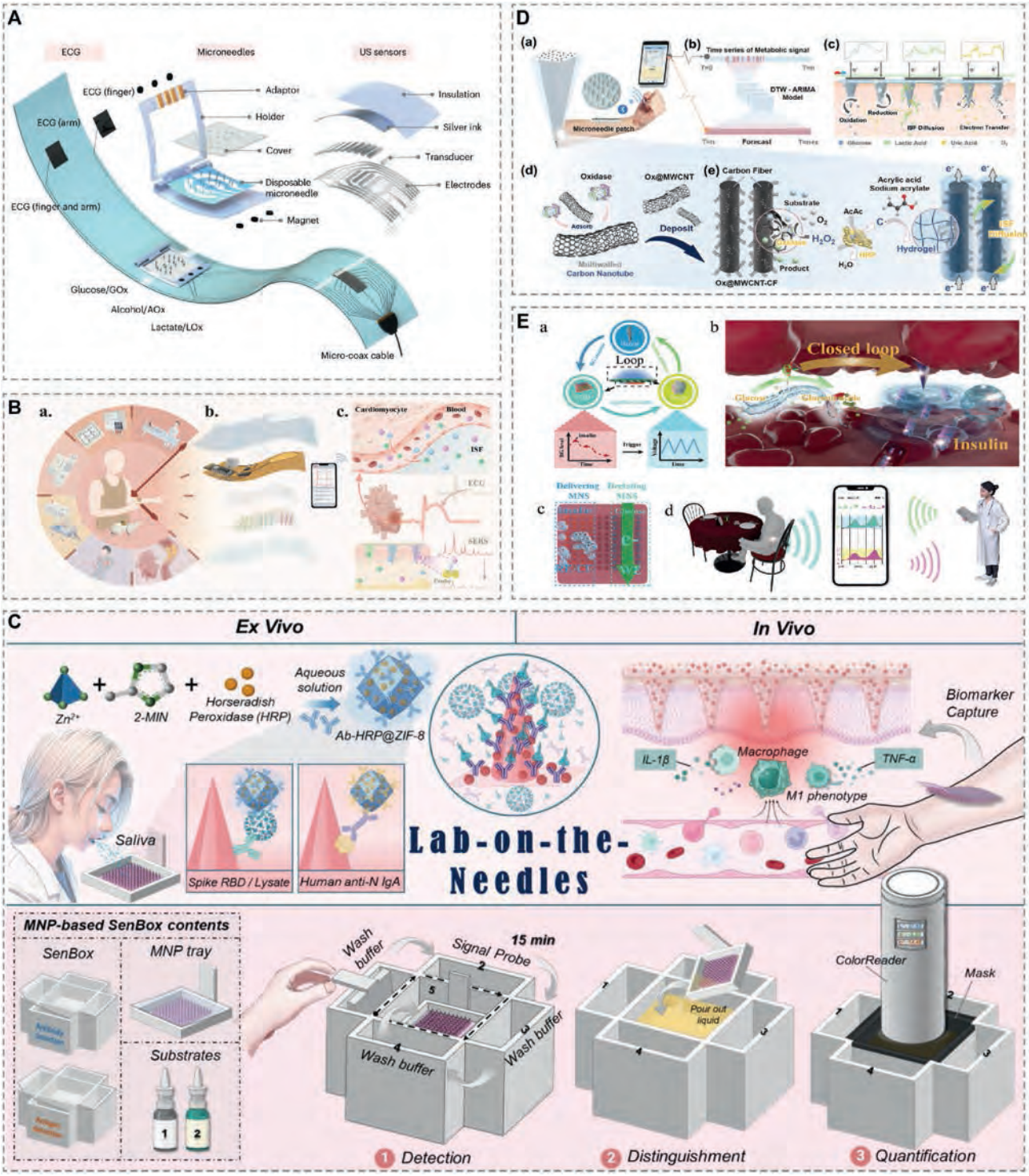

Figure 15 Wearable MNs for diagnosis and monitoring. (A) The fabrication of the multimodal BLUE platform. Reproduced with permission from Ref. 253. Copyright © 2025, Springer Nature. (B) Schematic illustration of wearable e-SERS MN. Reproduced with permission from Ref. 254. Copyright © 2025, American Chemical Society. (C) Schematic of the MNP-based SenBox for protein biomarker detection. Reproduced with permission from Ref. 28. Copyright © 2025, American Chemical Society. (D) Illustration of Gel MNs bioelectrodes system. Reproduced with permission from Ref. 255. Copyright © 2025, Wiley. (E) Principle and structural schematic of a MN-based closed-loop system for the treatment of diabetes. Reproduced with permission from Ref. 256. Copyright © 2023, American Chemical Society.

application for data display and real-time analysis. As a result, this MN decreased the time necessary for identifying ischemia to 50 min post-onset.

In addition to the detection of glucose and its metabolism, as well as inflammatory cytokines, wearable MNs are employed to identify protein biomarkers. The researchers integrated

horseradish POD into ZIF-8 (HRP@ZIF-8) to build a sensitive and stable signal probe, thereby improving the limit of detection for various target protein biomarkers and significantly expediting the biomarker detection process (Fig. 15C)[28]. Furthermore, they accomplished homogeneous deposition of gold NPs (AuNPs) on MNs by a layer-by-layer technique, thereby enabling the self-assembly of antigens or antibodies on the MNs. Utilizing clinical saliva and sputum samples alongside an inflammation rat model, they illustrated that the MN-based sensing box facilitated ultrasensitive and quantitative assessment of diverse protein biomarkers *via* a simple stick-and-peel method succeeded by on-needle analysis.

The forthcoming advancement in MN-based diagnostic systems incorporates the application of modern AI techniques to improve their diagnostic proficiency. AI-driven systems show great performance in enhancing data gathering, signal processing, and analysis, thereby facilitating more precise and individualized health insights. Integrating AI with MN sensors establishes an adaptive biosensing system that benefits from detecting minor fluctuations in biomarker levels, forecasting disease progression, and providing real-time feedback to users[44]. For instance, Guo et al.[255] designed a gel MN bioelectrode that initiates a rigid gel shell array from aligned carbon fibers through interfacial enzymatic polymerization, ensuring the complete encapsulation of three oxidases and efficient substrates, thereby achieving trace detection of glucose, lactic acid and uric acid (Fig. 15D). Their design could accurately detect stimuli such as food intake and exercise, thus allowing accurate prediction of biomarker dynamics in the next 20 min. This property was achieved by validating the integration of data acquisition and the AI-assisted analysis system in diabetic rats. Specifically, they constructed a machine learning model that integrated the dynamic temporal warping (DTW) algorithm with the autoregressive integrated moving average (ARIMA) model to detect stimulus events and forecast signals. The comparison of the test samples of lactic acid and uric acid over 180 min with the reference template indicated that the DTW algorithm effectively identifies feature alterations induced by similar stimuli, and the accuracy of singularity recognition was enhanced by the usage of templates. In addition to predict dynamic of biomarkers, the incorporation of AI technology and wearable MNs facilitated closed-loop system, making the right and intelligent decisions for the daily management of disease management. For example, Luo et al.[256] designed a three-component integrated closed-loop minisystem for diabetes management (Fig. 15E). It was specifically integrated with a MN glucose sensor for blood glucose detection, an ultrasonic pump utilizing a piezoelectric ring and a steel sheet for insulin delivery, and a printed circuit board (PCB) with an algorithm based on suspension control. Upon detecting elevated interstitial glucose levels, the closed-loop control algorithm activated the ultrasonic pump to administer insulin into the ISF *via* the hollow channel of the PLA MNs. More interestingly, this system could transmit daily blood glucose readings and the quantity of administered insulin to a mobile application, reliably tracking and recording swings in glucose levels. Furthermore, the data could be transmitted to a health database cloud storage, which can develop a rational therapeutic regimen and offer a nutritional management plan for physicians or patients themselves. In summary, the integration of this AI technology has opened a new paradigm for the development of intelligent diabetes management systems. Similarly, Liu et al.[257] created an MN patch comprising a graphene composite ink-printed sensor, a PEG-functionalized electroosmotic micropump, a polystyrene-based hollow needle, and a PCB for accurate and intelligent regulation of the sensor to monitor interstitial glucose and administer insulin *via* the hollow channels. The PCB was connected to the computer *via* a USB cable. Users could set the threshold and operating potential of the biosensor and micropump on the software interface of the computer, and check the current value detected by the biosensor. If the measured glucose level exceeded the threshold, the PCB automatically started the electroosmotic micropump, and the insulin solution stored in the drug reservoir was released for 10 min, and quickly reached the interstitial fluid *via* the hollow channel of the MNs. The sensor was then restarted to detect interstitial glucose. The device alternated between glucose sensing and insulin delivery until the detected glucose concentration reached a threshold. The above function was mediated by an alternative two-step control mode. Overall, the integration of AI algorithms effectively regulating blood glucose levels in diabetic rats with an autonomous closed-loop system.

In summary, wearable MNs designed for diagnosis and detection address the challenges of discomfort, bulkiness, and signal instability inherent in conventional testing procedures. Simultaneously, its integration with AI yields more precise and tailored health insights. These innovative MN devices provide remarkable benefits regarding precision, comfort, and user-friendliness.

7. Conclusion, challenges and future perspectives

7.1. Conclusion

The emergence and development of intelligent MNs have provided a new paradigm for the prevention, diagnosis, treatment, and ongoing monitoring of diseases. The payload that intelligent MNs can carry is diverse. Specifically, they can efficiently deliver or absorb various chemical and biological substances from ISF, including various small molecule compounds, biomacromolecules, cells, and microorganisms. Through the selection and structural design of MN tips and backing materials, as well as the regulation of the types of substances encapsulated in the tips, intelligent MNs can not only serve as a device for delivering substances firmly fixed at the application site but also engage in chemical reactions with the numerous molecules present in the skin or tissues. The use of these MNs enables the sequential, cascading, and controlled release of various payloads. These characteristics enable intelligent MNs to fulfill the primary objective of drugs delivery: improving efficacy and minimizing toxicity. Intelligent MNs have exhibited remarkable potential for application in vaccine delivery, cancer therapy, immunotherapy, tissue regeneration, and glucose regulation and diagnosis.

7.2. Challenges

Intelligent MNs display a transformative advancement in the field of biomedical interventions. Despite the increasing research on the design and application of intelligent MNs, they still face significant obstacles to clinical success. According to data from the clinical trial database (www.clinicaltrials.gov), approximately 69 MN products are currently undergoing clinical trials, primarily focusing on vaccination, wound healing, diabetes, and psoriasis. In clinical trials, MNs have been mainly used for simple sampling and detection, or for drug delivery after dissolution, while the

application of multi-functional, complex design and integrated close-loop devices is lacking. The clinical implementation of MN products still needs to overcome several key challenges.

For bio-inspired MNs and MNs with special structural designs, the limited drug loading and large-scale consistent production and manufacturing are major challenges that need to be faced. One approach to address the issue of restricted drug loading is to enhance the drug quality, for instance, by encapsulating solid drug powder at the needle tip or incorporating it with wearable devices to create a drug reservoir, while another method involves increasing the quantity of needle tips[258]. The unique structural design of MNs has posed challenges in manufacture and manufacturing. The existing techniques for MN fabrication include hot embossing, micromolding, thermal drawing lithography, magnetorheological lithography, laser drilling, and 3D/4D printing[259]. In contrast to conventional production techniques, 3D printing technology can fabricate any intricate geometric object with consistent quality. Besides facilitating large-scale printing, 3D printing technology is highly customizable and applicable for individualized medicine therapy. Moreover, 3D mechanical manufacturing diminishes human error, leading to enhanced repeatability[258]. Nonetheless, the fabrication of intricate structures (*e.g.* bee-inspired barbed MNs) poses challenges even for conventional 3D printers (static printing). In most cases, they are virtually impossible to reproduce using replicative molding techniques. The matter may be addressed by the advancement of 4D printing, wherein materials with pre-defined geometry or functionality are activated by external stimuli. Consequently, we believe that 3D and 4D printing will significantly enhance the production and fabrication of MNs including unique structural designs.

Bioactivity and immunogenicity concerns are the obstacles that should be addressed for the clinical advancement of enzyme-loaded intelligent MNs and living MNs. To sustain the functionality of biological enzymes, cells, organelles, and microbes encapsulated in living MNs, it is imperative to develop superior biocompatible materials. The application and development of living MNs are significantly constrained by their inherent constraints, which are represented for the scarcity of biocompatible materials, the specialized production process of frozen MNs, and the requisite storage conditions. The design of special structures of MNs can improve the survival rate of organisms in living MNs to a certain extent, such as promoting cell absorption of nutrients by increasing the porosity of porous MNs or designing groove structures to promote cell loading. Meanwhile, the immunogenicity problems associated with transdermal administration of cells and microbes need to be considered. To diminish immunogenicity and enhance the safety of intelligent MNs, it is preferable to collect live cells and organelles from the body for loading into the needle tip. Simultaneously, it is imperative to consider sterile production and radiation sterilization technologies to guarantee the sterility of intelligent MNs[258].

One of main challenge for closed-loop therapeutic systems utilizing wearable MN devices is the delicate "sense-and-act" mechanism, which is attributed to that minor alterations can result in erroneous dosing protocols, potentially leading to life-threatening complications for the user[43]. Currently, the detection principles for chemical molecules (such as glucose, insulin, lactic acid, cortisol and cytokines) in ISF are limited. There is an urgent need to develop MN devices based on novel detection principles to achieve real-time monitoring of multiple analytes throughout the body. At the same time, the restricted volume of ISF that can be harvested, along with the intrinsic concentration disparities of macromolecules in blood and ISF, presents challenges for the closed-loop treatment of wearable MN devices, necessitating the advancement of monitoring techniques with reduced detection thresholds and enhanced sensitivity. The integration of wearable MN devices with AI offers a feasible remedy to the aforementioned constraints. MN devices can integrate AI-driven calibration models to improve the accuracy of biomarkers, especially to address the time lag effect in ISF-glucose correlation. AI-integrated MN wearables provide real-time data processing, predictive analytics, and adaptive treatment modifications, enabling personalized, patient-centered diagnostics[44]. In addition, the wearer's sweating, exercise and other conditions also need to be considered, which will seriously affect the adhesion and comfort of the MN wearable devices.

7.3. Future perspectives

7.3.1. Integration of MNs with material science

The biological function of MNs significantly depends on the choice of materials. Firstly, the type of material is related to the mechanical strength and adhesion properties of the MNs. By adjusting the type of material, it is possible to impart controllable mechanical strength and Young's modulus to the needle tips, while also regulating the adhesion of the MNs to tissues. These properties enable them to be suitable for various tissues and organs, thereby expanding their application scenarios. Moreover, the material of the needle tip is closely related to drug release behavior. By regulating the types and proportions of materials, precise control over the drug release rate, release sequence, and penetration depth can be achieved. In addition, the development of responsive materials has also paved the way for the manufacturing of intelligent responsive MNs. More importantly, recent research has established a materials library to screen some novel materials for use as the tips or backing of MNs. In addition to providing support and a matrix, these materials also possess specific physiological functions, such as activating immune responses, inhibiting tumor growth, and promoting tissue regeneration. Moreover, the arrangement and 3D structure of the needle tip material significantly influence the activity of the payload contained within it. At the same time, progress in materials science can propel the advancement of wearable MNs. For instance, recent groundbreaking developments in nanosensors have resulted in the creation of various wearable MN devices for closed-loop diagnostics. In summary, paying attention to advancements in materials science, whether through the discovery of novel materials, the modification of existing ones, or the exploration of their new biological functions, is of transformative importance for the production of intelligent MNs.

7.3.2. Integration of MNs with engineering

The restricted drug loading capacity and the challenges of large-scale batch production have consistently hindered the clinical translation of MNs. Conventional techniques enhance drug loading capacity by increasing the number and length of the MNs. However, the benefits of this approach are limited. Novel strategies have been devised to address this issue by engineering the structure of the MNs. Recently, researchers developed dissolvable MNs including hollow chambers, enabling the direct incorporation of drug powder into these chambers, thus significantly enhancing the drug load. In addition, the porous and hollow structures of the needle tips also facilitate drug loading and delivery. Moreover,

specially shaped needle tips (for example, those inspired by the shapes of natural organisms) enhance the efficacy of the medication by improving adhesion or penetration. The unique structural design incorporates knowledge of engineering, facilitating the development of intelligent MN platforms characterized by high drug loading capacity, robust mechanical performance, and diverse functionality. On the other hand, the uniform and large-scale production of MNs relies on the integration of engineering. Traditional MN manufacturing methods, such as micro-molding, typically require complex steps like centrifugation and vacuum suction, which are not conducive to large-scale production. To overcome these obstacles, advancements in manufacturing technologies, such as 3D printing, or precision coating, will ensure that MNs can be produced efficiently, reliably, and economically. Overall, the integration of MN design and casting with engineering, alongside the development of MNs including innovative structures, diverse functionality, and scalable manufacturing capabilities, is essential for the advancement of intelligent MNs.

7.3.3. Integration of MNs with AI

Integrating AI with MNs equipped with multiplexed biosensors into a closed-loop therapeutic system can promote autonomous disease management through adaptive biomarker-responsive drug release, particularly for metabolic and cancer-related diseases. AI-assisted wearable biosensors play a crucial role in helping users interpret and benefit from high-dimensional, complex data. Meanwhile, machine learning and deep learning methods can quickly denoise, calibrate, and convert the collected signals into actionable insights, addressing the noise, drift, and patient-specific variations encountered when collecting biomarkers with MNs, ultimately enabling more timely and informed decisions. Therefore, the integration of MNs biosensors with AI lays the foundation for closed-loop therapeutic systems. The integration of MNs and AI represents a novel paradigm for comprehensive health monitoring, real-time treatment modifications, and improved user experiences.

7.3.4. Integration of MNs with pathophysiology

MNs can be applied to the skin or deep organs, which biological structure, physiology, and pathophysiological state can guide the design of MNs. For example, the skin microenvironment is a highly complex and dynamic system characterized by an acidic pH, diverse microbiota, various metabolites, and multiple enzymes. Once MNs infiltrate the layers of skin, they function as *in situ* chemical reaction chambers. They can administer chemical reactants or catalysts into the skin, thereby triggering precise chemical reactions. Furthermore, after the onset of certain diseases, the levels of specific biological markers change significantly. The drugs encapsulated in the MNs can chemically react with these signals, thereby dynamically regulating the release of the drugs. Consequently, comprehending the pathophysiological attributes of diseases is crucial for the development of intelligent MNs. A comprehensive understanding of pathophysiology can facilitate the creation and production of intelligent responsive MN delivery systems.

Acknowledgments

This work was funded by the National Nature Science Foundation of China (Nos. 82573579, 32071387 and 31872756), Six Talent Peaks Project in Jiangsu Province (JY-079, China). Lu Tang acknowledges the Alexander von Humboldt Foundation for financial support.

Author contributions

Conceptualization, Wei Wang, Lu Tang, Jing Shang, and Yue Yin; Original draft preparation, Yue Yin; Schematic illustration, Yue Yin, Qiaoqiao Zhao, Zihan Wang, Zixuan Li, Hening Liu, Fatemeh Eghbalitabar; Review and editing, Wei Wang, Lu Tang, Jing Shang, and Yue Yin; Supervision, Wei Wang, Lu Tang, and Jing Shang. All authors have read and agreed to the published version of the manuscript.

Declaration of Generative AI and AI-assisted technologies in the writing process

During the preparation of this work the authors used AI tools to improve language and readability. After using these tools, the authors reviewed and edited the content critically. The authors take full responsibility for the scientific accuracy, comprehensiveness, and impartiality of the work.

Conflicts of interest

The authors declare no conflicts of interest.

References

1. Zheng M, Sheng T, Yu J, Gu Z, Xu C. Microneedle biomedical devices. *Nat Rev Bioeng* 2023;**2**:324−42.
2. Han J, Wu Z, Zhan S, Sheng T, You J, Yu J, et al. Biorhythm-mimicking growth hormone patch. *Nat Mater* 2025;**24**:1283−94.
3. He P, He C, Wu F, Ou Y, Luo S, Zhang Y, et al. Microneedle-delivered adeno-associated virus vaccine amplified anti-viral immunity by improving antigen-presenting cells infection. *J Control Release* 2025;**10**:1045−57.
4. Wang Z, Yang Z, Jiang J, Shi Z, Mao Y, Qin N, et al. Silk microneedle patch capable of on-demand multidrug delivery to the brain for glioblastoma treatment. *Adv Mater* 2021;**34**:e2106606.
5. Zheng B, Yang L, Feng S, Zhu Y, Du L, Zhang J, et al. Organoid-loaded cryomicroneedles for biomimic hair regeneration. *Adv Funct Mater* 2023;**34**:2304950.
6. Zheng B, Li Q, Fang L, Cai X, Liu Y, Duo Y, et al. Microorganism microneedle micro-engine depth drug delivery. *Nat Commun* 2024; **15**:8947.
7. Wang H, Dong Y, Zhang J, Zhang H, Chen J, Wang S, et al. Living microecological microneedle patches enable proregenerative microenvironmental remodeling for promoting infected diabetic wound healing. *ACS Nano* 2025;**19**:21739−56.
8. Chang H, Chew SWT, Zheng M, Lio DCS, Wiraja C, Mei Y, et al. Cryomicroneedles for transdermal cell delivery. *Nat Biomed Eng* 2021;**5**:1008−18.
9. Khattak S, Xu H-T, Shen J. The microneedle bandages provide new hope for healing diabetic wounds. *Acta Pharm Sin B* 2024;**14**:5085−7.
10. Jiang X, Lai Y, Xia W, Yang W, Wang J, Pan J, et al. Self-oxygenating PROTAC microneedle for spatiotemporally-confined protein degradation and enhanced glioblastoma therapy. *Adv Mater* 2025;**37**: e2411869.
11. Creighton RL, Faber KA, Tobos CI, Doan MA, Guo T, Woodrow KA. Oral mucosal vaccination using integrated fiber microneedles. *J Control Release* 2024;**367**:649−60.
12. Ruan S, Li J, Ruan H, Xia Q, Hou X, Wang Z, et al. Microneedle-mediated nose-to-brain drug delivery for improved Alzheimer's disease treatment. *J Control Release* 2024;**366**:712−31.

13. Glover K, Mishra D, Gade S, Vora LK, Wu Y, Paredes AJ, et al. Microneedles for advanced ocular drug delivery. *Adv Drug Deliv Rev* 2023;**201**:115082.
14. Yu K, Yu X, Cao S, Wang Y, Zhai Y, Yang F, et al. Layered dissolving microneedles as a need-based delivery system to simultaneously alleviate skin and joint lesions in psoriatic arthritis. *Acta Pharm Sin B* 2020;**11**:505−19.
15. Hu S, Zhu D, Li Z, Cheng K. Detachable microneedle patches deliver mesenchymal stromal cell factor-loaded nanoparticles for cardiac repair. *ACS Nano* 2022;**16**:15935−45.
16. Mei X, Zhu D, Li J, Huang K, Hu S, Xing M, et al. Minimally invasive snakebite inspired microneedle delivery system for internal organs. *Bioact Mater* 2025;**49**:576−85.
17. Chen S, Sang Z, Li Y, Li H, Chen Z, Mei X, et al. NIR responsive microneedles patch used for promoting spinal cord injury repair by modulating mitochondrial ROS microenvironment. *Chem Eng J* 2025;**511**:162247.
18. Prausnitz MR, Gomaa Y, Li W. Microneedle patch drug delivery in the gut. *Nat Med* 2019;**25**:1471−2.
19. Hao T, Tang L, Xu Q, Wang W, Li Z, Shen Y, et al. Silk fibroin formed bioadhesive ophthalmic gel for dry eye syndrome treatment. *AAPS PharmSciTech* 2024;**25**:92.
20. Wang C, Yang Y, Zhang J, Zhang H, Wang Q, Ma S, et al. Microneedles at the forefront of next generation theranostics. *Adv Sci* 2025; **12**:e2412140.
21. Xiao Q, Tang L, Chen S, Mei Y, Wang C, Yang J, et al. Two-pronged attack: dual activation of fat reduction using near-infrared-responsive nanosandwich for targeted anti-obesity treatment. *Adv Sci (Weinh)* 2024;**11**:e2406985.
22. Kang Y, Zhang S, Wang G, Yan Z, Wu G, Tang L, et al. Nanocarrier-based transdermal drug delivery systems for dermatological therapy. *Pharmaceutics* 2024;**16**:1384.
23. Xiao Q, Wang C, Yang J, Gao X, Chen Z, Niu Z, et al. Dual-targeting nanoplatform to regulate metabolic disorders: from obesity to obesity-related metabolic dysfunction-associated steatotic liver disease. *Nano Lett* 2025;**25**:15416−27.
24. Wang Y, Chu Z, Wang P, Li T, Jin Y, Wu S, et al. Dual-ferroptosis induction-based microneedle patches for enhanced chemodynamic/photothermal combination therapy against triple-negative breast cancer. *Acta Pharm Sin B* 2025;**15**:4210−24.
25. Li Z, Wen X, Lu S, Zheng Y, Zhao P, Mu S, et al. Ice-pop making inspired photothermal ultra-swelling microneedles to facilitate loading and intradermal vaccination of tumor antigen. *J Control Release* 2025;**379**:77−88.
26. Driskill MM, Coates IA, Hurst PJ, Rajesh NU, Dulay MT, Waymouth RM, et al. Lyophilized SARS-CoV-2 self-amplifying RNA vaccines for microneedle array patch delivery. *J Control Release* 2025;**384**:113944.
27. Li N, Mu W, Xia Z, Ma Q, Feng R, Gu P, et al. Soluble-microneedle enhance three T-cell activation signals as efficient tumor vaccines for melanoma prevention and treatment. *J Control Release* 2025;**383**: 113726.
28. Hsu YP, Li NS, Pang HH, Pan YC, Tsai HP, Chen HC, et al. Lab-on-the-needles: a microneedle patch-based mobile unit for highly sensitive *ex vivo* and *in vivo* detection of protein biomarkers. *ACS Nano* 2025;**19**:3249−64.
29. Ashraf G, Wang H, Ahmed K, Xiong H, Kong J, Fang X. Microneedle-integrated FePc−MOF−MXene nanozyme patch for *in vivo* l-cysteine monitoring. *Adv Mater* 2025;**23**:e2502804.
30. Wu M, Liu L, Xing Y, Wu Z, Huang P, Li B. Plasmonic nanodiamond—microneedle bioinspired system for ultrarapid sampling and quantum sensing of melanoma-related miRNA. *Adv Funct Mater* 2025;**35**:2422305.
31. Mei Y, Hu J, Cao Y, Gao X, Tang L, Wang W. Versatile hydrogel-based drug delivery platform for multimodal cancer therapy from bench to bedside. *Appl Mater Today* 2024;**39**:102341.
32. Vora LK, Sabri AH, McKenna PE, Himawan A, Hutton ARJ, Detamornrat U, et al. Microneedle-based biosensing. *Nat Rev Bioeng* 2023;**2**:64−81.
33. Tang L, Li J, Zhao Q, Pan T, Zhong H, Wang W. Advanced and innovative nano-systems for anticancer targeted drug delivery. *Pharmaceutics* 2021;**13**:1151.
34. Liao H, Zhang F, Chen F, Li Y, Sun Y, Sloboda DD, et al. Application of artificial intelligence in laboratory hematology: advances, challenges, and prospects. *Acta Pharm Sin B* 2025;**15**:5702−33.
35. Pooyan M, Aziz M, Majid S, Aaron RJH, Melissa K, Rezvan J, et al. Bioinspired microneedle patches: biomimetic designs, fabrication, and biomedical applications. *Matter* 2022;**5**:390−429.
36. Ai Y, Hu ZN, Liang X, Sun Hb, Xin H, Liang Q. Recent advances in nanozymes: from matters to Bioapplications. *Adv Funct Mater* 2021; **32**:2110432.
37. Tian Y, Xia L, Song X, Chen Y. Dissolving microneedles as *in situ* chemical reaction chambers: from design strategies to versatile biomedical applications. *Adv Funct Mater* 2025;**35**:2422274.
38. Makvandi P, Jamaledin R, Chen G, Baghbantaraghdari Z, Zare EN, Di Natale C, et al. Stimuli-responsive transdermal microneedle patches. *Mater Today* 2021;**47**:206−22.
39. Tang L, Zhang A, Zhang Z, Zhao Q, Li J, Mei Y, et al. Multifunctional inorganic nanomaterials for cancer photoimmunotherapy. *Cancer Commun* 2022;**42**:141−63.
40. Xu Y, Wu X, Zhang X, Zu Y, Tan Q, Zhao Y. Living microneedle patch with adipose-derived stem cells embedding for diabetic ulcer healing. *Adv Funct Mater* 2022;**33**:2209986.
41. Jia J, Guo X, Wang Y, Wu M, Wang X, Zhao M, et al. Living photosynthetic microneedle patches for *in situ* oxygenation and postsurgical melanoma therapy. *J Nanobiotechnol* 2024;**22**:698.
42. Pei S, Babity S, Sara Cordeiro A, Brambilla D. Integrating microneedles and sensing strategies for diagnostic and monitoring applications: the state of the art. *Adv Drug Deliv Rev* 2024;**210**:115341.
43. Teymourian H, Tehrani F, Mahato K, Wang J. Lab under the skin: microneedle based wearable devices. *Adv Healthcare Mater* 2021;**10**: e2002255.
44. Ashraf G, Ahmed K, Aziz A, Asif M, Kong J, Fang X. Microneedle wearables in advanced microsystems: unlocking next-generation biosensing with AI. *Trends Anal Chem* 2025;**187**:118208.
45. Su Y, Wang W, Xiao Q, Tang L, Wang T, Xie M, et al. Macrophage membrane-camouflaged lipoprotein nanoparticles for effective obesity treatment based on a sustainable self-reinforcement strategy. *Acta Biomater* 2022;**152**:519−31.
46. Wegst UG, Bai H, Saiz E, Tomsia AP, Ritchie RO. Bioinspired structural materials. *Nat Mater* 2015;**14**:23−36.
47. Petővári G, Moldvai D, Raffay R, Dankó T, Sztankovics D, Reszegi A, et al. Mimicking breast cancer tissue—3D bioprinted models in accurate drug sensitivity tests. *View* 2025;**6**:20250092.
48. Gan N, Li X, Wei M, Li Z, Zhou S, Gao B. Tongue prick bionic angularly adjustable microneedles for enhanced scarless wound healing. *Adv Funct Mater* 2025;**35**:2422602.
49. Liu Y, Luo X, Li L, Chen L, Qiao Z, Si C, et al. Wearable, battery-free, and wireless microneedle-based bioelectronics for robustly-integrated chronic wound management and therapeutic diagnosis. *Nano Energy* 2025;**138**:110909.
50. Hu C, Liu B, Huang X, Wang Z, Qin K, Sun L, et al. Sea cucumber-inspired microneedle nerve guidance conduit for synergistically inhibiting muscle atrophy and promoting nerve regeneration. *ACS Nano* 2024;**18**:14427−40.
51. Zhu Z, Wang J, Pei X, Chen J, Wei X, Liu Y, et al. Blue-ringed octopus-inspired microneedle patch for robust tissue surface adhesion and active injection drug delivery. *Sci Adv* 2023;**9**:eadh2213.
52. Hu T, Lui KS, Ko EB, Zhao Y, Zhang Q, Yang H, et al. Microneedles with an anisotropic porous microstructure facilitate the transdermal delivery of small molecules, lipid nanoparticles, and T cells. *Matter* 2025;**8**:102038.

53. Gong Y, Tong S, Li X, Chen X, Liu Y, Li N, et al. Intestinal villi-inspired mathematically base-layer engineered microneedles (IMBEMs) for effective molecular exchange during biomarker enrichment and drug deposition in diversified mucosa. *ACS Nano* 2023;**17**:15696−712.
54. Huang L, Li L, Jiang Y, Cai J, Cai S, Ren Y, et al. Tumbler-inspired microneedle containing robots: achieving rapid self-orientation and peristalsis-resistant adhesion for colonic administration. *Adv Funct Mater* 2023;**33**:2304276.
55. Guo M, Wang Y, Gao B, He B. Shark tooth-inspired microneedle dressing for intelligent wound management. *ACS Nano* 2021;**15**: 15316−27.
56. Zhang X, Chen G, Cai L, Wang Y, Sun L, Zhao Y. Bioinspired pagoda-like microneedle patches with strong fixation and hemostasis capabilities. *Chem Eng J* 2021;**414**:128905.
57. Gao X, Li J, Li J, Zhang M, Xu J. Pain-free oral delivery of biologic drugs using intestinal peristalsis−actuated microneedle robots. *Sci Adv* 2024;**10**:eadj7067.
58. Liu Y, He C, Qiao T, Liu G, Li X, Wan Q, et al. Coral-inspired hollow microneedle patch with smart sensor therapy for wound infection. *Adv Funct Mater* 2024;**34**:2314071.
59. Montaruli A, Castelli L, Mulè A, Scurati R, Esposito F, Galasso L, et al. Biological rhythm and chronotype: new perspectives in health. *Biomolecules* 2021;**11**:487.
60. Chen Z, Li B, Zhang Y, Shang X, Ma C, Gao W, et al. Bioinspired rational design of nanozymes. *Mater Horiz* 2025;**12**:5957−74.
61. Xiong Y, Mi B, Liu G, Zhao Y. Microenvironment-sensitive nanozymes for tissue regeneration. *Biomater* 2024;**309**:122585.
62. Tang L, Cao Y, Yin Y, Liu H, Feng J, Fu C, et al. Dual-targeting nanozyme combined with aPD-L1-based immunotherapy for combating cancer recurrence and metastasis. *Mater Today* 2024;**73**: 79−95.
63. Lee J, Liao H, Wang Q, Han J, Han JH, Shin HE, et al. Exploration of nanozymes in viral diagnosis and therapy. *Exploration* 2022;**2**: 20210086.
64. Li Z, Song J, Zhao X, Wang K, Liang Y, Zhang L, et al. Mito-nanozyme: mitochondria-targeted nanozyme for cancer therapy. *Coord Chem Rev* 2025;**542**:216899.
65. Tang L, Li J, Pan T, Yin Y, Mei Y, Xiao Q, et al. Versatile carbon nanoplatforms for cancer treatment and diagnosis: strategies, applications and future perspectives. *Theranostics* 2022;**12**:2290−321.
66. Chen D, Tan G, Tian S, Han L, Li Y, Tan Y, et al. Advancements in nanozymes research for the management of chronic wounds. *Chem Eng J* 2024;**500**:157299.
67. Tang L, Xiao Q, Yin Y, Mei Y, Li J, Xu L, et al. An enzyme-responsive and NIR-triggered lipid−polymer hybrid nanoplatform for synergistic photothermal/chemo cancer therapy. *Biomater Sci* 2022;**10**:2370−83.
68. Fu C, Tang L, Cao Y, Yin Y, Liu H, Feng J, et al. Bacterial outer membrane vesicles-clothed nanoparticles delivered by live macrophages for potentiating antitumor photoimmunotherapy. *Chem Eng J* 2024;**499**:156420.
69. Hu Z, Shan J, Cui Y, Cheng L, Chen XL, Wang X. Nanozyme-incorporated microneedles for the treatment of chronic wounds. *Adv Healthcare Mater* 2024;**13**:2400101.
70. Zhu W, Mei J, Zhang X, Zhou J, Xu D, Su Z, et al. Photothermal nanozyme-based microneedle patch against refractory bacterial biofilm infection *via* iron-actuated janus ion therapy. *Adv Mater* 2022; **34**:e2207961.
71. Kong B, Liu R, Shan J, Li M, Zhou X, Zhao Y. Frozen reinforced microneedles loaded with NIR-photothermal nanozyme for keratitis treatment. *Nano Today* 2023;**52**:102000.
72. Wang B, Zhang W, Pan Q, Tao J, Li S, Jiang T, et al. Hyaluronic acid-based cus nanoenzyme biodegradable microneedles for treating deep cutaneous fungal infection without drug resistance. *Nano Lett* 2023;**23**:1327−36.
73. Liu S, Bai Q, Jiang Y, Gao Y, Chen Z, Shang L, et al. Multienzyme-like nanozyme encapsulated ocular microneedles for keratitis treatment. *Small* 2023;**20**:2308403.
74. Sun S, Liu X, Meng X, Yang Z, Zhang X, Dong H. Bimetallic metal−organic framework microneedle array for wound healing through targeted reactive oxygen species generation and electron transfer disruption. *ACS Nano* 2025;**19**:15109−19.
75. Chen Z, Zhang L, Yang Y, Cheng W, Tu L, Wang Z, et al. Photothermal nanozyme-encapsulating microneedles for the synergistic treatment of infected wounds. *Adv Funct Mater* 2024;**35**: 2417415.
76. Chen H, Yu N, Wang J, Zhang S, Cao L, Zhou M, et al. Construction of versatile fibroin/nanozyme hybrid microneedles with controllable phototherapeutic sterilization property against periodontitis. *Nano Today* 2024;**56**:102297.
77. Duan W, Xu K, Gao Y, Huang S, Xia X, Liu X, et al. Bimetallic plasmonic nanozyme-based microneedle for synergistic ferroptosis therapy of melanoma. *Adv Sci* 2025;**12**:e04203.
78. Shi S, Jiang Y, Yu Y, Liang M, Bai Q, Wang L, et al. Piezo-augmented and photocatalytic nanozyme integrated microneedles for antibacterial and anti-inflammatory combination therapy. *Adv Funct Mater* 2022;**33**:2210850.
79. Zhao J, Duan W, Liu X, Xi F, Wu J. Microneedle patch integrated with porous silicon confined dual nanozymes for synergistic and hyperthermia-enhanced nanocatalytic ferroptosis treatment of melanoma. *Adv Funct Mater* 2023;**33**:2308183.
80. Yuan A, Xia F, Bian Q, Wu H, Gu Y, Wang T, et al. Ceria nanozyme-integrated microneedles reshape the perifollicular microenvironment for androgenetic alopecia treatment. *ACS Nano* 2021;**15**:13759−69.
81. Zhu Y, Li S, Li Y, Tan H, Zhao Y, Sun L. Antioxidant nanozyme microneedles with stem cell loading for *in situ* endometrial repair. *Chem Eng J* 2022;**449**:137786.
82. Jing S, Liu Y, Wang B, Zhou H, Zhang H, Siwakoti P, et al. Microneedle-mediated hypoxic extracellular vesicle-encapsulated selenium nanoparticles delivery to treat androgenetic alopecia. *J Control Release* 2025;**381**:113597.
83. Tang Q, Xue N, Ding X, Tsai KH, Hew JJ, Jiang R, et al. Role of wound microbiome, strategies of microbiota delivery system and clinical management. *Adv Drug Deliv Rev* 2023;**192**:114671.
84. Del Mastro L, Poggio F, Blondeaux E, De Placido S, Giuliano M, Forestieri V, et al. Fluorouracil and dose-dense adjuvant chemotherapy in patients with early-stage breast cancer (GIM2): end-of-study results from a randomised, phase 3 trial. *Lancet Oncol* 2022; **23**:1571−82.
85. Giroux V, Rustgi AK. Metaplasia: tissue injury adaptation and a precursor to the dysplasia-cancer sequence. *Nat Rev Cancer* 2017;**17**: 594−604.
86. Zhang J, Chatham JC, Young ME. Circadian regulation of cardiac physiology: rhythms that keep the heart beating. *Annu Rev Physiol* 2020;**82**:79−101.
87. Thornton C, Panagiotopoulou M, Chowdhury FA, Diehl B, Duncan JS, Gascoigne SJ, et al. Diminished circadian and ultradian rhythms of human brain activity in pathological tissue *in vivo. Nat Commun* 2024;**15**:8527.
88. Morris A. Rhythms found in skin. *Nat Rev Endocrinol* 2018;**15**:3.
89. Wu T, Duan Y, Jiang J, Gu T, Zhang P, Bi Y. A century of prolactin: emerging perspectives as a metabolic regulator. *Diabetes Metab Res Rev* 2024;**40**:e3836.
90. Yin H, Tang W, Huang D, Gan J, Zhang P, Zhao Y, et al. Bioinspired prolactin pulse release from responsive microneedles for inhibiting fatty liver formation. *Adv Sci* 2025;**13**:e08364.
91. Cao Y, Tang L, Fu C, Yin Y, Liu H, Feng J, et al. Black phosphorus quantum dot loaded bioinspired nanoplatform synergized with aPD-L1 for multimode cancer immunotherapy. *Nano Lett* 2024;**24**: 6767−77.

92. Wei H, Wang E. Nanomaterials with enzyme-like characteristics (nanozymes): next-generation artificial enzymes. *Chem Soc Rev* 2013;**42**:6060−93.
93. Liu H, Zhu Y, Shu W, Zhang Y, Hou Y, Tang L, et al. Photoactive nanoplatforms with immunomodulation effect for antibacterial therapy. *Adv Healthcare Mater* 2025;**14**:e03365.
94. Liu H, Zhu Y, Li Z, Shu W, Yin Y, Hou Y, et al. Bioengineered violet phosphorus hybrid nanoassembly for pathogen-specific eradication of multidrug-resistant bacteria. *Adv Funct Mater* 2025:e18779. Available from: https://doi.org/10.1002/adfm.202518779.
95. Wu J, Wang X, Wang Q, Lou Z, Li S, Zhu Y, et al. Nanomaterials with enzyme-like characteristics (nanozymes): next-generation artificial enzymes (II). *Chem Soc Rev* 2019;**48**:1004−76.
96. Tang L, Fu C, Liu H, Yin Y, Cao Y, Feng J, et al. Chemo-immunotherapeutic nanogel for pre- and postsurgical treatment of malignant melanoma by reprogramming tumor-associated macrophages. *Nano Lett* 2024;**24**:1717−28.
97. Tang L, Yin Y, Zhang Z, Fu C, Cao Y, Liu H, et al. Size-switchable and dual-targeting nanomedicine for cancer chemoimmunotherapy by potentiating deep tumor penetration and antitumor immunity. *Chem Eng J* 2024;**493**:152590.
98. Hou X, Wang H, Yao X, Zhou Q, Niu X. Pt-induced sublattice distortion facilitates enzyme cascade reactions for eradicating intracellularly methicillin-resistant *Staphylococcus aureus* and enhancing diabetic wound healing. *ACS Nano* 2025;**19**:17709−27.
99. You W, Cai Z, Xiao F, Zhao J, Wang G, Wang W, et al. Biomolecular microneedle initiates fe3o4/mxene heterojunction-mediated nanozyme-like reactions and bacterial ferroptosis to repair diabetic wounds. *Adv Sci* 2025;**12**:e2417314.
100. Xuan Q, Cai J, Gao Y, Qiao X, Jin T, Peydayesh M, et al. Amyloid-templated ceria nanozyme reinforced microneedle for diabetic wound treatments. *Adv Mater* 2025;**37**:e2417774.
101. Hirobe S, Azukizawa H, Hanafusa T, Matsuo K, Quan YS, Kamiyama F, et al. Clinical study and stability assessment of a novel transcutaneous influenza vaccination using a dissolving microneedle patch. *Biomaterials* 2015;**57**:50−8.
102. Chu SY, Chou CH, Huang HD, Yen MH, Hong HC, Chao PH, et al. Mechanical stretch induces hair regeneration through the alternative activation of macrophages. *Nat Commun* 2019;**10**:1524.
103. Yap CX, Sidorenko J, Wu Y, Kemper KE, Yang J, Wray NR, et al. Dissection of genetic variation and evidence for pleiotropy in male pattern baldness. *Nat Commun* 2018;**9**:5407.
104. Yu J, Zhang Y, Kahkoska AR, Gu Z. Bioresponsive transcutaneous patches. *Curr Opin Biotechnol* 2017;**48**:28−32.
105. Yang J, des Rieux A, Malfanti A. Stimuli-responsive nanomedicines for the treatment of non-cancer related inflammatory diseases. *ACS Nano* 2025;**19**:15189−219.
106. Tang L, Liu H, Feng J, Yao Y, Cao Y, Yin Y, et al. Site-specific antibacterial strategy for multi-pathway treatment of drug-resistant skin infections. *Adv Healthcare Mater* 2025:e04240. Available from: https://doi.org/10.1002/adhm.202504240.
107. Chu H, Xue J, Yang Y, Zheng H, Luo D, Li Z. Advances of smart stimulus-responsive microneedles in cancer treatment. *Small Methods* 2023;**8**:e2301455.
108. Tang L, Xiao Q, Mei Y, He S, Zhang Z, Wang R, et al. Insights on functionalized carbon nanotubes for cancer theranostics. *J Nanobiotechnol* 2021;**19**:423.
109. Han J, Kanelli M, Liu Y, Daristotle JL, Pardeshi A, Forster TA, et al. On-patient medical record and mRNA therapeutics using intradermal microneedles. *Nat Mater* 2025;**24**:794−803.
110. Yin Y, Tang L, Cao Y, Liu H, Fu C, Feng J, et al. Microneedle patch-involved local therapy synergized with immune checkpoint inhibitor for pre- and post-operative cancer treatment. *J Control Release* 2025;**379**:678−95.
111. Mei Y, Tang L, Zhang L, Hu J, Zhang Z, He S, et al. A minimally designed PD-L1-targeted nanocomposite for positive feedback-based multimodal cancer therapy. *Mater Today* 2022;**60**:52−68.
112. Liu H, Mei Y, Zhao Q, Zhang A, Tang L, Gao H, et al. Black phosphorus, an emerging versatile nanoplatform for cancer immunotherapy. *Pharmaceutics* 2021;**13**:1344.
113. Liu H, Tang L, Yin Y, Cao Y, Fu C, Feng J, et al. Photoresponsive multirole nanoweapon camouflaged by hybrid cell membrane vesicles for efficient antibacterial therapy of *Pseudomonas aeruginosa*-infected pneumonia and wound. *Adv Sci (Weinh)* 2024;**11**:e2403101.
114. Li Y, Li Y, He G, Li X, Ding R, Yan R, et al. Activatable enzymatic nanoplatform incorporated into microneedle patch for relieving tumor hypoxia augmented photodynamic therapy. *Adv Mater* 2025;**37**:e2504258.
115. Lai S, Cao B, Ouyang X, Zhang S, Li J, He W, et al. Fluorescent microneedle-based theranostic patch for naked-eye monitoring and on-demand photo-therapy of bacterial biofilm infections. *Adv Funct Mater* 2024;**35**:2415559.
116. Shao J, Li X, Li Y, Lin J, Huang P. Self-heating multistage microneedle patch for topical therapy of skin cancer. *Adv Mater* 2024;**36**:e2308217.
117. Lin X, Jia Q, Lin X, Shi J, Gong W, Shen K, et al. Galvanic cell bipolar microneedle patches for reversing photoaging wrinkles. *Adv Mater* 2025;**37**:e2500552.
118. Zhang X, Chen G, Fu X, Wang Y, Zhao Y. Magneto-responsive microneedle robots for intestinal macromolecule delivery. *Adv Mater* 2021;**33**:e2104932.
119. Li S, Yu J, Shen Y, Xiong B, Zhao D, Xu W, et al. Transdermal microneedle-assisted ultrasound-enhanced CRISPRa system to enable sono-gene therapy for obesity. *Nat Commun* 2025;**16**:1499.
120. Zhang W, Qin X, Li G, Zhou X, Li H, Wu D, et al. Self-powered triboelectric-responsive microneedles with controllable release of optogenetically engineered extracellular vesicles for intervertebral disc degeneration repair. *Nat Commun* 2024;**15**:5736.
121. Chen Z, Lai Y, Xu S, Zhu M, Sun Y, Cheng Y, et al. A self-powered controllable microneedle drug delivery system for rapid blood pressure reduction. *Nano Energy* 2024;**123**:109344.
122. Jiang Y, Huang J, Xu C, Pu K. Activatable polymer nanoagonist for second near-infrared photothermal immunotherapy of cancer. *Nat Commun* 2021;**12**:742.
123. Akomeah F, Nazir T, Martin GP, Brown MB. Effect of heat on the percutaneous absorption and skin retention of three model penetrants. *Eur J Pharmaceut Sci* 2004;**21**:337−45.
124. Tang L, Zhang A, Mei Y, Xiao Q, Xu X, Wang W. NIR light-triggered chemo-phototherapy by ICG functionalized MWNTs for synergistic tumor-targeted delivery. *Pharmaceutics* 2021;**13**:2145.
125. Cheng Y, Zhang X, Wu X, Ding Y, Zhu L, Pan J, et al. Multifunctional microneedle patches for perivascular gene delivery and treatment of vascular intimal hyperplasia. *ACS Nano* 2024;**18**:32578−88.
126. Yang B, Shi J. Developing new cancer nanomedicines by repurposing old drugs. *Angew Chem Int Ed Engl* 2020;**59**:21829−38.
127. Zare EN, Makvandi P, Ashtari B, Rossi F, Motahari A, Perale G. Progress in conductive polyaniline-based nanocomposites for biomedical applications: a review. *J Med Chem* 2019;**63**:1−22.
128. Hou Y, Guo X, Ran J, Lu X, Xie C. Conductive polyphenol microneedles coupled with electroacupuncture to accelerate wound healing and alleviate depressive-like behaviors in diabetes. *Bioact Mater* 2024;**44**:516−30.
129. Chen T, Cai Y, Ren B, Sánchez BJ, Dong R. Intelligent micro/-nanorobots based on biotemplates. *Mater Horiz* 2024;**11**:2772−801.
130. Guo Y, Luo Y, Hua S, Ding C-F, Yan Y. Application of magnetic nanomaterials in peptidomics: a review in the past decade. *Chin Chem Lett* 2024;**36**:110070.
131. Ze Q, Kuang X, Wu S, Wong J, Montgomery SM, Zhang R, et al. Magnetic shape memory polymers with integrated multifunctional shape manipulation. *Adv Mater* 2020;**32**:e1906657.
132. Tu L, Liao Z, Luo Z, Wu YL, Herrmann A, Huo S. Ultrasound-controlled drug release and drug activation for cancer therapy. *Exploration* 2021;**1**:20210023.
133. Shakya G, Cattaneo M, Guerriero G, Prasanna A, Fiorini S, Supponen O. Ultrasound-responsive microbubbles and nanodroplets:

a pathway to targeted drug delivery. *Adv Drug Deliv Rev* 2024;**206**: 115178.
134. Xiang Y, Lu J, Mao C, Zhu Y, Wang C, Wu J, et al. Ultrasound-triggered interfacial engineering-based microneedle for bacterial infection acne treatment. *Sci Adv* 2023;**9**:eadf0854.
135. Li R, Wang J, Lin Q, Yin Z, Zhou F, Chen X, et al. Mechano-responsive biomaterials for bone organoid construction. *Adv Healthcare Mater* 2024;**14**:e2404345.
136. Wu Z, Ding X, Chen X, Chen J, Chang X, Liu Z, et al. Recent progress of polymer-based piezoelectric nanogenerators. *Adv Compos Hybrid Mater* 2025;**8**:225.
137. Conta G, Libanori A, Tat T, Chen G, Chen J. Triboelectric nanogenerators for therapeutic electrical stimulation. *Adv Mater* 2021;**33**: e2007502.
138. Mahapatra SD, Mohapatra PC, Aria AI, Christie G, Mishra YK, Hofmann S, et al. Piezoelectric materials for energy harvesting and sensing applications: roadmap for future smart materials. *Adv Sci* 2021;**8**:e2100864.
139. Bairagi S, Shahid-ul-Islam n, Kumar C, Babu A, Aliyana AK, Stylios G, et al. Wearable nanocomposite textile-based piezoelectric and triboelectric nanogenerators: progress and perspectives. *Nano Energy* 2023;**118**:108962.
140. Wang Y, Zhang X, Chen G, Lu M, Zhao Y. Multifunctional structural color triboelectric microneedle patches for psoriasis treatment. *Matter* 2023;**6**:1555−68.
141. Tang L, Fu C, Zhang A, Li X, Cao Y, Feng J, et al. Harnessing nanobiotechnology for cerebral ischemic stroke management. *Biomater Sci* 2023;**11**:791−812.
142. Pan T, Tang L, Chu R, Zheng S, Wang J, Yang Y, et al. Microfluidic-enabled assembly of multicomponent artificial organelle for synergistic tumor starvation therapy. *ACS Appl Mater Interfaces* 2024;**16**: 40667−81.
143. Wang W, Chen K, Su Y, Zhang J, Li M, Zhou J. Lysosome-independent intracellular drug/gene codelivery by lipoprotein-derived nanovector for synergistic apoptosis-inducing cancer-targeted therapy. *Biomacromolecules* 2018;**19**:438−48.
144. Zhang F, Li M, Su Y, Zhou J, Wang W. A dual-targeting drug co-delivery system for tumor chemo- and gene combined therapy. *Mater Sci Eng C* 2016;**64**:208−18.
145. Tang L, Yin Y, Liu H, Zhu M, Cao Y, Feng J, et al. Blood−brain barrier-penetrating and lesion-targeting nanoplatforms inspired by the pathophysiological features for synergistic ischemic stroke therapy. *Adv Mater* 2024;**36**:2312897.
146. Li X, Yue R, Guan G, Zhang C, Zhou Y, Song G. Recent development of pH-responsive theranostic nanoplatforms for magnetic resonance imaging-guided cancer therapy. *Exploration* 2023;**3**: 20220002.
147. Zhang F, Wang X, Xu X, Li M, Zhou J, Wang W. Reconstituted high density lipoprotein mediated targeted co-delivery of HZ08 and paclitaxel enhances the efficacy of paclitaxel in multidrug-resistant MCF-7 breast cancer cells. *Eur J Pharmaceut Sci* 2016;**92**:11−21.
148. Wang F, Xu Z, Zheng F, Yang D, Xu K, Ke M, et al. Cardiac organoid model inspired micro-robot smart patch to treat myocardial infarction. *Adv Mater* 2025;**37**:e2417327.
149. Qian Y, Zhang B, Xu Y, Liang J, Yang X, Gu Y, et al. Coordination of functional oligonucleotides yields a versatile nanocomposite microneedle patch to facilitate local wound microenvironment remodeling *via* systemic hyperglycemia regulation. *Adv Funct Mater* 2025;**35**: 2423012.
150. Zhao B, Guo W, Zhou X, Xue Y, Wang T, Li Q, et al. Ferroptosis-mediated synergistic therapy of hypertrophic scarring based on metal−organic framework microneedle patch. *Adv Funct Mater* 2023;**33**:2300575.
151. Hao T, Guo H, Wang C, Jing S, Zhang W, Zeng Y, et al. Mitochondria-targeted microneedles reverse doxorubicin resistance *via* apoptosis−ferroptosis synergy. *ACS Nano* 2025;**19**:23315−33.
152. Sun J, Zhao B, Wo K, Xia Y, Liu Y, Li S, et al. Cell microparticles loaded with pro-inflammatory factors and chloroquine collaborate with mechanical force to facilitate orthodontic tooth movement. *J Control Release* 2025;**384**:113868.
153. Zhang A, Zeng Y, Xiong B, Jiang X, Jin Y, Wang S, et al. A pH-responsive core−shell microneedle patch with self-monitoring capability for local long-lasting analgesia. *Adv Funct Mater* 2023; **34**:2314048.
154. Hu Y, Miao Y, Zhang Y, Wang X, Liu X, Zhang W, et al. Co-assembled binary polyphenol natural products for the prevention and treatment of radiation-induced skin injury. *ACS Nano* 2024;**18**: 27557−69.
155. Tan H, Wang S, He X, Yang G, Zhu Y, Yang S, et al. Microneedles loaded with nitric-oxide driven nanomotors improve force-induced efferocytosis impairment and sterile inflammation by revitalizing macrophage energy metabolism. *ACS Nano* 2025;**19**:9390−411.
156. Yu F, Zhao X, Wang Q, Fang PH, Liu L, Du X, et al. Engineered mesenchymal stromal cell exosomes-loaded microneedles improve corneal healing after chemical injury. *ACS Nano* 2024;**18**:20065−82.
157. Wang S, Yang C, Zhang W, Zhao S, You J, Cai R, et al. Glucose-responsive microneedle patch with high insulin loading capacity for prolonged glycemic control in mice and minipigs. *ACS Nano* 2024; **18**:26056−65.
158. GhavamiNejad A, Liu JF, Mirzaie S, Lu B, Samarikhalaj M, Giacca A, et al. Catechol-based chemistry for hypoglycemia-responsive delivery of zinc-glucagon *via* hydrogel-based microneedle patch technology. *Nat Commun* 2025;**16**:3124.
159. Saravanakumar G, Kim J, Kim WJ. Reactive-oxygen-species-responsive drug delivery systems: promises and challenges. *Adv Sci* 2016;**4**:1600124.
160. Gao F, Xiong Z. Reactive oxygen species responsive polymers for drug delivery systems. *Front Chem* 2021;**9**:649048.
161. Tao W, He Z. ROS-responsive drug delivery systems for biomedical applications. *Asian J Pharm Sci* 2018;**13**:101−12.
162. Bi D, Qu F, Xiao W, Wu J, Liu P, Du H, et al. Reactive oxygen species-responsive gel-based microneedle patches for prolonged and intelligent psoriasis management. *ACS Nano* 2023;**17**:4346−57.
163. Zelzer M, Todd SJ, Hirst AR, McDonald TO, Ulijn RV. Enzyme responsive materials: design strategies and future developments. *Biomater Sci* 2012;**1**:11−39.
164. de la Rica R, Aili D, Stevens MM. Enzyme-responsive nanoparticles for drug release and diagnostics. *Adv Drug Deliv Rev* 2012;**64**: 967−78.
165. Mu J, Lin J, Huang P, Chen X. Development of endogenous enzyme-responsive nanomaterials for theranostics. *Chem Soc Rev* 2018;**47**: 5554−73.
166. Zeng Y, Wang C, Lei J, Jiang X, Lei K, Jin Y, et al. Spatiotemporally responsive cascade bilayer microneedles integrating local glucose depletion and sustained nitric oxide release for accelerated diabetic wound healing. *Acta Pharm Sin B* 2024;**14**:5037−52.
167. Ye Y, Wang J, Hu Q, Hochu GM, Xin H, Wang C, et al. Synergistic transcutaneous immunotherapy enhances antitumor immune responses through delivery of checkpoint inhibitors. *ACS Nano* 2016; **10**:8956−63.
168. Mir M, Permana AD, Ahmed N, Khan GM, Rehman AU, Donnelly RF. Enhancement in site-specific delivery of carvacrol for potential treatment of infected wounds using infection responsive nanoparticles loaded into dissolving microneedles: a proof of concept study. *Eur J Pharm Biopharm* 2020;**147**:57−68.
169. Veiseh O, Tang BC, Whitehead KA, Anderson DG, Langer R. Managing diabetes with nanomedicine: challenges and opportunities. *Nat Rev Drug Discov* 2014;**14**:45−57.
170. Perkins BA, Sherr JL, Mathieu C. Type 1 diabetes glycemic management: insulin therapy, glucose monitoring, and automation. *Science* 2021;**373**:522−7.
171. Gordijo CR, Koulajian K, Shuhendler AJ, Bonifacio LD, Huang HY, Chiang S, et al. Nanotechnology-enabled closed loop insulin delivery device: *in vitro* and *in vivo* evaluation of glucose-regulated insulin release for diabetes control. *Adv Funct Mater* 2010;**21**:73−82.

172. Yang C, Sheng T, Hou W, Zhang J, Cheng L, Wang H, et al. Glucose-responsive microneedle patch for closed-loop dual-hormone delivery in mice and pigs. *Sci Adv* 2022;**8**:eadd3197.
173. Oh JY, Son D, Katsumata T, Lee Y, Kim Y, Lopez J, et al. Stretchable self-healable semiconducting polymer film for active-matrix strain-sensing array. *Sci Adv* 2019;**5**:eaav3097.
174. Faure E, Falentin-Daudré C, Jérôme C, Lyskawa J, Fournier D, Woisel P, et al. Catechols as versatile platforms in polymer chemistry. *Prog Polym Sci* 2012;**38**:236−70.
175. Luan X, Du S, Liu Z, He B, Pan Y, Yang J, et al. Microneedle-loaded gene-editable nanohybrids engineer cancer cells by telomere stress induction and metabolic interference for enhanced cuproptosis and immunotherapy. *Adv Funct Mater* 2024;**35**:2416285.
176. Wang P, Wu J, Yang H, Liu H, Yao T, Liu C, et al. Intelligent microneedle patch with prolonged local release of hydrogen and magnesium ions for diabetic wound healing. *Bioact Mater* 2023;**24**:463−76.
177. Zhang X, Gan J, Fan L, Luo Z, Zhao Y. Bioinspired adaptable indwelling microneedles for treatment of diabetic ulcers. *Adv Mater* 2023;**35**:e2210903.
178. Li D, Hu D, Xu H, Patra HK, Liu X, Zhou Z, et al. Progress and perspective of microneedle system for anti-cancer drug delivery. *Biomaterials* 2021;**264**:120410.
179. Gao F, Liu X, Ma Z, Tang M, Tang Z, Wu J, et al. An integrated modular vaccination system for spatiotemporally separated perioperative cancer immunotherapy. *Adv Mater* 2025;**37**:e2418322.
180. Minnick G, Tajvidi Safa B, Rosenbohm J, Lavrik NV, Brooks J, Esfahani AM, et al. Two-photon polymerized shape memory microfibers: a new mechanical characterization method in liquid. *Adv Funct Mater* 2023;**33**:2206739.
181. Tang L, Liu H, Yin Y, Pan T, Fu C, Cao Y, et al. Micro/nano system-mediated local treatment in conjunction with immune checkpoint inhibitor against advanced-stage malignant melanoma. *Chem Eng J* 2024;**497**:154499.
182. Li L, Wang F, Mo S, Deng J, Wang X, Ai J, et al. A spatially distributed microneedle system for bioorthogonal T cell-guided cancer therapy. *Adv Sci* 2025;**12**:e2416841.
183. Tang L, Yin Y, Cao Y, Liu H, Qing G, Fu C, et al. Bioorthogonal chemistry-guided inhalable nanoprodrug to circumvent cisplatin resistance in orthotopic nonsmall cell lung cancer. *ACS Nano* 2024;**18**:32103−17.
184. Qu Y, Zeng H, Wang L, Ge Z, Liu B, Fan Z. Microenvironment-regulated dual-layer microneedle patch for promoting periodontal soft and hard tissue regeneration in diabetic periodontitis. *Adv Funct Mater* 2025;**35**:2418076.
185. Zhang B, Qian Y, Li J, Fan Y, Gao M, Wu Q, et al. Double-layer nucleoside-microneedles co-delivering dexamethasone vesicles and adenosine overcome pseudomembrane barriers for the treatment of oral ulcer. *ACS Nano* 2025;**19**:25204−27.
186. Song W, Guo Y, Liu W, Yao Y, Zhang X, Cai Z, et al. Circadian rhythm-regulated adsc-derived sEVs and a triphasic microneedle delivery system to enhance tendon-to-bone healing. *Adv Mater* 2024;**36**:e2408255.
187. Pan X, Kang Y, Zhou S, Zhang T, Zheng Y, Jin Q, et al. A multifunctional rocket-like microneedle system with thrusters for self-promoted deep drug penetration and combination treatment in melanoma. *Adv Funct Mater* 2024;**34**:2405696.
188. Tang L, Mei Y, Shen Y, He S, Xiao Q, Yin Y, et al. Nanoparticle-mediated targeted drug delivery to remodel tumor microenvironment for cancer therapy. *Int J Nanomed* 2021;**16**:5811−29.
189. Wang K, Ding Q, Qi M, Zhang W, Hou Y, Cao R, et al. Integrated bilayer microneedle dressing and triboelectric nanogenerator for intelligent management of infected wounds. *Adv Funct Mater* 2024;**34**:2316820.
190. Shan Y, Zhong J, Sun Q, Gao W, Zhang C, Chen H, et al. Dual nanozymes-loaded core−shell microneedle patches with antibacterial and NETs-degradation bifunctional properties for periodontitis treatment. *Bioact Mater* 2025;**53**:161−77.
191. He X, Zhao W, Xu H, Li H, Chen M, Fu Y, et al. Smart core−shell microneedles for psoriasis therapy: *in situ* self-assembly of calcium ion-coordinated dexamethasone hydrogel. *J Control Release* 2025;**379**:786−96.
192. Liu M, Zhou X, Wang Y, Zhao W, Zhao X, Li L, et al. A strategy involving microporous microneedles integrated with CAR-TREM2-macrophages for scar management by regulating fibrotic microenvironment. *Adv Mater* 2024;**36**:e2406153.
193. Le Z, Shou Y, Li RR, Liu L, Tan R, Charles CJ, et al. Sponge-like microneedles spatially sequester chemokines and deplete monocytes to alleviate inflammatory skin disorders. *Adv Funct Mater* 2024;**34**:2402539.
194. Fan L, Zhang X, Wang L, Song Y, Yi K, Wang X, et al. Bio-inspired porous microneedles dwelled stem cells for diabetic wound treatment. *Adv Funct Mater* 2024;**34**:2316742.
195. Cao Y, Kim D, Koh SS, Li Z, Rigoldi F, Fortmueller JE, et al. Nanofabrication of silk microneedles for high-throughput micronutrient delivery and continuous sap monitoring in plants. *Nat Nanotechnol* 2025;**20**:1142−51.
196. Lu Z, Cai R, Xie T, Zhao S, Juengpanich S, Topatana W, et al. Microneedle patch for *in situ* neutrophil monitoring. *Adv Sci* 2025;**12**:e2417801.
197. Zhou S, Chino Y, Kasama T, Miyake R, Mitsuzawa S, Luan Y, et al. Biocompatible core−shell microneedle sensor filled with zwitterionic polymer hydrogel for rapid continuous transdermal monitoring. *ACS Nano* 2024;**18**:26541−59.
198. Li H, Zheng X, Gao Z, Mu T, Liu M, Li J, et al. ROS-responsive core−shell microneedles based on simultaneous efficient type I/II photosensitizers for photodynamic against bacterial biofilm infections. *Adv Funct Mater* 2024;**25**:2401477.
199. Zhang Y, Wang S, Yang Y, Zhao S, You J, Wang J, et al. Scarless wound healing programmed by core−shell microneedles. *Nat Commun* 2023;**14**:3431.
200. Xu B, Zhang S, Liu H, Yang G, Zhou Z, Gao Y. Double-layered core−shell microneedle patch integrated with microparticles for long-acting treatment of osteoporosis. *J Control Release* 2025;**384**:113898.
201. Fang A, Wang Y, Guan N, Zuo Y, Lin L, Guo B, et al. Porous microneedle patch with sustained delivery of extracellular vesicles mitigates severe spinal cord injury. *Nat Commun* 2023;**14**:4011.
202. Chen X, Wang L, Yu H, Li C, Feng J, Haq F, et al. Preparation, properties and challenges of the microneedles-based insulin delivery system. *J Control Release* 2018;**288**:173−88.
203. Li W, Tang J, Terry RN, Li S, Brunie A, Callahan RL, et al. Long-acting reversible contraception by effervescent microneedle patch. *Sci Adv* 2019;**5**:eaaw8145.
204. Li W, Chen JY, Terry RN, Tang J, Romanyuk A, Schwendeman SP, et al. Core−shell microneedle patch for six-month controlled-release contraceptive delivery. *J Control Release* 2022;**347**:489−99.
205. Luo M, Zhang Y, He S, Guo Y, Cao X, Gong T, et al. Effervescent microneedles for the codelivery of chitosan nanoparticles and indocyanine green to enhance the treatment of diet-induced obesity in mice. *ACS Nano* 2025;**19**:11792−806.
206. You J, Yang C, Han J, Wang H, Zhang W, Zhang Y, et al. Ultrarapid-acting microneedles for immediate delivery of biotherapeutics. *Adv Mater* 2023;**35**:2304582.
207. Yu W, Fu J, Jia F, Jin Q, Wang Y, Ji J. Removable photocatalysis microneedle reactor for carbon monoxide delivery to enhance chemosensitization. *Nano Lett* 2024;**24**:10024−31.
208. Cai L, Chen G, Sun L, Miao S, Shang L, Zhao Y, et al. Rocket-inspired effervescent motors for oral macromolecule delivery. *Adv Mater* 2023;**35**:2210679.
209. Andrabi SM, Shahriar SMS, Tian Y, Hayati F, Su Y, Zhang F, et al. Engineered peptides-based hybrid-nested microneedle effectively treats biofilm-infected diabetic wounds. *Adv Funct Mater* 2025;**35**:2422150.
210. Zhou R, Yu H, Sheng T, Wu Y, Chen Y, You J, et al. Grooved microneedle patch augments adoptive T cell therapy against solid

tumors *via* diverting regulatory T cells. *Adv Mater* 2024;**36**: e2401667.
211. Choi H, Hong J, Seo Y, Joo S-H, Lim H, Lahiji SF, et al. Self-assembled oligopeptoplex-loaded dissolving microneedles for adipocyte-targeted anti-obesity gene therapy. *Adv Mater* 2024;**36**: e2309920.
212. Xu R, Guo H, Chen X, Xu J, Gong Y, Cao P, et al. Smart hydrothermally responsive microneedle for topical tumor treatment. *J Control Release* 2023;**358**:566−78.
213. Hu S, Zhu M, Xing H, Xue Y, Li J, Wang Z, et al. Thread-structural microneedles loaded with engineered exosomes for annulus fibrosus repair by regulating mitophagy recovery and extracellular matrix homeostasis. *Bioact Mater* 2024;**37**:1−13.
214. Tang L, He S, Yin Y, Liu H, Hu J, Cheng J, et al. Combination of nanomaterials in cell-based drug delivery systems for cancer treatment. *Pharmaceutics* 2021;**13**:1888.
215. Facklam AL, Volpatti LR, Anderson DG. Biomaterials for personalized cell therapy. *Adv Mater* 2020;**32**:e1902005.
216. Tang L, He S, Yin Y, Li J, Xiao Q, Wang R, et al. Combining nanotechnology with the multifunctional roles of neutrophils against cancer and inflammatory disease. *Nanoscale* 2022;**14**:1621−45.
217. Fuchs E. Skin stem cells in silence, action, and cancer. *Stem Cell Rep* 2018;**10**:1432−8.
218. Saxena M, Bhardwaj N. Re-emergence of dendritic cell vaccines for cancer treatment. *Trends Cancer* 2018;**4**:119−37.
219. Li H, Wang Z, Ogunnaike EA, Wu Q, Chen G, Hu Q, et al. Scattered seeding of CAR T cells in solid tumors augments anticancer efficacy. *Natl Sci Rev* 2021;**9**:nwab172.
220. Yao WD, Zhou JN, Tang C, Zhang JL, Chen ZY, Li Y, et al. Hydrogel microneedle patches loaded with stem cell mitochondria-enriched microvesicles boost the chronic wound healing. *ACS Nano* 2024; **18**:26733−50.
221. Wu X, Huang D, Xu Y, Chen G, Zhao Y. Microfluidic templated stem cell spheroid microneedles for diabetic wound treatment. *Adv Mater* 2023;**35**:e2301064.
222. Shi Q, Yin T, Zeng C, Pan H, Chen Z, Wang L, et al. Cryomicroneedle delivery of nanogold-engineered *Rhodospirillum rubrum* for photochemical transformation and tumor optical biotherapy. *Bioact Mater* 2024;**37**:505−16.
223. Wang F, Zhang X, Chen G, Zhao Y. Living bacterial microneedles for fungal infection treatment. *Research* 2020;**2020**:2760594.
224. Gao S, Rao Y, Wang X, Zhang Q, Zhang Z, Wang Y, et al. *Chlorella*-loaded antibacterial microneedles for microacupuncture oxygen therapy of diabetic bacterial infected wounds. *Adv Mater* 2024;**36**: e2307585.
225. Bitto A. Mitochondrial transplants to treat mitochondrial dysfunction. *Nat Metab* 2024;**6**:1846−7.
226. Fu L, Zhang W, Zhou X, Fu J, He C. Tumor cell membrane-camouflaged responsive nanoparticles enable MRI-guided immunochemodynamic therapy of orthotopic osteosarcoma. *Bioact Mater* 2022;**17**:221−33.
227. Dong Z, Liu X, Li S, Fu X. Inhibition and rescue of hyperglycemia-induced cellular senescence by mitochondrial transfer from enucleated mesenchymal stem cell-derived microvesicles for chronic wound healing. *Adv Sci* 2025;**12**:e01612.
228. Rossi G, Manfrin A, Lutolf MP. Progress and potential in organoid research. *Nat Rev Genet* 2018;**19**:671−87.
229. Hughes CS, Postovit LM, Lajoie GA. Matrigel: a complex protein mixture required for optimal growth of cell culture. *Proteomics* 2010; **10**:1886−90.
230. Kuang R, Zhang Z, Jin X, Hu J, Shi S, Ni L, et al. Nanofibrous spongy microspheres for the delivery of hypoxia-primed human dental pulp stem cells to regenerate vascularized dental pulp. *Acta Biomater* 2016;**33**:225−34.
231. Glanville N, Prevosto C, Domingos-Pereira S, Polak L, Morel V, Leblond M, et al. Abstract 1673: advancing bladder cancer treatment with live attenuated salmonella ZH9: from monotherapy to combination strategies. *Cancer Res* 2025;**85**:1673.
232. Liu Y, Wang W, Li R, Zhang H, Guo W, Yuan B, et al. Inhaled predatory bacteria-loaded large porous microspheres to eradicate drug-resistant Pseudomonas aeruginosa from the lung. *Mater Today Bio* 2025;**31**:101562.
233. Jiang J, Ma Y, Zhou L, Han W, Liang Y, Dong J, et al. Synergistic genetic and chemical engineering of probiotics for enhanced intestinal microbiota regulation and ulcerative colitis treatment. *Adv Mater* 2025;**37**:e2417050.
234. Shen H, Aggarwal N, Wun KS, Lee YS, Hwang IY, Chang MW. Engineered microbial systems for advanced drug delivery. *Adv Drug Deliv Rev* 2022;**187**:114364.
235. Gao J, Tang L, Fu C, Cao Y, Liu H, Yin Y, et al. A nano-strategy for advanced triple-negative breast cancer therapy by regulating intratumoral microbiota. *Nano Lett* 2025;**25**:6134−44.
236. Shaw LP, Chau KK, Kavanagh J, AbuOun M, Stubberfield E, Gweon HS, et al. Niche and local geography shape the pangenome of wastewater- and livestock-associated Enterobacteriaceae. *Sci Adv* 2021;**7**:eabe3868.
237. Wu Y, Yuan M, Song J, Chen X, Yang H. Hydrogen gas from inflammation treatment to cancer therapy. *ACS Nano* 2019;**13**: 8505−11.
238. Ma Y, Lai X, Luo X, Luo Z, Mao L, Zhu H, et al. Multifunctional silver-enzyme nanogels assembly with efficient trienzyme cascades for synergistic diabetic wound healing. *Adv Funct Mater* 2024;**34**: 2405644.
239. Wang YH, Peng WY, Li CF, Wu YL, Sheng J, Zi CT, et al. The improvement effect of ellagic acid and urolithins on metabolic diseases: pharmacology and mechanism. *Food Med Homol* 2025;**2**: 9420058.
240. Kellersztein I, Tish D, Pederson J, Bechthold M, Daraio C. Multifunctional biocomposite materials from *Chlorella vulgaris* microalgae. *Adv Mater* 2024;**37**:e2413618.
241. Jayathilaka WADM, Qi K, Qin Y, Chinnappan A, Serrano-García W, Baskar C, et al. Significance of nanomaterials in wearables: a review on wearable actuators and sensors. *Adv Mater* 2018;**31**: e1805921.
242. Du-Harpur X, Watt FM, Luscombe NM, Lynch MD. What is AI? Applications of artificial intelligence to dermatology. *Br J Dermatol* 2020;**183**:423−30.
243. Jiang YL, Zhao G, Wang SH, Li N. Leveraging artificial intelligence for clinical decision support in personalized standard regimen recommendation for cancer. *Mil Med Res* 2025;**12**:31.
244. Wang T, Shi X, Wang Y, Sun H, Sun Y, Wang G, et al. Lidocaine-loaded iontophoresis-driven fiber-based microneedle patch for controllable and long-lasting transdermal local analgesia. *Adv Fiber Mater* 2024;**7**:281−95.
245. Wang H, Cai R, Wang S, Yang Y, Sheng T, Zhang W, et al. A wearable transdermal device for on-demand drug delivery. *Matter* 2025;**8**:102040.
246. Zou Y, Lyu L, Xie Y, Yan S, Zhao Y, Chen W, et al. Active chemical messenger-driven immune activation *via* electrochemical patch for *in-situ* tumor vaccination. *ACS Nano* 2025;**19**: 22424−41.
247. Qian L, Jin F, Wei Z, Li T, Sun Z, Lai C, et al. Wearable, self-powered, drug-loaded electronic microneedles for accelerated tissue repair of inflammatory skin disorders. *Adv Funct Mater* 2023;**33**: 2209407.
248. Yang C, Zhou A, Lin Y, Fang T, Qin C, Bai C, et al. Stretchable and microneedle-integrated electronic patches with actively controlled chemothermal therapy for cancer treatment. *Adv Funct Mater* 2025; **5**:eaav3097.
249. Jin T, Wang H, Ullah I, Xie W, Lin T, Tan Q, et al. A wireless operated flexible bioelectronic microneedle patch for actively controlled transdermal drug delivery. *Adv Mater* 2025;**37**: e2417136.
250. Xue H, Jin J, Huang X, Tan Z, Zeng Y, Lu G, et al. Wearable flexible ultrasound microneedle patch for cancer immunotherapy. *Nat Commun* 2025;**16**:2650.

251. Zhao S, Lu Z, Cai R, Wang H, Gao S, Yang C, et al. A wearable osmotic microneedle patch provides high-capacity sustained drug delivery in animal models. *Sci Transl Med* 2024;**16**: eadp3611.
252. Himawan A, Vora LK, Permana AD, Sudir S, Nurdin AR, Nislawati R, et al. Where microneedle meets biomarkers: futuristic application for diagnosing and monitoring localized external organ diseases. *Adv Healthcare Mater* 2023;**12**:e2202066.
253. Chang AY, Lin MY, Yin L, Reynoso M, Ding SC, Liu RX, et al. Integration of chemical and physical inputs for monitoring metabolites and cardiac signals in diabetes. *Nat Biomed Eng* 2025. Available from: https://doi.org/10.1038/s41551-025-01439-z.
254. Yang K, Dong QQ, Yao ZB, Liang JJ, Zhao JJ, Wu L, et al. A wearable dual-modal patch for rapid pre-hospital diagnosis of acute myocardial infarction. *ACS Nano* 2025;**19**:23969−81.
255. Guo Y, Shang Y, Han X, Tang Y, Ma T, Shen H, et al. Carbon-nanotube synergized robust enzymatic-fuel-cell in gel microneedle for self-powered monitoring and forecasting. *Adv Mater* 2025;**37**:2313837.
256. Luo X, Yu Q, Yang L, Cui Y. Wearable, sensing-controlled, ultrasound-based microneedle smart system for diabetes management. *ACS Sens* 2023;**8**:1710−22.
257. Liu Y, Yang L, Cui Y. A wearable, rapidly manufacturable, stability-enhancing microneedle patch for closed-loop diabetes management. *Microsyst Nanoeng* 2024;**10**:112.
258. Li J, Xia Q, Ma S, Wang Z, Guo T, Feng N, et al. Progressive microneedles for targeting and intelligent drug delivery. *Asian J Pharm Sci* 2025;**20**:101051.
259. Yang J, Zhang H, Hu T, Xu C, Jiang L, Shrike Zhang Y, et al. Recent advances of microneedles used towards stimuli-responsive drug delivery, disease theranostics, and bioinspired applications. *Chem Eng J* 2021;**426**:130561.